FABRICATION OF MESA STRUCTURES ON SUPERCONDUCTING $Bi_2Sr_2CaCu_2O_{8+\delta}$ SINGLE CRYSTALS

A Thesis Submitted to
the Graduate School of Engineering and Sciences of
İzmir Institute of Technology
in Partial Fulfillment of the Requirements for the Degree of

MASTER OF SCIENCE

in Physics

by
Cihan KURTER

June 2005
İZMİR

We approve the thesis of **Cihan KURTER**

Date of Signature

……. **06 June 2005**
Assoc. Prof. Lütfi ÖZYÜZER
Supervisor
Department of Physics
İzmir Institute of Technology

……. **06 June 2005**
Prof. Doğan ABUKAY
Department of Physics
İzmir Institute of Technology

……. **06 June 2005**
Asst. Prof. Yusuf SELAMET
Department of Physics
İzmir Institute of Technology

……. **06 June 2005**
Asst. Prof. Salih Okur
Department of Physics
İzmir Institute of Technology

……. **06 June 2005**
Prof. Mustafa EROL
Department of Physics Education
Dokuz Eylül University

……. **06 June 2005**
Prof. Durmuş Ali DEMİR
Head of Department
İzmir Institute of Technology

……
Assoc. Prof. Semahat Özdemir
Head of the Graduate School

ACKNOWLEDGEMENTS

There is no perfect work which can be done without any help. This thesis is the consequence of a three-year study evolved by the contribution of many people and now I would like to express my gratitude to all the people supporting me from all the aspects for the period of my M.S.

First of all, I would like to thank my thesis advisor, Assoc. Professor Lütfi Özyüzer who introduced me to fascinating aspects of superconductivity, for his extremely good guidance and inspiring suggestions during the preparation of this thesis. I am also thankful to Dr. Kenneth E. Gray and Dr. John F. Zasadzinski for their supports and providing some facilities in each step of tunneling measurements. I wish to extend my thanks Dr. Dave G. Hinks and Dr. Paris Barnes from Argonne National Laboratory who grew the high quality BSCCO single crystals for the characterization. I would also like to acknowledge Dr. Chris Kendziora from Naval Research Laboratory for supplying some of the BSCCO crystals. Moreover, I appreciate the thesis committee members; Dr. Doğan Abukay, Dr. Yusuf Selamet, Dr. Salih Okur and Dr. Mustafa Erol for their remarkable comments and advice.

I am greatly indebted to the staff of Center for Material Research of İzmir Institute of Technology for their contribution whilst doing pre-characterization. This research was partially supported both TUBITAK (TBAG-2031) and TUBA. I acknowledged research assistantship from İzmir Institute of Technology throughout my graduate study. I am also grateful to my friends especially Çağlar Karadağ and lab-mates; Kaan Oğuz, Mehtap Özdemir, and Savaş Ulucan for their helps and creating a nice environment while studying together. Besides, I would like to thank Mehmet Eğilmez for his encouragement when I most needed it.

Finally, special thanks to my family especially my father and my dear Sinem for being with me all the time and letting me feel their sincere love whenever I bogged down.

ABSTRACT

There have been tremendous efforts to understand the relatively much more sophisticated mechanism of superconductivity in high temperature superconductors (HTSC). In order to investigate the inherent features and tunneling characteristics just only peculiar to HTSC, micron-sized mesa structures were fabricated on the surfaces of both pristine optimally doped and $HgBr_2$ intercalated $Bi_2Sr_2CaCu_2O_{8+\delta}$ (Bi-2212) single crystals using photolithography and Argon ion beam etching techniques. The surface topography and heights of the mesas were examined with atomic force microscopy. Hysteretic I-V curves with multiple branches and temperature dependence of tunneling characteristics were investigated by means of a novel technique, point contact tunneling (PCT) and experiments were carried out in a large range of temperatures from 4.2 K to 300 K. The results of SIN single junctions and SIS break junctions obtained by tunneling measurements using PCT technique on bulk crystals were compared with intrinsic Josephson junction quasiparticle spectra generally showing sharp peaks at the gap voltages and no dip/hump structures; which are reconciled with overheating in the mesa. The IJJ measurements performed with $HgBr_2$ intercalated Bi-2212 samples showed far more enhanced characteristics indicating less heating. The zero bias conductance versus temperature plots were examined to scrutinize the existence of pseudogap in electronic excitation spectra of investigated samples. Besides, the normalized gap voltages were plotted against normalized temperature to show the deviation from BCS fit, which displays the novelty of HTSC.

ÖZET

Kristal yapıları, düşük sıcaklık üstüniletkenlerine kıyasla hayli karmaşık olan yüksek sıcaklık üstüniletkenlerinin mekanizmalarının tümüyle anlaşılabilmesi için büyük emek harcanmaktadır. Bu çalışmada, yüksek sıcaklık üstüniletkenlerine özgü bazı özellikleri araştırmak ve tünelleme karekteristiklerini elde edebilmek amacıyla optimal katkılanmış ve $HgBr_2$ molekülleriyle intercalate edilmiş $Bi_2Sr_2CaCu_2O_{8+\delta}$ (Bi-2212) tek kristalleri üzerine mikron boyutta mesa yapılar üretilmiştir. Fotolitografi ve Ar iyon aşındırması teknikleri kullanılarak elde edilen özgün Josephson eklemi yığınlarının, akım-gerilim ve tünelleme iletkenlikleri, yüzeylerinden nokta kontak alınarak geniş bir sıcaklık aralığında (4.2-300 K) ölçülmüştür. Elde edilen mesaların yüzey topografileri ve yükseklikleri atomik kuvvet mikroskobu yardımıyla belirlenmiştir. Özgün Josephson eklemlerinin tünelleme iletkenliğinin, Bi-2212 ye ait durum yoğunluğunun spektral özelliklerini (örneğin sankiparçacık-quasiparticle-pikleri, "dip" ve "hump" yapıları) göstermesi gerektiğinden yola çıkılarak tünelleme ölçümleri sonucu alınan I-V ve dI/dV-V karakteristikleri ile bu özellikler gözlenmeye çalışılmış ve sonuçlar SIN ve SIS eklemlerinin karakteristikleriyle karşılaştırılmıştır. Kristalde herhangi bir şekillendirme yapılmaksızın PCT tekniğinin direk yüzeye uygulandığı ölçümlerden elde edilen spektra ile mesa yapılardan alınan verilerin uyumsuzluğu özgün Josephson eklemlerindeki aşırı ısınmanın ve sankiparcacık enjeksiyonun varlığı ile açıklanmıştır. Bi-2212 kristalinin çok düşük termal iletkenliğe sahip olması deneyler esnasında aşırı ısınma problemiyle karşılaşma olasılığını tetiklemektedir. Bu sorunu aşmada en etkili yöntemlerinden birisi, Bi-2212 üstüniletkeni içerisine kristalin yapısal sistemini bozmayacak yabancı bir molekül enjekte etmektir. $HgBr_2$ intercalate edilmiş Bi-2212 kristallerle yapılan deneylerden alınan sonuçlarda ısınma probleminin etkin bir şekilde yenilebildiği gözlenmiştir. Normalize edilmiş pik voltajı değerlerinin normalize edilmiş sıcaklığa bağlılığı, BCS fitiyle beraber incelendiğinde yüksek sıcaklık üstün iletkenlerinin kritik sıcaklığın çok üstündeki değerlerde dahi enerji aralığı sergilediği gözlenmiş ve sanki enerji aralığının varlığı incelenmiştir.

TABLE OF CONTENTS

LIST OF FIGURES

LIST OF TABLES

CHAPTER 1

INTRODUCTION

1.1. Motivation

High Temperature Superconductors (HTSC) have excited a great curiosity in scientific community since Bednorz and Müller discovered the first cuprate compound in 1986. Although researchers made significant progress in this field, mechanism of high temperature superconductivity is still an enigma and there are many unanswered questions about it.

It is realized that the symmetry of the superconducting wave function of the pairs has a great significance for identifying the underlying mechanism of HTSC. The pair can be depicted by quantum theory by means of a single wave function, which mathematically specifies the probability distribution showing where the two electrons are most likely to be. The wave function of the electrons in the conventional superconductors is spherical, which means that a pair has an equal chance of traveling in any direction. Such a pairing is said to show s-wave symmetry; in other words, Cooper pairs have zero orbital angular momentum. The pairing mechanism can be explained by vibrations in the crystal lattice; especially after the discovery of transition temperature dependence on isotopic mass as predicted, this theory gained substance to reveal the nature of conventional superconductors. The involvement of the phonon interaction in superconductivity explains why the good normal conductors such as gold can not exhibit superconducting phase, since in good conductors the lattice interaction is weak (Petley 1971). However, in HTSC the situation is a little bit different, i.e. phonons alone are not powerful enough to maintain the essential electron pairing at higher temperatures. Most of the experiments such as tunneling spectroscopy, angle-resolved photoemission spectroscopy (ARPES) and Raman spectroscopy propose that superconducting order parameter in HTSC likely has d-wave symmetry although there are some studies which display evidence for s-wave or mixed symmetries in these kinds of materials.

There have been enormous efforts to understand electronic and superconducting behaviors of HTSC and reveal their distinguishing features. One of the experimental techniques, electron tunneling spectroscopy gives the valuable information about the pairing mechanism owing to subgap conductance analyses. Also, it is one of the most powerful techniques to determine the energy gap and density of states (DOS) of a superconductor which are fundamental superconducting characteristics.

Though, high temperature superconductivity has many similarities with the well-understood BCS superconductivity, it exhibits inherent properties and novel electronic phases ever examined. The considerably deviation of strong coupling ratio $\left(2\Delta/k_B T_c\right)$ in HTSC from the BCS prediction based on weak electron-phonon interaction can exemplify the intrinsic structure of these components.

1.2. High Temperature Superconductivity

After the discovery of superconductivity by chance in mercury at 4.2 K in 1911, most researchers have continued to search for the new superconducting materials with higher critical temperatures. In 1986, a new era was opened in the field of superconductivity by the synthesis of a ceramic compound, lanthanum barium copper oxide (LBCO), $La_{2-x}Ba_xCuO_4$, with the critical temperature (T_c) of 36 K. Up to this breakthrough, the highest recorded transition temperature in superconductors was 23.3 K for a thin film of Nb_3Ge and the new material found was pretty interesting because BCS theory had predicted a theoretical limit of about 30-40 K for T_c (due to the thermal vibrations). The invention was so remarkable not only because it represented a significant increase in the maximum critical temperature but also because the material $La_{2-x}Ba_xCuO_4$ was the first cuprate ever created-a new class of superconducting materials known as copper oxide superconductors (Bednorz and Müller 1986). Before them, most of the encountered superconductors were metals. Because the ceramics are normally antiferromagnetic insulating materials, no scientist had considered them as potential HTSC candidates. Following year another cuprate, yttrium barium copper oxide compound (YBCO), $YBa_2Cu_3O_{7-x}$ (Y-123), was found with T_c around 90 K (Wu et al. 1987), whose critical temperature is well above the boiling point of liquid nitrogen. So, it enabled to use the liquid nitrogen as a coolant instead of liquid helium, more expensive and unpractical cryogen. Soon after YBCO was found, two bismuth

strontium calcium copper oxide compounds (BSCCO) were formed; $Bi_2Sr_2CaCu_2O_{8+x}$ (Bi-2212) and $Bi_2Sr_2Ca_2Cu_3O_{10+x}$ (Bi-2223) (Chu et al. 1998). Their critical temperatures are 95 K and 110 K respectively for the optimally doped crystals. The critical temperature reached to 125 K with the discovery of thallium barium calcium copper oxide compound (TBCCO), $Tl_2Ba_2Ca_2Cu_3O_x$ (Tl-2223) (Hazen et al. 1988). At the present time, the maximum transition temperature is around 135 K in $HgBa_2Ca_2Cu_3O_{8+x}$ (Hg-1223) known as mercuric cuprate (Schilling et al. 1993). The T_c of this material shows an increase under pressure up to 160-165 K (Gao et al. 1994).

In January 2001, a new superconductor with baffling properties was discovered, MgB_2. Before this superconductor with T_c= 39 K, the known intermetallic compound with the highest critical temperature up to that time was also Nb_3Ge with T_c= 23.3 K. Although MgB_2 obeys conventional models of superconductivity and has relatively basic structure if compared with the cuprates, it is considered as type II superconductor like all HTSC.

HTSC have been continuing to capture a great attention of researchers around the world. Each high T_c superconductor belongs to a certain system containing several extensive families delineated by elemental compositions. It means that different families in the same system involve the same elements but in different proportions. The members of the families are named by the ratios of the elements and the chemical symbols of the first elements in the superconductors to shorten the notation.

The crystal structures of all copper oxide superconductors are based on oxygen-defect modifications of the perovskite structure. The name “perovskite” refers to the compound $CaTiO_3$ with a cubic or almost cubic unit cell in which calcium atom is in the center, Ti atoms are on each of the eight vertices and O atoms are in the middle of the each edge. Because all the valences of the system are saturated, this material is an electrical insulator (Kadin 1999). All HTSC can be thought as a stack of some basic perovskite cells along the c-axis with the vacancy of some oxygen sites; which eliminates the electronic neutralization and lets the material show superconducting properties.

Copper oxide superconductors exhibit unusual features apart from having relatively higher critical temperatures. All HTSC are extremely type II superconductors whose magnetic properties can be well explained by Ginzburg- Landau Theory (Schmidt 1997). The multi-layered structures of HTSC make them highly anisotropic; all of them include copper oxide sheets providing superconductivity separated by non-

superconducting layers. In these kinds of structures, there are two fundamental axes: the in plane direction and the direction perpendicular to the planes or c-axis. According to these axes, characteristic physical parameters such as critical fields, London penetration depth, superconducting coherence length, resistivity, energy gap also show anisotropic behaviors. The d-wave model of the superconducting energy gap for cuprate superconductors indicates the gap anisotropy which means that the gap should be maximum along a and b directions and go to zero between the two. Furthermore, this model suggests that the superconducting wave function should actually change sign between the two directions, i.e. the phase shifts by 180^0 (Kadin 1999). The superconducting order parameter, which reflects the local density of superconducting electrons, is suppressed in the vortex core with the size ξ and the magnetic field of the vortex decays on the characteristic distance of the London penetration depth λ. For all type two superconductors, $\kappa = \lambda/\xi$ should be greater than $\sqrt{2}$ where κ is the Ginzburg-Landau parameter and it is typically on the order of 100 in HTSC (Soibel 2001). The coherence length values of HTSC are excessively short (less than 2 nm along the a-b axes) and correspondingly they have large critical fields (generally greater than 180 T), the two parameters are inversely related (Tallon 2000).

In the sandwiched structure of HTSC, within the parallel two dimensional sheets containing cooper and oxygen, each copper atom has the potential to relinquish one loosely bound electron which can then move from one copper atom to another and carry electricity, which actually depends on the p value (the number of the holes per CuO_2). When the p value is zero and the temperature is sufficiently low, the material is antiferromagnetic insulator known as Mott insulator (Buchanan 2001). When the doping is increased above a critical value, i.e. the holes are injected into the CuO_2 layers by adding oxygen atoms, the material first turns from an antiferromagnetic insulator into a reasonable conductor, at larger values of p, it gains the ability to be superconducting when cooled. The name of this region in the related phase diagram (temperature versus doping) is pseudogap region or more specifically underdoped region. Various experimental techniques bring to light two different kinds of pseudogaps and correspondingly two different pseudogap temperatures: T* (low energy pseudogap temperature) and T^m (high energy pseudogap temperature). Although the first pseudogap has almost the same energy scale as the superconducting gap disappearing at T*, the latter is a gap-like feature whose scale is pretty much larger than that of

superconducting energy gap. It is believed that low energy pseudogap is the precursor of superconductivity and the high energy pseudogap is of magnetic origin forming hump features roughly at 3Δ values in SIN (S: superconductor, I: insulator, N: normal metal) point contact characteristics (Miyakawa et al. 2001b). Namely, the hump feature may be caused by short-range magnetic correlations (Miyakawa et al. 2000). Sometimes, the hump positions have the values slightly more than 3Δ in SIN or 4Δ in SIS tunneling conductance curves. This trend of hump feature scaling with the superconducting gap is associated with doping range (Zasadzinski et al. 2000).

The existence of pseudogap can be probed by interlayer tunneling experiments exploiting the dependence of c-axis conductance characteristics on temperature. Besides, ARPES experiments investigate the pseudogap by revealing the relation between superconducting gap and the direction in which the photon is fired into the material. This shows the d-wave behavior of the Cooper pairs and anisotropy in the superconducting energy gap. A dazzling observation can be obtained when the superconducting material is heated above T_c, the energy gap does not go away, this aberration is known “pseudogap”.

Since their indisputable peculiarities, the nature of HTSC needs satisfying explanation. According to some researchers, the fluctuations in electron spins of HTSC may play a role similar to phonons in the s-wave superconductors. The spin of one traveling electron might deform the neighboring spins of electrons by exerting an attractive force on other electrons; which causes to bind them together into pairs.

Another idea focuses on lightly doped Mott insulators in which charge holes can move from atom to atom. Because the movement of the holes is not easy in such a largely antiferromagnetic material, the stripes including linear regions of holes come into existence in the antiferromagnetic pattern. Being forced together into the stripes, the holes can become bound together into pairs even at high temperatures, which leads to pseudogap (Buchanan 2001). At lower temperatures, the pairs within the each stripe would condense into single quantum states encouraging superconductivity. That is, below the critical temperature, pairs can move from stripe to stripe resulting in phase coherence and superconductivity. This theory is quite controversial, because superconducting properties call for vibration of the stripes and stripes can exist in just only certain compounds as claimed by some scientist.

A model has been developed based on the hypothesis of two dimensional arrangements of stripes in CuO_2 planes. In such a superstructure, there exists hole states

localized either between the stripes (a states) or inside the stripes (b states). If the position independent on-site energies for a and b states are named ε_a and ε_b respectively, $|\varepsilon_a - \varepsilon_b|$ can be told a measure of the pseudogap according to suggested model. This pseudogap is an authentic feature in the normal density of states, i.e. it is not associated with the superconducting fluctuations above T_c. The model pseudogap will be zero when $\varepsilon_a = \varepsilon_b$, which can correspond to the doping concentration 0.19 (Fine 2005).

1.3. Superconductive Tunneling

In 1957, the discovery of tunnel diode caused that tunneling phenomena drew so much interest and this sophisticated concept was put into applications (Esaki 1957). The first experiments on superconductive tunneling were conducted by Giaever in 1960 by measuring current-voltage characteristics of a superconductor-insulator-normal metal (SIN) junction. What he observed was that the resistance of the junction suddenly increased when the superconductor under investigation began to show superconducting properties. He claimed that superconducting energy gap is responsible for reducing the electron flow through the junction by not accepting electrons with small excitation energies. He was able to show the tunneling current was controlled primarily by the density of states in the superconductor (Ozyuzer 1999a).

In general meaning, tunneling is a quantum mechanical process according to which an atomic particle such as electron is able to penetrate a potential barrier, though classically its kinetic energy is not sufficient to surmount the height of the barrier. If two conducting materials are brought together and interrupted with an ultra thin insulating layer, different kinds of tunneling junctions such as NIN, SIN, SIS (N: normal metal, I: insulator, S: superconductor) can be created.

In an SIS junction, two fundamental types of tunneling effect can be observed: single particle tunneling and Cooper pair tunneling. Single particles, so-called quasiparticles are unpaired electronlike or holelike excitations in superconductors which can tunnel through the insulating layer. There are two types of process to form quasiparticle. A pair may be broken by creating a hole excitation on the side where the pair was and injecting the electron into the other side. The second type is the transfer of

an excited electron from one side to the other (Duzer and Turner 1999). Apart from single particle tunnel current, there is another current passing through the junction which is supercurrent or Josephson current. In 1962, Brain Josephson predicted that Cooper pairs can tunnel through a sufficiently thin non superconducting barrier (less than 1nm) even in the absence of an external voltage, known as dc Josephson effect (Josephson 1962). The first experimental authentication of the Josephson tunneling effect was done by Rowell (Rowell 1963), then soon Shapiro found steps in the I-V characteristics which confirm the existence of supercurrent (Shapiro 1963). Josephson also predicted that if a constant nonzero voltage V is applied across the tunnel barrier, an alternating supercurrent will flow through the barrier in addition to the current produced by the tunneling of single electrons which is called ac Josephson Effect. These effects can be observed in a circuit containing weak links such as SIS junctions, cracks, grain boundaries, point contacts or linear contacts. SIS tunneling junctions, known as Josephson junctions can be categorized in two general groups: conventional Josephson junctions (CJJ) and intrinsic Josephson junctions (IJJ). By separating two superconductors with an extremely thin non-superconducting layer, a single CJJ can be obtained. If the structures of HTSC are examined, it can be easily realized that so many SIS junctions are ordered periodically in a natural way; such kinds of Josephson junctions are called IJJ.

Although approximately 20 years have passed since the discovery of the first cuprate, this area is still a challenge for researchers. For this reason, IJJ which constitute the structure of HTSC are getting more and more important for the studies of these materials theory. Stacked series arrays of IJJ can be formed in various ways, and measurements of these special structures shed onto light many spectral features to investigate underlying mechanism of HTSC. Recent developments have showed that the observation of Josephson effects is strongly associated with crystal quality and convenience of patterned images geometry on the investigated sample. Understanding of these effects on HTSC is a key factor to study the c-axis current transport under magnetic fields and to develop a theoretical model for vortex dynamics (Yurgens and Claeson 2001).

Fabrication of cube shaped mesa structures is one way to reach one of the appropriate geometries related to this matter. Applying some particular techniques such as optical photolithography and mechanical/wet etching (Ar ion beam or chemical etching depending on the study), proper mesas can be formed for facility in

measurements. Recently, much more precise experiments have been performed with e-beam technology (Heim et al. 2000) or focused ion beam technique (Kim et al. 1999, Latyshev et al.1999) to pattern the images onto the crystals. All CuO_2 superconductors have a comparatively low thermal conductivity, so it is inevitable to face overheating locally. The reason why we need such kind of construction is to get rid of excess Joule heating which affects the results of experiments negatively. Mesa fabrication and some phenomena related to this subject are going to be explained in details in the third chapter.

Another alternative to create effective stacks of IJJ is to make HTSC whiskers which are known perfect geometry without requiring any crucible or substrate and they are completely free of macroscopic defects and dislocations (Latyshev et al. 1997) Although many IJJ preparation methods call for advanced techniques, whiskers are the structures much more easily to fabricate. These structures are grown in the direction of a-axis but aside from this longitudinal axis, whiskers usually have small dimensions in both b and c directions. With some studies on fabricating Bi-2212 cross-whiskers on MgO single crystal substrate even without microfabrication, electrical transport properties of Bi-2212 have been investigated, and also by means of I-V curves at certain temperatures, significant information can be gained about Josephson Effects (Takano et al. 2001).

Micrometer scale IJJ structures have been created on epitaxial Bi-2212 thin film (grown on its substrate with the same vicinal direction) with tilted c-axis (Tsai et al. 1995). The applied current flows along both a-b plane and c-axis directions. This geometry is advantageous in practical applications and helps to escape the excess heat from stack into the substrate.

Many technological improvements in the area of the superconducting devices are based on Josephson effects. One of the most important inventions related to both effects is SQUID (superconducting quantum interference device) magnetometer which was first introduced by James Zimmerman in the late 1960s. SQUID, made up by a tiny superconducting loop employing one or more Josephson junctions is capable of detecting extremely sensitive magnetic fields (on the order of fermtotesla) even that of human brain or heart. According to the mechanism, there are two types of SQUIDs which are rf and dc SQUIDs. The dc SQUID consists of two Josephson junctions connected in parallel to form a superconducting ring. In the existence of a magnetic field an appropriate circulating current is induced in the ring and thus a voltage is

developed across the junctions. As the applied external magnetic field is changed, this voltage oscillates back and forth with a period of one flux quantum. Namely, the magnitude of the circulating current varies periodically according to the strength of external flux. A change in magnetic field can be detected by measuring the resulting change in voltage across the SQUID using conventional electronics.

The very rapid switching time (less than 10^{-9} sec) and the lower power dissipation as compared semiconducting switches let Josephson junctions be used as a computer switching element (Petley 1971). Because most of the electronic devices such as computers depend on time required to transmit short electrical signal pulses, using Josephson junctions is very advantageous for designing high speed mechanisms.

When a DC voltage is applied to a Josephson junction, an oscillation occurs with a characteristic frequency proportional to the applied voltage across the junction. Because this relationship between voltage and frequency involves just only fundamental constants and frequency can be detected with a great accuracy, then "the standard volt" is determined by means of Josephson junctions.

The radiation emitted by point contact systems or other kind of tunneling junctions enables them to be used as a simple source of millimeter or submilimeter waves. The former alternative is more useful in many respects because the frequency of the radiation emitted is dependent on the resonant frequency of the containing cavity; it is thus a broader band device (Petley 1971).

Recently, terahertz spectroscopy has been an outstanding measurement tool in some special fields such as radio astronomy, physical chemistry, atmospheric studies, biological investigations and plasma researches. The realization of IJJ along the c-axis in layered high temperature superconductors as high frequency devices has been promising. The Josephson vortex dynamics of mesa structures consisting of IJJ which is closely related to external magnetic field applied parallel to a-b axes is extensively important not only in terms of physics but also designing tunable-solid state terahertz wave sources. However, terahertz region in electromagnetic spectrum is still unclear and needs reliable and tunable sources. The researchers have managed to obtain terahertz radiation in femtosecond duration, after the experiments done with semiconductor crystals. But trends begin to change; the recent advances in the field of terahertz studies are based on high T_c superconductors. For this purpose, generally preferred material is $Bi_2Sr_2CaCu_2O_{8+\delta}$ (Bi-2212) which is an extremely anisotropic high temperature superconductor with the critical temperature of 95 K for optimally doped

crystals. Local overheating in created Bi-2212 mesas precludes the terahertz resonance conditions and raises the temperature of the mesa due to the overinjection of the quasiparticles. Since tunneling current is inversely proportional to the thickness of insulating layers in the crystal structure, Bi-2212 can be intercalated with some inert molecules such as $HgBr_2$ molecules to eliminate heating problem and correspondingly increase resonance possibility.

1.4. Point Contact Tunneling Technique

There are a lot of techniques to reveal tunneling spectroscopy of superconductors for studying the DOS near the Fermi level (Wolf 1985). Scanning Tunneling Microscopy (STM), point contact tunneling (PCT), break junctions and planar junctions (single junctions or IJJ) can be considered among the powerful tools exhibiting reproducible results in terms of tunneling.

The PCT method has been used comprehensively to construct tunneling junctions up to now and the feasibility of this technique on low T_c superconductors has been supported by some experiments performed with Nb (Huang et al. 1990). Basically, a point contact can be created by being approached with a pointed tip of electrode such as Au, Pt etc. to a flat surface of examined sample so that the contact area can be sufficiently small.

PCT has been also believed to be one of the most important probes for tunneling of HTSC as well as that of conventional superconductors. However, a measurement over the wide temperature range of HTSC is difficult because of the thermal expansions in the PCT apparatus. The conditions of point contact tunnel junction can change or the junction can be totally spoiled as the temperature is varied (Ozyuzer et al. 1998)

The experimental point contact tunneling conductances obtained by tunneling between a normal metal and a cuprate show uncommonly high degree of symmetry, while this usually exists in conductances of conventional superconductors (Chen et al. 1994). In general, all stable SIN junctions exhibit weakly decreasing background conductance with increasing voltage values as observed in experiments done with HTSC. Besides, there are some exceptions for cuprates showing increasing or flat background conductance among the results of PCT measurements.

This thesis divided into mainly 4 parts including theoretical and experimental parts as well as tunneling characteristics of pristine optimally doped and $HgBr_2$ intercalated Bi-2212 single crystals. Chapter 2 provides a brief overview of the relevant theory providing a foundation for the subsequent parts. Chapter 3 details the investigated material, Bi-2212, used experimental techniques for the mesa fabrication such as photolithography and the design of a new devise for PCT measurements. Chapter 4 presents tunneling results obtained by PCT measurements on various Bi-2212 single crystals. Finally, Chapter 5 summarizes the results and concludes this thesis.

The aim of this study is to investigate the structure of HTSC with their extremely distinguishing properties and try to understand the ambiguity in underlying mechanism of the cuprates. For this reason, superconducting Bi-2212 single crystals were chosen to probe the high T_c superconducting properties and to study their tunneling characteristics which give a direct insight about DOS near the Fermi level. In order to observe the generic behaviors of HTSC, stacked arrays of IJJ were fabricated on the surfaces of Bi-2212 single crystals using photolithography and Argon ion beam etching techniques. Due to the extremely small mesa areas, a novel technique, PCT, were used for interlayer tunneling and results obtained from the measurements were discussed in the light of various theoretical explanations.

CHAPTER 2

THEORETICAL BACKGROUND

This chapter is mainly concerned with the fundamental tunneling picture of superconductors. Besides, the existence of pseudogap in high T_c superconductors is discussed by giving characteristic phase diagram (temperature as a function of carrier doping) based on experimental results.

2.1. Tunneling Spectroscopy

Existence of energy gap in superconductors can be proved by some experimental measurements such as specific heat, thermal conductivity, nuclear relaxation, ultrasonic attenuation and electromagnetic absorption (Giaver and Megerle 1961). Among these methods, tunneling is the one of the most sensitive probes to investigate the energy gap. This quantum mechanical process was first employed by Giaver in 1960 with a quite simple design which is shown in Figure 2.1. (Giaver 1960a, Giaver 1960b). In order to generate a tunneling junction, it is sufficient an ultra-thin insulating oxide layer sandwiched between two evaporated metal films. If both metals are normal, as soon as they are brought together, their Fermi levels become equal. When a small potential difference V is applied to the junction, the Fermi levels of the metals will shift apart by the amount of eV with respect to each other, so tunnel current will begin to flow. The possible transitions of the single electrons are straight across from filled states in negatively biased metal to the empty states of the second metal. The current-voltage relation of the tunneling junction obeys Ohm's law, because tunneling current passing through the junction is directly proportional to the applied voltage.

Aside from tunneling in normal metal-insulator-normal metal junctions (NIN), tunneling can occur through an insulating layer between a normal metal and a superconductor (SIN) or between two superconductors (SIS).

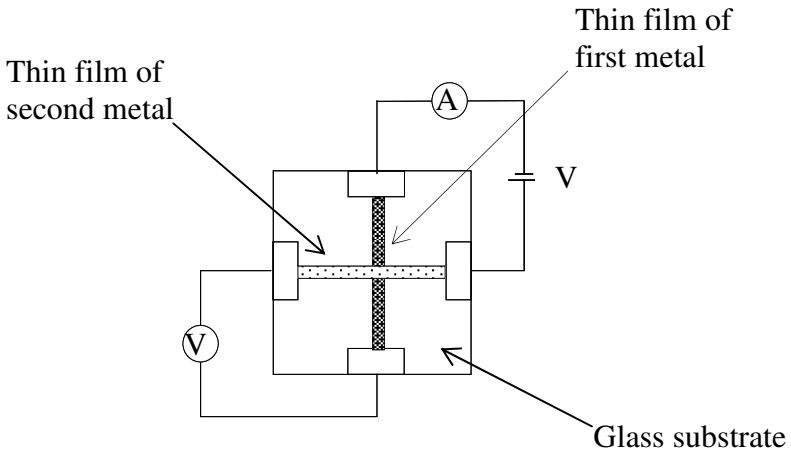

Figure 2.1. The schematic representation of the metal-insulator-metal (NIN) junction created by Giaver. The intersection of the two films forms a tunnel junction.

Giaver found that if one of the metals forming the tunneling junction is superconducting, so current-voltage characteristics deviate from straight line observed in NIN junctions (Giaver 1960b). This change is caused by the existence of energy gap in the electron density of states of superconductors. There are two different representation of the energy levels associated with superconductors which are semiconductor and Bose condensation representations. According to semiconductor model of superconductors, superconducting materials are believed to have an energy gap $E_g = 2\Delta$ between a lower energy band, full of superelectrons and an upper energy band, totally empty at absolute zero. If the temperature is increased, some of the electrons are excited from the lower band to the upper band. These individual electrons moving at the Fermi velocity are called quasiparticles. The approach of this model is based on single electron picture and it does not take into account Cooper pairs. Another representation of the energy levels in superconductors, Bose-condensation representation, suggests just only one level for the superelectrons at 0 K. In other words, at absolute zero, all the Cooper pairs, boson particles with zero spin, are condensed into a level located at a distance Δ below the bottom of the conduction band, so called ground state for superconductors. Above the 0 K, some of the Cooper pairs break up and by this way, quasiparticles occur.

If one of the metals is superconductor, likewise, no net tunneling occurs in the unbiased case. In the normal metal, the energy of the elementary excitations is measured

from the Fermi level. Hence when a SIN tunnel junction is established, the energy levels to be equalized are the Fermi level of the normal metal and the ground state level of the superconductor. Application of the positive bias voltage V to the superconductor causes that the Fermi level of the normal metal is moved up by the value of eV above the ground state of the superconductor. In the case of $eV \geq \Delta$, electrons can tunnel from the conduction band of the normal metal to the empty states above the superconducting gap. Figure 2.2 shows Bose-condensation representation of SIN tunneling process.

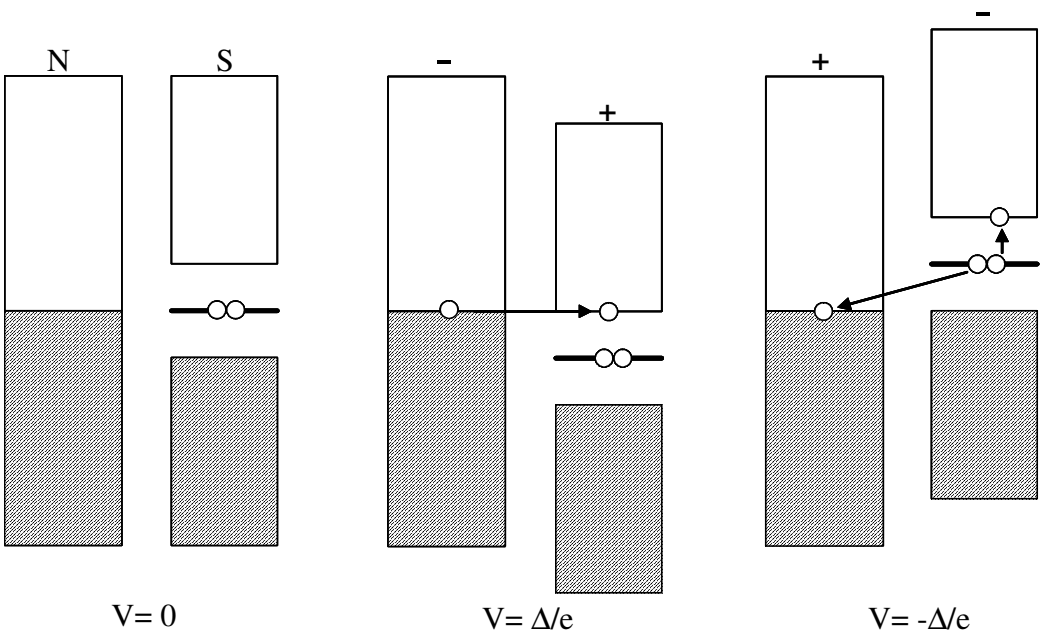

Figure 2.2. Schematic representation of SIN tunneling process

I-V characteristics or more accurately tunneling conductances are related to the density of states of quasiparticles in the superconductor, because the metal density of states can be taken as constant in the few milielectronvolts of interest. If the polarity of the applied voltage is reversed, the transition process changes. According to Boson condensation model, the tunneling involves the breakup of a Cooper pair, with one electron of the pair tunneling down to the top of the normal metal conduction band and the other one jumping upward to the quasiparticle energy band of the superconductor. Hence breaking up a pair creates a quasiparticle inside the superconductor and a electron passing through the insulating layer to reach the normal metal (Poole et al. 1995) The total tunneling current in an SIN junction can be determined by the independent particle approximation (Tinkham 1996).

$$I(V) = c\int |T|^2 N_{1n}(E) N_{2s}(E+eV)[f(E) - f(E+eV)]dE \qquad (2.1)$$

In the formula above, $f(E) = [1 + \exp(E/k_B T)]^{-1}$ is the Fermi-Dirac function, $N_{2s}(E)$ is DOS of the superconductor, N_{1n} (E) is DOS of the normal metal which is gold in our case, $|T|^2$ is the tunneling matrix element and c is the proportionality constant. The quasiparticle energy is given by E, which is defined relative to the Fermi level. For a rough estimation of tunneling current at T=0 K, it can be assumed N_{1n} has a constant value near the Fermi level and the tunneling matrix element is dependent on energy weakly over the voltage range of the energy gap, which may be ignored.

$$dI/dV \equiv \sigma_s = c|T|^2 N_{2s}(E) = c|T|^2 N_s(E) N_n(E) \qquad (2.2)$$

where N_s (E) is the superconducting part of the DOS and $N_n(E)$ is the normal state DOS of the superconductor. In most s-wave superconductors, $N_n(E)$ is usually a constant over the energy range of interest. The superconducting DOS can be found from the ratio of superconducting conductance to normal state conductance. According to BSC theory the superconducting DOS

$$N_s(E) = \mathrm{Re}\left(\frac{E}{\sqrt{E^2 - \Delta^2}}\right), \ |E| \geq \Delta$$

$$N_s(E) = 0, \ |E| < \Delta \qquad (2.3)$$

HTSC are commonly assumed to have d-wave pairing symmetry while conventional superconductors are considered to show s-wave nature. For s-wave superconductors, the superconducting energy gap,Δ, is constant in k space. That is, superconducting energy gap isotropic in conventional superconductors near the Fermi level while high temperature superconducting energy gap is anisotropic. Some experiments indicate that the shape of the tunneling spectra encountered on

conventional superconductors deviates from equation 2.3. This smearing is introduced into the BCS density of states with a broadening parameter, Γ (Dynes et al. 1978).

$$N_s(E) = \mathrm{Re}\left(\frac{E - i\Gamma}{\sqrt{(E - i\Gamma)^2 - \Delta^2}} \right) \qquad (2.4)$$

If two superconductors are put close enough to each other an SIS junction can be obtained. Bose-condensation representation of SIS tunneling process can be seen from Figure 2.3.

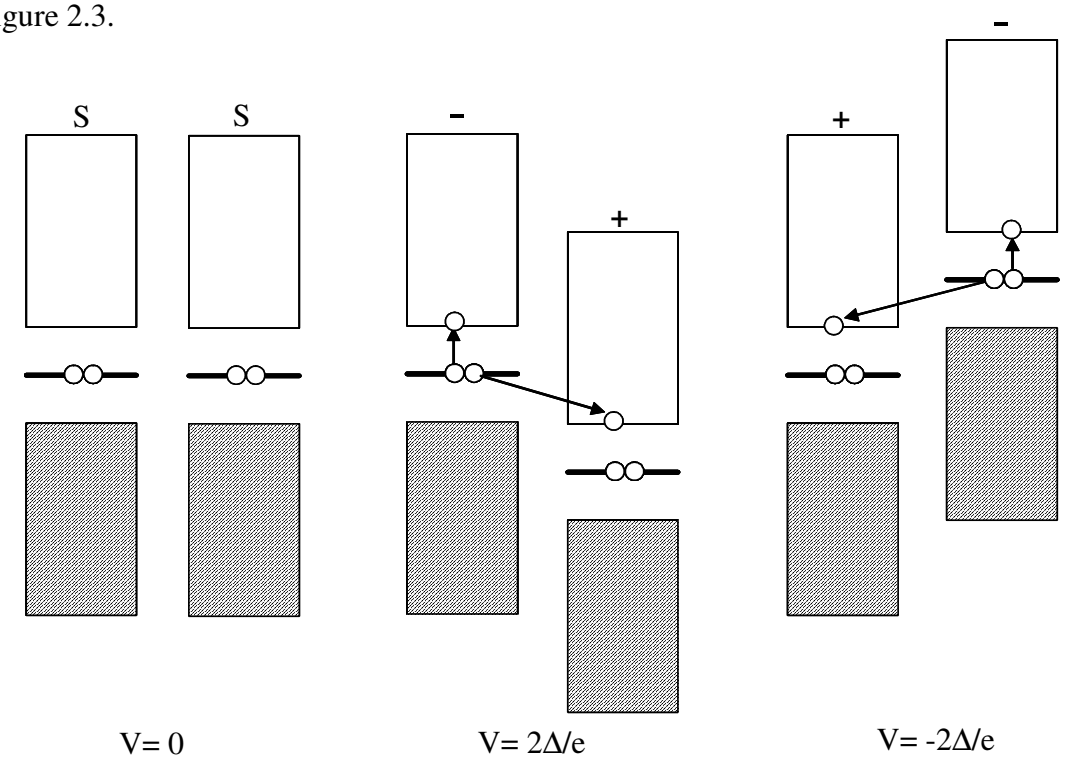

Figure 2.3. Schematic representation of SIS tunneling process

In such kinds of the junctions, the cases T=0 K and $T \neq 0$ K are fundamentally different. In the former situation, tunneling current begins to flow only when the voltage across the junction is $V > (\Delta_1 + \Delta_2)/e$ where Δ_1 is the energy gap of the first superconductor while Δ_2 is that of the second one. According to the tunneling process, a Cooper pair breaks up in the first superconductor and one of the electrons belongs to pair tunnels to quasiparticle energy bands of the second superconductor, thereby releasing energy equal to or greater than Δ_1. The released energy is absorbed by the second electron of the broken pair, which is subsequently excited to the quasiparticle

energy band of first superconductor (Schmidt 1997). In the I-V characteristics, there is a discontinuous jump in current at $V = (\Delta_1 + \Delta_2)/e$ because of the infinitive value of the density of states. If the temperature is different from 0 K, there is already a certain number of thermally excited normal electrons in the quasiparticle states of both superconductors. The Cooper pair-quasiparticle equilibrium is determined by temperature. In this case, if there is no voltage applied to the junction, the number of the excited states at the same energy levels in both superconductors is equal. Hence the number of the particles passing from first superconductor to second one is the same as the number of the particles tunneling in the opposite direction, which provides total zero tunneling current through the insulator. If a voltage V is applied, the equilibrium between superconductors will be spoiled and quasiparticles start to flow immediately from one superconductor to the other and the current will increase with increasing voltage values until $V = (\Delta_1 - \Delta_2)/e$ at which the current gives a drastic rise. If the voltage value is increased further, this time current begins to decrease. This reduction goes on until $V = (\Delta_1 + \Delta_2)/e$ value and after this value there is again a substantial rise in tunneling current, since DOS will increase greatly. The SIS tunneling current passing through the barrier is denoted as equation 2.5.

$$I(V) = c\int |T|^2 N_{1s}(E) N_{2s}(E+eV)[f(E) - f(E+eV)]dE$$

$$= c|T|^2 N_{1n}(0) N_{2n}(0) \int \left[\frac{|E|}{\sqrt{E^2 - \Delta_1^{\,2}}} \frac{|E+eV|}{\sqrt{(E+eV)^2 - \Delta_2^{\,2}}} \left(f(E) - f(E+eV)\right) \right] dE \qquad (2.5)$$

the range of the integration excludes values of E such that $|E| < \Delta_1$ and $|E+eV| < \Delta_2$.

The characteristic picture at $|\Delta_1 - \Delta_2|/e$ and $|\Delta_1 + \Delta_2|/e$ enables to determine Δ_1 and Δ_2 from the tunneling data. If both superconductors are the same materials, the quasiparticle peaks occur at +2Δ and -2Δ values. SIS junctions differ from other junction types in that they show supercurrent tunneling due to Cooper pair transfer between two superconductors which is called Josephson current apart from the quasiparticle tunneling. The existence of the Josephson current, I_c, depends on the

junction resistance and given by Ambegaokar-Baratoff theory (Ambegaokar and Baratoff 1963) for BCS superconductors. This theory can be explained as following:

$$I_c R_n = \frac{\pi \Delta(0)}{2e} \tag{2.6}$$

where I_c is the Josephson current, R_n is the normal state resistance of the junction and $\Delta(0)$ is the energy gap at absolute zero temperature . Josephson current at zero bias can be seen from the Figure 2.4.

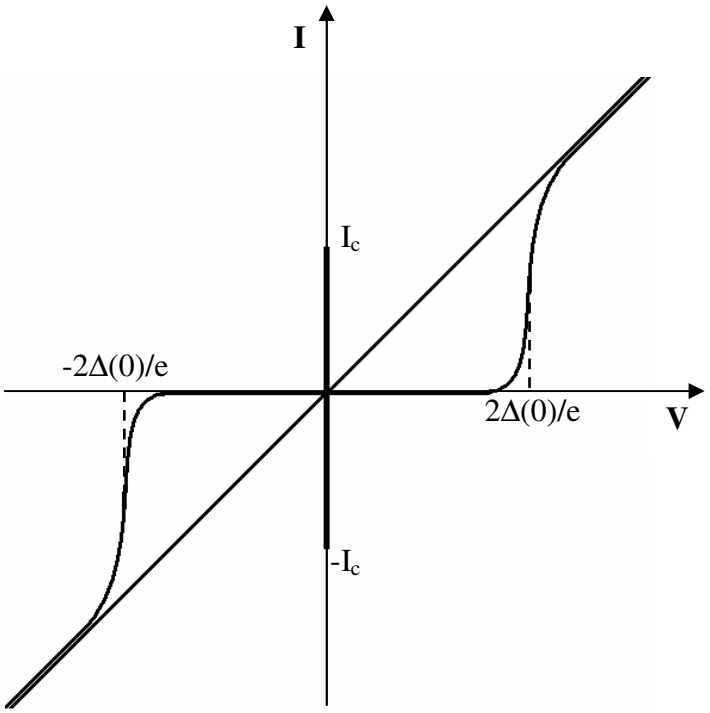

Figure 2.4. I-V characteristics of an SIS junction showing Josephson current

Superconducting energy gap of s-wave superconductors is isotropic in k-space, because tunneling measurements obtain just only single gap value without dependence of any tunneling direction. However, all HTSC have very sophisticated structure due to their multilayered constructions. Because they exhibit extremely anisotropic behaviors, their physical properties depend on the direction. So, for HTSC tunneling, direction is very important, d-wave gap function related this issue is given as following:

$$\Delta(k) = \Delta_0 \left(\cos k_x - \cos k_y\right)/2 \tag{2.7}$$

where Δ_0 is the maximum superconducting energy gap value. There is a π phase shift of superconducting order parameter in orthogonal k-space; which leads to appear positive or negative sign of the pairing potential in these k-space directions. The nodes are along the [110] direction in the CuO_2 plane (Misra 2004).

The cusp-like feature at zero bias value is a characteristic of momentum averaged DOS with the d-wave gap symmetry. According to Won and Maki, in a two dimensional superconductor, d-wave DOS can be stated as given equation 2.8 (Won and Maki 1994).

$$N_s(E,k) = \mathrm{Re}\left(\frac{E - i\Gamma}{\sqrt{(E - i\Gamma)^2 - \Delta(k)^2}} \right) \tag{2.8}$$

This time, the gap function becomes k-dependent, $\Delta(k) = \Delta_0 \cos(2\Phi)$ and Φ is the polar angle that the quasiparticle momentum makes with the k_x axis in the k_x-k_y space. The new defined gap function having lines of nodes at the directions $\pi/4$ from the k_x and k_y axes, is of d-wave symmetry and the approximate polar form of the equation 2.7. The total superconducting DOS is calculated by an integral over the polar angle:

$$N_s(E) = \int N_s(E,k)dk \tag{2.9}$$

It can be considered that the tunneling matrix element is reconciled with the k, because it couples electrons in the tip (normal metal) to those in the Cu-O layer (superconductor). Thus an additional term should be available in the equation 2.8 indicating $|T|^2$ dependence on k. Mallet et al. have taken into account a weighting function, f(Φ), in the equation 2.8 (Mallet et al.1996):

$$N_s(E,\Phi) = f(\Phi)\,\mathrm{Re}\left(\frac{E - i\Gamma}{\sqrt{(E - i\Gamma)^2 - \Delta(\Phi)^2}} \right) \tag{2.10}$$

where $f(\Phi) = 1 + \alpha \cos(4\Phi)$, and α is the directionality strength weighting the tunneling probability toward the (π,0) direction. This function makes the subgap region more round, so if the α value is increased, directionality is enlarged; which results in the BCS DOS resemblance of tunneling conductance.

A Fortran program was developed by Chen which enables us to create SIN and SIS conductances. Running the program, SIS curve can be generated at the end of convolution of two SIN DOS obtained by experimentally or from BCS theory. Figure 2.5 exhibits SIN conductance created by this program. The cusp-like feature at zero bias and sharp conductance peaks at ±20 mV can be recognized easily from the curve. Note that the smearing parameter is taken as 0.1 meV and also $\alpha = 0$.

.

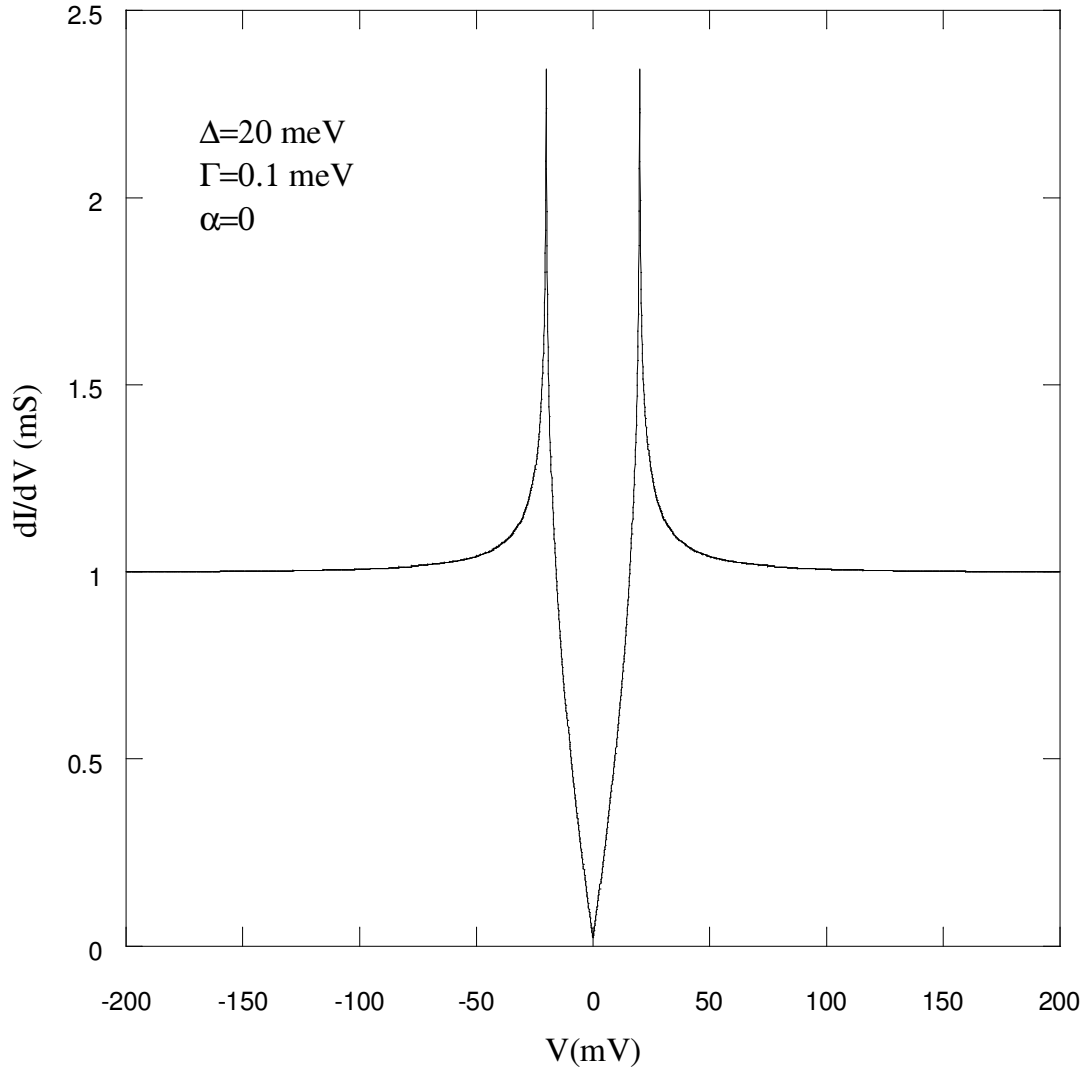

Figure 2.5. SIN conductance obtained by Fortran program

2.2. Phase Diagram of Cuprates and Pseudogap

High T_c superconductors are layered metal oxides and superconducting properties originates from dopable CuO_2 planes. Superconductivity can exemplify the strongly correlated systems; the doping-temperature phase diagram of the HTSC gives insight into these systems in the phenomenological sense. The extremes of this diagram are still in controversy, the underdoped insulator appears to be an antiferromagnet and the heavily overdoped superconductor appears to be a quasi-two dimensional metallic BCS superconductor (Misra 2004). Figure 2.6 illustrates the doping dependence on temperature in HTSC. The two regions of the diagram, antiferromagnetic insulating state (AF)-below 320 K and with hole doping $p \leq 0.02$ and the superconducting state (SC)-below 100 K and p is between 0.06 and 0.26 are well-established.

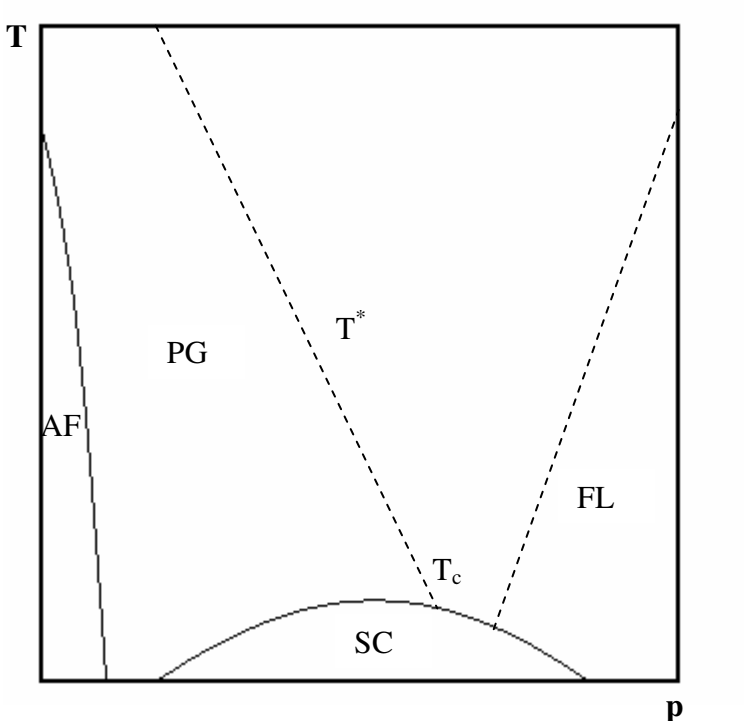

Figure 2.6. Characteristic phase diagram for HTSC

Superconducting region in the phase diagram can be divided into 3 different parts-underdoped region where the T_c decreases as doping becomes lower, optimally doped region where T_c value is highest for related material, overdoped region where T_c decreases with further doping while the material becomes more metallic. The doping

dependence of all the HTSC is generally same and convenient with the phase diagram above. The highest T_c is at the optimal hole concentration near 0.16 per CuO_2 unit for cuprates, which can be defined as;

$$\frac{T_c}{T_c^{\max}} = 1 - 82.6(p - 0.16)^2 \qquad (2.11)$$

However some parts of the diagram are not precise, e.g. enigmatic pseudogap regime (PG) occur below optimal doping (p= 0.16) but can not be defined exactly. Typically charge carriers in the form of holes are inserted by oxygen doping (e.g. in $Bi_2Sr_2CaCu_2O_{8+x}$), by substituting a monovalent atom with a divalent atom (e.g. replacing La with Sr in $La_{2-x}Sr_xCuO_2$), or by removal of oxygen from their stoichiometric positions (e.g. in $YBa_2Cu_3O_{7-x}$). In any case, the carrier concentration is a considerable parameter upon which the properties of the material depend strongly. The mechanism of the ground state in the conventional superconductors is based on long-range order of condensed Cooper pairs. However, HTSC show much more complicated phase behavior indicating the presence of other competing ground states within the spectra. For instance, pseudogap which is a suppression of accessible electronic states at the Fermi level in the normal state of high T_c superconductors can be given as an example to create such kind of intricate structure (Alff et al. 2003).

According to the recent studies there are two kinds of pseudogap in the electronic excitation spectra: low temperature and high temperature pseudogaps. Tunneling measurements in Bi-2212 revealed that the energy scale of the low temperature pseudogap whose characteristic temperature is denoted by T^* has strong correlation with magnitude of the superconducting gap measured at low temperatures (Miyakawa et al. 2001a). In other words, the superconducting gap below T_c smoothly evolves into the pseudogap just above T_c, where pseudogap has nearly the same energy scale as the superconducting gap.

Another kind of the pseudogap, called high energy pseudogap whose transition temperature is characterized by T^m, has the energy scale much higher than that of superconducting gap. It is commonly believed that high energy pseudogap is associated with the hump structures existing in the tunneling conductance characteristics (Miyakawa et al. 2001a).

CHAPTER 3

EXPERIMENTAL

This chapter concerns with experimental facilities used while preparing this thesis. The mechanism and inherent features of investigated cuprate, $Bi_2Sr_2CaCu_2O_{8+\delta}$ (Bi-2212), are presented in the first part. The second part of this chapter is associated with micron-sized mesa fabrication on Bi-2212 single crystals and in the following part, the novel method, point contact tunneling technique to get the I-V and tunneling conductance characteristics is explained in details.

3.1. Material

The experiments were performed on both optimally doped pristine and $HgBr_2$ intercalated Bi-2212 single crystals. Optimally doped crystals with the critical temperature around 93 K were grown using self flux technique by Chris Kendziora at Naval Research Laboratory, US (Kendziora et al. 1996). In order to provide phase stabililization to these samples, a small amount of yttrium was substituted. For this thesis, apart from the optimally doped specimens (T_c=93 K), additional $HgBr_2$ intercalated Bi-2212 compounds were measured (T_c=74 K). $HgBr_2$ intercalated Bi-2212 single crystals were prepared by D.G. Hinks at Argonne National Laboratory using a different technique to grow pristine crystals, floating zone technique.

The complicated HTSC series, $(BiO)_2Si_2Ca_{n-1}Cu_nO_{2+2n}$, contains perovskite-type layers and $(BiO)_2$ layers of bismuth in the unit cell. Number of the perovskite units or equivalently the number of the consecutive copper oxide layers in the unit cell can be denoted by “n”. If n is equal to one, there is no calcium in the unit cell which results in formation of $Bi_2Sr_2CuO_6$ (Bi-2201) structure with T_c ranging from 8 K up to as high as 22 K. When the value of n is 2, then we can obtain $Bi_2Sr_2CaCu_2O_{8+\delta}$ (Bi-2212) phase. Besides, there is another configuration for n=3, $Bi_2Sr_2Ca_2Cu_3O_{10}$ (Bi-2223) whose transition temperature is around 110 K. All of them have layered atomic arrangement with planes of weak bonding, the $(BiO)_2$ (Romano et al. 1998).Among the cuprates, or more specifically within the BSCCO family, the Bi-2212 is the most examined material

and many researchers have focused on it since years. The optimally doped sample of Bi-2212 has approximately a onset critical temperature of 95 K which is the maximum value of T_c for this compound and its transition temperature can be reduced either by additional oxygen content (overdoping) or by the removal of oxygen with vacuum annealing (underdoping). Therefore, by means of doping phase diagram of this cuprate, its physical properties can be investigated (Ozyuzer et al. 2000). The most important advantage of this material is that it can be grown in the way of single crystal without any macroscopic defects or dislocations. Besides it can be cleaved easily in a simple manner; thus flat and convenient regions are able to be created for surface sensitive measurements such as STM, Raman spectroscopy or ARPES. However, in this case, cleaving exposes the Bi-O layer which sits 4.5 A^0 above the pair of CuO_2 planes in the unit cell of Bi-2212. This layer contains the excess oxygens used to dope Bi-2212 and therefore the Bi-O plane has been reckoned as a doping plane, with the Sr-O and Ca planes acting as spacer layers (Misra 2004).

The Ginzburg-Landau parameter,κ, is larger than 100 for the Bi-2212 compound; which means that it exhibits strong type II superconducting behavior. Associated with this parameter, it has an extremely short coherence length $\xi_{ab}(0)$= 20-40 A^0 and $\xi_c(0) \cong$ 0.1-0.3 A^0 at low temperatures and relatively large penetration depth λ_{ab}=2000 A^0 (Ting Wei-Li 1995).

Like all HTSC, the structure of Bi-2212 is formed by stacked series arrays of intrinsic Josephson tunnel junctions along the direction of crystal c-axis. The nature of the Bi-2212 single crystal is based on a set of different layers; which are Cu-O, Bi-O, Sr-O in the unit cell of the material. This layered structure makes the crystal fairly intricate and show excessively anisotropic properties. There are two models developed to be able to explain the mechanism of this material: multilayer model and proximity model (Yurgens et al. 1996a) which are represented in Figure 3.1.

According to the multilayer model; Bi-2212 single crystals act as stacks of Josephson coupled Cu-O double layers with the thickness of 3 A^0 separated by non-superconducting Sr-O and Bi-O layers of thickness 12 A^0. This configuration forms natural Josephson tunnel junctions array going on like SISIS... inside the single crystal and enables to observe both dc and ac Josephson effects. Superconducting properties of the multilayered high Tc superconductors stem mainly from the double CuO_2 layers in which coupling occurs, while the role of the other layers can not be defined exactly; it is

commonly believed that Sr-O and Bi-O intermediate planes behave as passive spacers or charge reservoirs. As stated above, the superconducting coherence length for Bi-2212 in the out of plane direction is approximately 0.1 A^0, which is relatively small if compared with the distance between two adjacent CuO_2 layers in the Bi-2212 unit cell. This point makes Josephson tunneling of Cooper pairs hard across the insulating layer (Yurgens et al.1996a).

Another adopted model is proximity model; which suggests that not only CuO_2 layers but also Bi-O planes make contribution to superconductivity of the HTSC. Some experiments show that Bi-O layers exhibit metal-like or even superconducting features rather than insulating character.

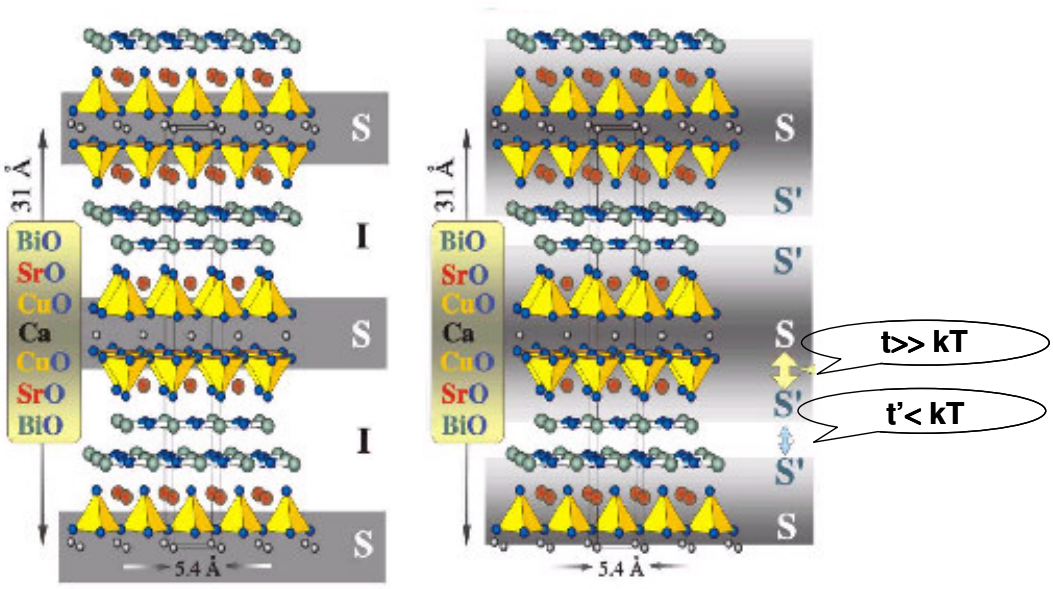

Figure 3.1. The crystal structure of Bi-2212. The left image corresponds to basic multilayer model, while the right image defines the proximity model.

According to the proximity effect, there is a strong coupling between the Cu-O and Bi-O layers (S-S') with weak Josephson coupling between neighboring Bi-O layers (S'-S'). Some researchers claim that the reduced energy gap value of Bi-2212 is the consequence of the proximity induced superconductivity of the Bi-O layers (Yurgens et al. 1996a).

The current-voltage characteristics obtained by means of a current sweeping back and forth from zero to a some maximum values show large hysteresis and multiple branches corresponding to IJJ inside the crystal. Each quasi-particle branch which belongs to a different IJJ has a well-developed gap structure.

3.2. Mesa Structures

3.2.1. General Features

In order to observe the intrinsic Josephson effects inside the single crystal of Bi-2212, it is sufficient to apply the current in the direction of crystal c-axis and monitor the voltage (Kleiner et al. 1992). Also, to see these effects, one should take into account to work with very small sized tunnel junction areas to be able to reach the critical current without overheating problem in the mesas (Yurgens 2000).

The thickness of the Bi-2212 single crystals is generally several micrometers; including around several thousand IJJ in series; thus it is pretty hard to investigate tunneling characteristics of an individual junction. To surmount this obstacle, and also decrease the heating, the arrays of the mesa structures can be fabricated on the surfaces of the Bi-2212 single crystals using photolithography and Ar ion beam etching techniques (Kurter and Ozyuzer 2005). Bi-2212 single crystal is a disadvantageous material because of its poor thermal and electrical conductivities; the Joule heating at high bias current values becomes inevitable. Overheating and nonequilibrium effects are the most encountered problems whilst obtaining I-V data, up to now various research groups have investigated this subject (Tanabe et al. 1996, Yurgens et al. 2004). One of the ways to eliminate heating problem is to use a short pulse of current and this has recently exhibited dip and hump features as seen by STM/STS and PCT (Anagawa et al. 2003). It is shown that these features are closely related to the fundamental pairing mechanism of HTSC (Zasadzinski et al. 2001). Another alternative method is to intercalate the Bi-2212 single crystals with inert guest molecules such as $HgBr_2$, HgI_2, or I_2 molecules to reduce the coupling between CuO_2 layers. The IJJ prepared from $HgBr_2$ intercalated Bi-2212 single crystals also showed dip and hump features; which is an indication of less heating (Yurgens et al. 1999). The intercalation of $HgBr_2$ is done by heating the vacuum sealed tube containing pristine Bi-2212 single crystals and $HgBr_2$ molecules at approximately 230 ^{0}C for 16 hours. After the intercalation process, it can be realized that the lattice expansion is around 12.6 A^0 by using X-ray analysis (Yurgens et al. 1999). From the Figure 3.2, this expansion can be seen.

Introduction of inert $HgBr_2$ molecules into the adjacent Bi-O layers results in considerable stretching in the Bi-2212 unit cell in the c-axis direction. The intercalation

causes to decrease in the c axis critical current by lengthening the tunneling barrier and increase in the normal state resistance; thus Joule heating can be substantially overcome.

Moreover, reducing the mesa size can be counted among the methods of suppressing the heating problem. Using photolithography and Argon ion beam etching facilities, we made areas as small as 10x10 μm^2 and heights down to 65 nm corresponding to about 12 IJJ in the fabricated Bi-2212 mesa structure.

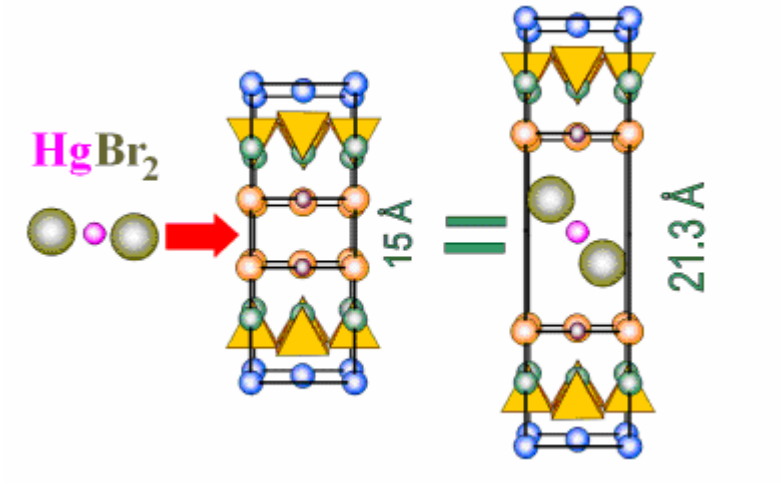

Figure 3.2. Schematic representation of the $HgBr_2$ intercalation

Applying the current in the direction of c-axis effectively is so important in terms of dependability and validity of the measurements. Annealing the mesas at high temperatures (higher than 450 ^{0}C) can assist to make good contacts; which leads to the diffusion of the gold deposition into the out of plane by reducing the contact resistance and allowing the current to pass easily.

3.2.2. Mesa Fabrication Process

In order to understand the mechanism of superconductivity in HTSC and to investigate fundamental features such as energy gap or density of states near the Fermi level, the arrays of small sized mesas were fabricated using some special techniques such as photolithography or argon ion beam etching.

The methods and technologies for mesa preparation can show subtle differences, but the general features remain the same. For mesa fabrication, a single crystal of Bi-

2212 having a smooth surface was first glued onto an alumina substrate by an epoxy. In order to get fresh and flat regions, the crystal was then cleaved with an aid of adhesive tape and was immediately placed in vacuum chamber of the evaporator. A thin film of gold was deposited onto the cleaved crystal to protect the surface from chemicals such as photoresist, developer and water during the photolithography and also to get electrical contacts for characterization. Photolithography was then applied to replicate different sized mask patterns, such as squares with the edge dimensions of 10 μm and 20 μm. For this purpose we used, Shipley Microposit 1813 positive photoresist to get the exact image on the photomask. Both positive and negative photoresists are complicated photosensitive organic materials, usually including a resin, photosentizer and a special solvent.

The mask having clear and opaque features defines the pattern to be created in the photoresist. The last main step, Ar ion beam etching was used to etch down the regions on the surface unprotected by photoresist and obtains proper mesa structures consisting of many IJJ and gold film. The samples were placed into the chamber with an angle of 45^0 with the direction of Ar ion beam and etched by Ar ions with various parameters, e.g. one of the optimally doped samples was etched by ions with the energy of 700 eV at 22 W for 15 minutes. Even after ion beam milling, some remaining of photoresist is still available on mesa, i.e. a skin like coating may stay on top of the gold film. Such cases can require oxygen plasma etching process. The basic configuration of the Ar ion beam system is shown in Figure 3.3 (a) and the photograph in Figure 3.3 (b) exhibits the system in our laboratory.

Many well-constructed mesa structures can be observed over the 300x300 μm^2 area. The steps of the mesa fabrication process are given in Figure 3.4. We designed various masks including squares with varied surface areas to be able to produce different images. The chromium coated glass photomasks were created by using special software named L-Edit and made by TUBITAK UEKAE utilizing advanced lithographic techniques. There are 9 different sized masks on a large glass; each mask is created by square array generating mesa structures and holders attached to the array of squares.

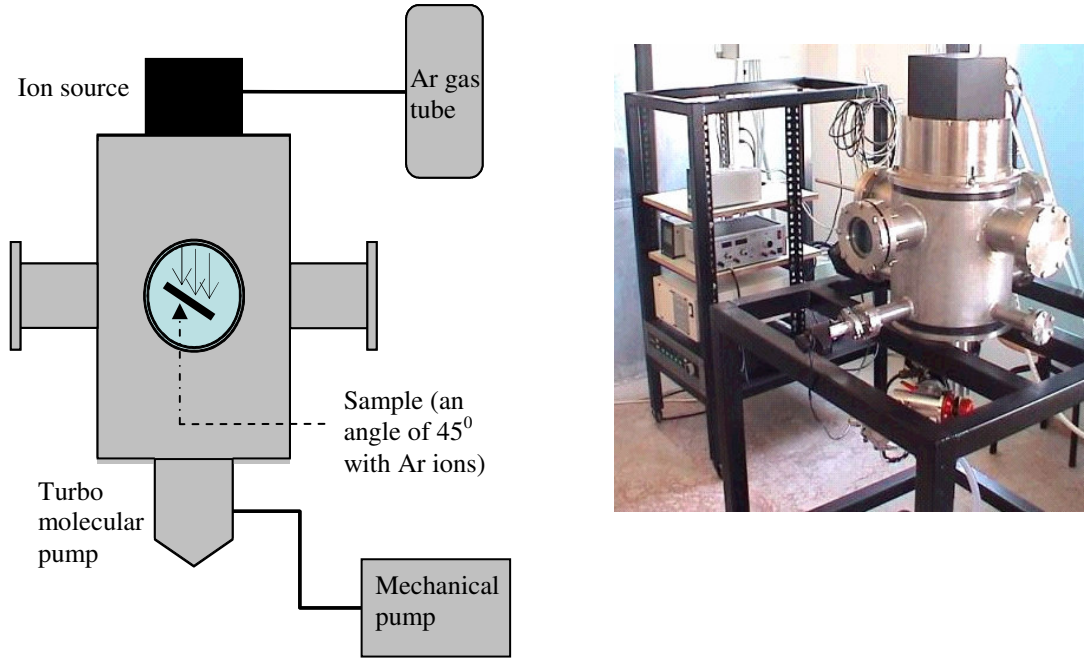

Figure 3.3. (a) Schematic representation of Ar-ion beam system (b) the photograph of the same system in our laboratory.

Each mask is designed as shown in Figure 3.5 and the photograph of the large glass containing all the masks is exhibited in Figure 3.6. The mask holders are also black squares with the edge of 3 mm while the area in the middle of the holders consisting of square array which will create the mesas is 0.5x0.5 mm^2.

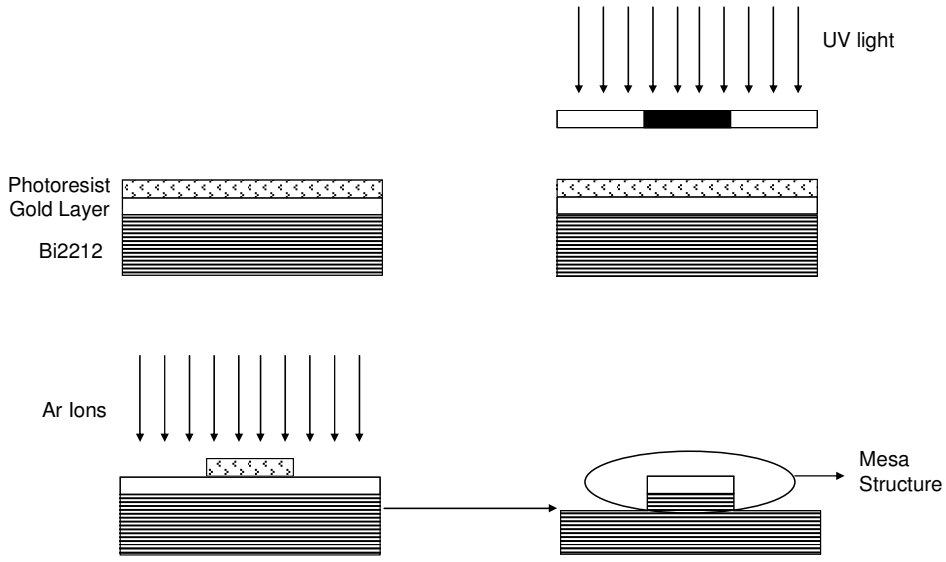

Figure 3.4. Fabrication processes of Bi-2212 mesa structures. In the figure alumina substrate attached to the Bi-2212 single crystal is not showed for facility.

The sizes of the images on the masks are just as following;

1) Squares with the area of 20x20 μm^2, distance between them 10 µm
2) Squares with the area of 10x10 μm^2, distance between them 10 µm
3) Squares with the area of 10x10 μm^2, distance between them 5 µm
4) Squares with the area of 10x10 μm^2, distance between them 4 µm
5) Squares with the area of 5x5 μm^2, distance between them 5 µm
6) Squares with the area of 5x5 μm^2, distance between them 4 µm
7) Squares with the area of 4x4 μm^2, distance between them 4 µm
8) Four point contact with the distance of 800 µm
9) Four point contact with the distance of 1000 µm

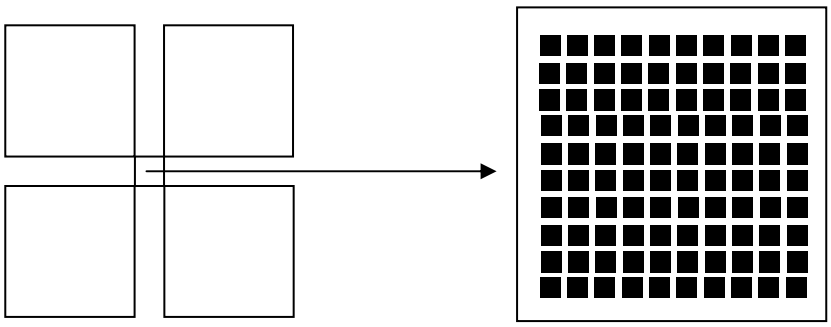

Figure 3.5. Holders and the area consisting of square array

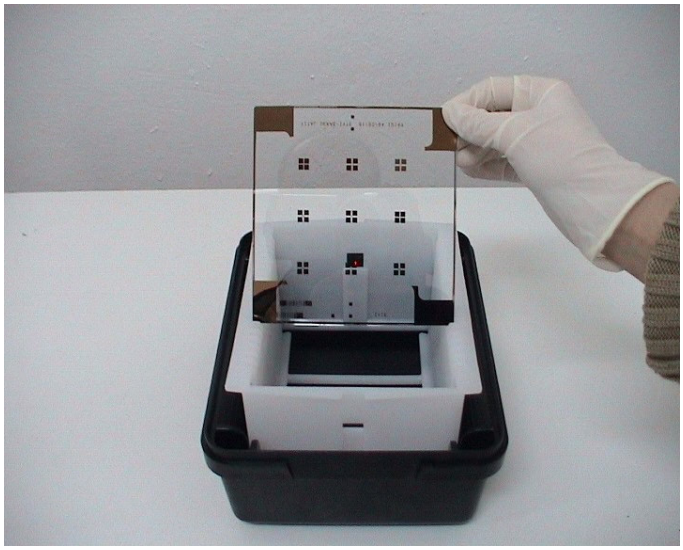

Figure 3.6. The glass containing 9 different masks

3.3. Experimental Method

3.3.1. Point Contact Tunneling (PCT) Measurements

The discovery of the HTSC has led to a significant effort to make Josephson junctions for not only research and investigations but also practical applications. In this part of thesis, Point Contact Tunneling (PCT) apparatus and inherit properties of this system are going to be given in details. This method is the simplest and one of the most suitable techniques to get information about the basics of superconducting phase such as energy gap, quasiparticle density of states, pairing symmetry and electron-phonon interaction.

Several experimental constructions have been developed for spectroscopic tunneling studies examining current-voltage characteristics or conductance curves. For this purpose, in the field of conventional superconductors, planar tunnel junctions which are the best understood Josephson devices were widely used. Although early studies on PCT were based on conventional superconductors such as Nb (Huang et al. 1990), it has been often employed in the field of high T_c superconductors later (Chen et al. 1994).

With s-wave superconductors, it is relatively easy to fabricate stable SIN and SIS planar type junctions and the tunneling spectra obtained from these have provided a direct measure of the temperature dependent energy gap $\Delta(T)$, and an explanation for electron-phonon interaction of strong coupled BCS theory (Wolf 1985). No satisfactory planar tunneling junction technology has still developed in HTSC field with the same degree of quality as evolved in conventional superconductors. Consequently, it is preferred to obtain the quasiparticle density of states by using PCT design forming a mechanical junction if the experiments are based on HTSC. Because all HTSC contain relatively thick insulating layers inside their structures, PCT tip can be used to mechanically scrape, clean or even cleave the specimen surface (Huang et al. 1990). Apart from these experiments, some researchers made some measurements for the superconducting energy gap in organic superconductors using PCT apparatus (Hawley et al. 1986).

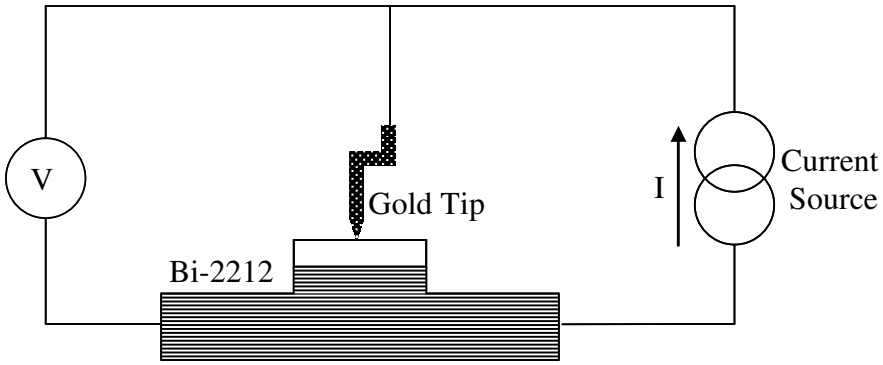

Figure 3.7. The schematic representation of PCT

The basic construction for PCT measurements on Bi-2212 single crystals is shown in Figure 3.7. There is one point to be taken into account while carrying out the PCT studies on Bi-2212. Probe (tip)-contact pressure on the sample surface creates extraordinary spectrum characteristics because of the surface deterioration. Since there is weak bonding strength between the double Bi-O layers in the unit cell of Bi-2212, freshly cleaved surface may be harmed easily. Existence of some additional features in zero bias conductances and superconducting gaps is reasoned with the surface cracks and layer detachments caused by PCT tip by some research groups (Murakami et al. 2000). Such kind of problem is possible in other surface sensitive probes but the experiments performed with IJJ are not affected in a large scale. The naturally formed and properly repeated IJJ inside the crystal provide a high degree of homogeneity and reproducibility. So, it can be said that surface deformation does not spoil the dependability of measurements in IJJ.

3.3.2. Setup for PCT

The mechanism of PCT is completely based on that of vacuum tunneling devices such as STM. The entire experimental setup consists of a electromagnetically and acoustically screened 6’ x 10’ x 10’ room, a vibration, isolation and damping system to obtain an acceptable signal to noise ratio, a cryostat, a point contact junction assembly and measurement circuits.

The quality of the data obtained from PCT is enhanced by acoustic, electric and magnetic shielding and by suppressing thermal fluctuations. The whole apparatus

should be placed in a quiet corner of the laboratory basement to reduce the noise effects on measurements. The helium dewar holding the apparatus is kept above the floor by four air suspension legs (NRC pneumatic isolation mounts type XL-A) to decouple it from low frequency ground vibrations. Besides, the cryostat walls are vacuum pumped before cooling it in order to manage thermal isolation. There are stacked bricks with the weight of approximately 500 kg around the perimeter of the upper plate of the platform to diminish the resonant frequency and to damp any oscillations of the air table. The dewar sits inside a sand-filled plastic drum on the lower plate of the platform. Fine silica sand isolates the sample region from acoustical noise. There is another silica sand box to get rid of vibration which comes from outside via cables and rubber vacuum hose. These systems make junction stable while getting data.

The tunneling junction assembly locating in a continuous flow cryostat is represented in Figure 3.8. This system enables to make measurements over a wide temperature range (1.5-300 K) and very high magnetic fields up to 6 T. To produce large magnetic field is so important to be able to obtain superconducting density of states at 0 K. In this situation, the ratio of the tunneling conductance of superconducting state (σ_s) to that of normal state (σ_n) gives superconducting DOS value. Although σ_s can be detected easily if the temperature is well below critical temperature, to measure σ_n is challenged because of the deterioration of junctions at high temperatures at which crystals are in the normal phase. Thus the most suitable way to quench the superconducting phase and to obtain the σ_n is to apply the sample a magnetic field whose value is above the upper critical field of the specimen. The most adverse effect of doing measurement at the temperatures larger than T_c is that quasiparticle peak positions can be affected by thermal smearing or other broadening mechanism.

The helium dewar is an aluminum superinsulated vessel (International Cryogenics Inc.) without liquid nitrogen jacket. The dewar is precooled by liquid nitrogen and then filled with liquid helium by blowing the liquid nitrogen out.

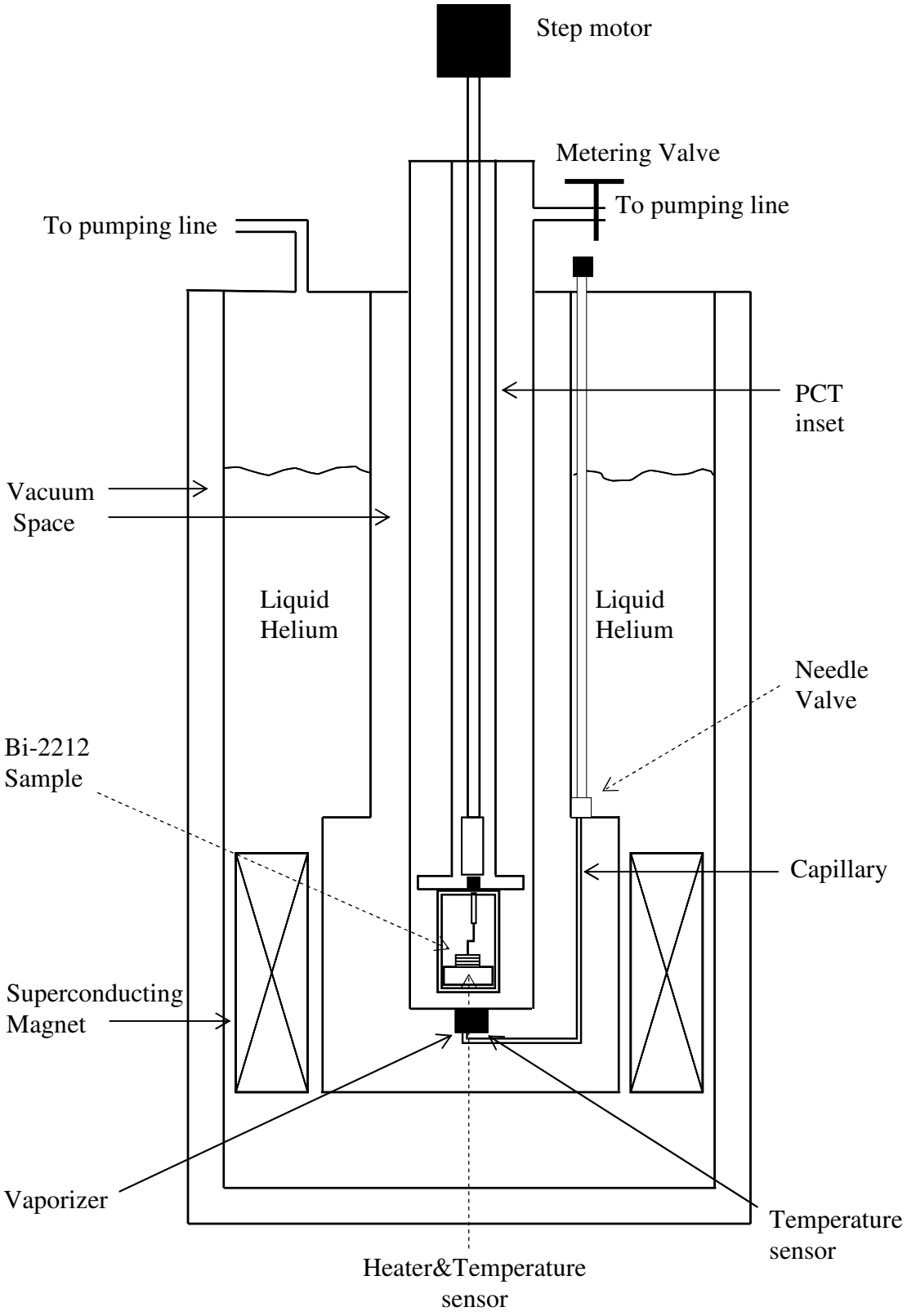

Figure 3.8. PCT apparatus

In continuous flow cryostats, cryogens (liquid helium or liquid nitrogen) flow from the main reservoir through a capillary tube to the can where sample is located. Flow rate of the cryogen can be changed to control the sample temperature. This can be in three different ways outlined as following:

1) Varying the flow rate of the cryogen through a needle valve
2) Utilizing the heat exchanger at the bottom of the sample
3) Pumping on the sample region to produce evaporative cooling

In the experiments, we used Al_2O_3 (alumina) substrates and Bi-2212 single crystals were placed on them owing to the epoxy. Alumina substrate provides good electronic insulation between Bi-2212 and platform whilst serving perfect thermal contact. To make electrical connections properly to a sample, silver filled conductive paint is used. After creating contacts, the assembly is mounted into the can and placed in cryostat. The resistance of formed point contact tunnel junction is on the order of kiloohms.

The rough approach of the sample to the tip along the direction perpendicular to the specimen surface is made by the plate on which sample is mounted. The coarse adjustment of the sample in the x-y plane is provided by a commercial micropositioner (Charles Supper Co.) attached to the copper block just below the sample. The tip-sample distance in the z-direction can be regulated sensitively by using differential micrometer which has a total travel of 0.4 mm and a z-displacement 11.5 nm per degree of revolution. A stainless steel tube holds the micrometer; inside this tube there is another stainless steel tube which exploits the micrometer for fine adjustment. There is a decoupling between a micrometer and this tube to prevent possible vibrations coming from the flange. This tube is run by a small electric motor placed out of the flange on top of the insert. There are three tiny windows on the sample cage to make adjustment of sample and protect the tip from the direct cooling of the gas coming from the vaporizer.

There is a temperature sensor near the vaporizer through the copper block on the micropositioner; which is used for monitoring the temperature and providing a feedback loop to arrange the temperature at a set value. Another temperature sensor (Cernox Sensor) is on the copper block attached to the micropositioner and also a heater is placed between the sample and copper block.

Because there are strong superconducting magnets at the bottom part of the PCT insert including sample and tip assembly, it is necessary that the material used in the structure is nonmagnetic over a substantial portion of the 6 T range. Hence differential micrometer connected to the tip and sample cage was made of titanium, which has a lower magnetic permeability than stainless steel. Besides, titanium has a lower thermal expansion coefficient than stainless steel, which is so advantageous in terms of reducing the effects of thermal expansion between sample and tip.

The tip of the insert assembly can be made from different materials like Nb, W, In, etc. depending on the research. In this study, we used gold tip because of its superior properties such as low oxidation rate, malleability, and good thermal and electrical conductivity. The gold tip is formed by knife and polished with various grades of diamond paper (the final one containing 3 μm diameter grit) and then tip is etched in aqua regia.

As mentioned above, the temperature of the sample can be changed with several ways. Adjusting the gas-flow needle is not a good choice for coarse temperature variation after a particular junction is created, because in this manner, the valve is subjected the direct contact with the cryostat. Using metering valve is recommended, since it is mechanically isolated from the cryostat with a rubber hose and a sand box. The vaporizer and sample heater are connected to Lakeshore 91C temperature controllers to fine regulation of the temperature with an accuracy of 0.01 K ranging from 1.5 K to 300 K. Two superconducting magnets being able to create 6T magnetic field can be regulated with the sensitivity of 1 mT.

The parts of the electronics which belong to system are placed in a rack. Current source of the PCT is a sweep circuit and two preamplifiers simultaneously measure current and voltage values reducing the interference which comes from the sweep generator or from x-y recorder or data acquisition system by means of its high input impedance. While the tip is pushed against the crystal, the $I(V)$ signal is continuously monitored using an oscilloscope until an acceptable junction is obtained. The extraordinally small area of the PCT junction with the contact diameter 0.24 μm and the easy motion from one point to another point increases the probability of finding a tunnel junction without any barrier defects. The data are obtained by the aid of data acquisition card (DAC) for fast response inside the hardware of the computer which shows the data

collected. The entire experiment is controlled by a computer program written in Lab View. The schematic representation of the parts of the system is given in Figure 3.9.

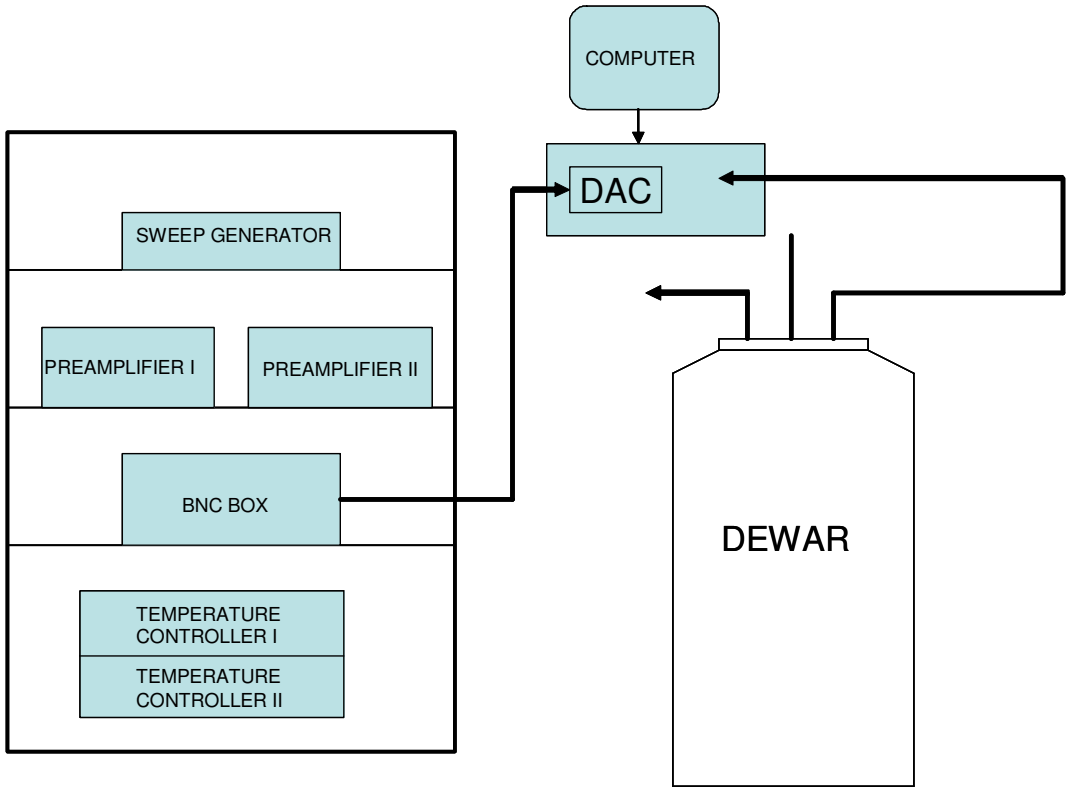

Figure 3.9. The parts of the PCT system

The design of the PCT system is a versatile development for tunneling into HTSC. The temperature dependence of the dynamical conductances obtained from tunneling measurements by PCT can give significant information about the energy gap and critical temperature of material measured in a particular region. Also these curves indicate the existence of pseudogap exhibiting flat features in tunneling conductances at elevated temperatures.

CHAPTER 4

RESULTS AND DISCUSSION

This chapter includes characterization consequences which belong to both single tunneling junctions (SIS and SIN) and various mesa structures (stacked IJJ) prepared from different Bi-2212 single crystals; optimally doped samples with T_c= 93 K and $HgBr_2$ intercalated samples with the critical temperature of 74 K.

4.1. General Remarks

All HTSC can be considered naturally stacked arrays of IJJ keeping their periodicity along the crystal c-axis. The generic features of HTSC have developed a promising research issue. Bi-2212 is a remarkable member of the HTSC family from many experimental aspects. It has been studied many times in various studies so far, because of its superior properties over other high T_c superconductors. Bi-2212 single crystals can be easily grown with a high degree of quality, also after cleavage process, atomically smooth and shiny regions can be created to facilitate the patterning. Moreover, the doping level of this material can be altered without any difficulty by annealing in argon or oxygen media. This property makes it an excellent candidate while investigating its physical characteristics over a large range of the doping.

With this thesis, it is mostly aimed to report the results of a novel method, PCT technique, on different Bi-2212 single crystal samples. Using interlayer tunneling based on PCT method, the inherent features of IJJ in small-sized mesas can be investigated and also by means of this technique, SIN single junctions and SIS break junctions can be produced. The advantage of PCT over other surface sensitive experimental methods such as STM, ARPES, Raman spectroscopy and Auger techniques is that the gold tip can be used to scrape, clean or even cleave the surface. In many cases, the non superconducting gold tip penetrates into the surface and reaches the crystal body of Bi-2212. Because of the weak bonding in the structure, with this process, SIS break junctions can be formed easily within the crystal as it is going to be described later.

The tunneling conductances are fairly effective to identify SIS and SIN junctions. A typical tunneling spectrum of SIN junction generally shows weakly decreasing background, asymmetric quasiparticle peaks at the $\pm\Delta/e$ points (sample relative to tip), well-defined asymmetric dip-hump features (generally at $\pm 2\Delta/e$ and $\pm 3\Delta/e$ respectively) related to strong coupling effects at higher bias values and as low as 10%-15% zero bias conductances. Yet SIS junctions have symmetric quasiparticle peaks at the $\pm 2\Delta/e$ values, symmetric dip and hump features (generally at $\pm 3\Delta/e$ and $\pm 4\Delta/e$ respectively), less than 1% zero bias conductance and hysteretic Josephson current at zero bias when the junction conductance exceeds a minimum value,G_{min}, obtained from Ambegaokar-Baratoff theory. In the measurements on small area mesas have generally been focused on the Josephson currents which can be detected at low bias voltages and the individual switching of each junction from the Josephson branch to the quasiparticle branch could be observed (Ozyuzer et al. 2005). Most of the PCT measurements show asymmetric SIN spectra, e.g. the dip and hump structures can be seen just only on the left side of the plot. In negative bias part of the conductances indicating the electron removal from the superconductor is observed a well-defined dip feature at nearly $-2\Delta/e$ and also hump structure at higher voltage values (more or less $-3\Delta/e$). For positive bias there is no sharp dip feature but rather an abrupt change of slope and hump structure is not clear. This asymmetric construction is also available in STM results but more enhanced. The reason of this effect is believed to be associated with different tunneling matrix elements for vacuum and PCT junctions along the c-axis (Zasadzinski et al. 2000). The asymmetry in SIN conductance peaks is reported to be a signature of the d-wave pairing (Yusof et al. 1998). The characteristic features of all Bi-2212 junctions are the quasiparticle peaks indicating single particle tunneling at the gap voltages that are both larger and broader than expected (with respect to d-wave DOS) as well as reproducible dip and hump structures at higher voltages which are believed to be related with strong coupling effects (DeWilde et al. 1998, Pan et al. 2001, Zasadzinski et al. 2001). Nevertheless, the dynamical conductances of tunneling junctions are much more consistent with d-wave symmetry than s-wave symmetry (Ozyuzer et al. 2000). Although SIS and SIN tunneling spectra of overdoped Bi-2212 exhibit similar features to that of optimally doped Bi-2212, the magnitude of superconducting energy gap is reduced, e.g. Δ=15-20 meV, this value is reported for optimally doped crystals around 38 meV (Miyakawa et al. 2003). The strong coupling ratio, $2\Delta/k_BT$ which is 9.3 for

optimally doped Bi-2212 approaches the BCS mean field value 3.52 with overdoping (Miyakawa et al. 1999). This result is accordant with the idea that overdoped compounds show behavior of Fermi liquid rather than that of antiferromagnetic insulator. In general, the reverse results are obtained with decreasing doping, i.e. the superconducting energy magnitude becomes larger, if one deals with underdoped crystals.

All the tunneling measurements were performed with the apparatus as described Chapter 3.3.2 in a large scale of temperature ranging from 4.2 K to 300 K. In the setup, gold tip was used as a counter electrode and it was mechanically and chemically cleaned before each run. SIN single junctions and SIS break junctions can be formed by the aid of this gold tip. The rough adjustment of the distance and contact force between the gold tip and investigated sample is made by differential micrometer after the sample is mounted to setup and its temperature is decreased to 4.2 K. When the tip pushes onto the crystal surface, a stable mechanical junction occurs between the tip and the sample surface. As mentioned before, after the cleavage process, what remains on the surface of the crystal is just single Bi-O layer because of the relatively weak bonding between the neighboring Bi-O layers. So, the tunneling barrier needed to form an SIN junction is the native surface of the crystal, namely, the insulating layer includes this single Bi-O plane and underlying Sr-O layer. Whilst the tip is approached to the crystal, the I-V characteristics are continuously monitored on an oscilloscope until a convenient junction displaying a superconducting gap in the curve can be obtained.

Increasing the force of the gold tip against the crystal generates an ohmic contact (≅1 ohm) between the tip and the crystal, the reason of that is believed a perforation of the insulating layer. When the tip is retracted, commonly a small piece of the Bi-2212 is separated from the entire crystal and fastened to the tip owing to a mechanical bond. Again the Bi-O pairs break easily leading to form SIS junction within the crystal body. The removed piece probably remains in a cavity in the larger crystal; which causes that these SIS junctions are mechanically stable. It is reported that raising the tip to form an SIS junction is not necessary, but it is essential to relieve the pressure applied (Ozyuzer et al. 1999b). This break junction method provides a fresh junction created in-situ deep in the crystal. The schematic representation of the SIS break junction forming inside the Bi-2212 single crystal is given by Figure 4.1.

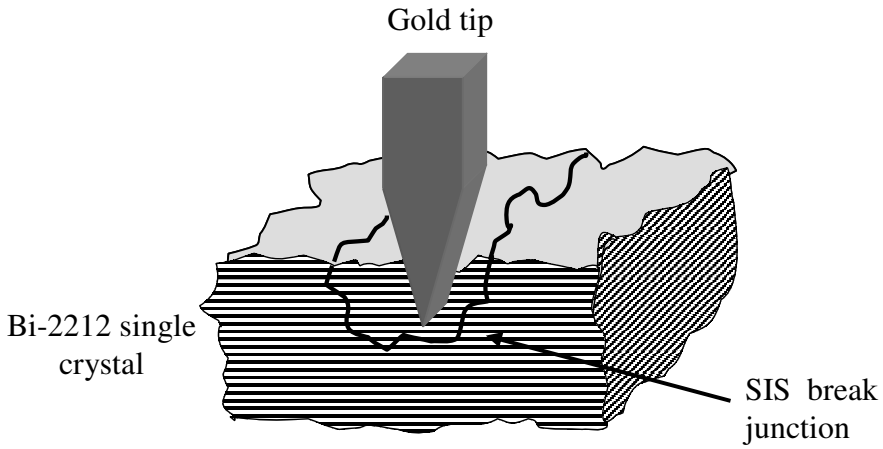

Figure 4.1. SIS break junction obtained by gold tip

In SIS break junction spectra, Josephson current can be seen as well as quasiparticle branches. The availability of supercurrent at zero bias depends on the junction resistance which can be tuned by changing the tip pressure.

4.2. Results of Optimally Doped Pristine Bi-2212 Single Crystals

The optimally doped single crystals of Bi-2212 with the transition temperature of approximately 93 K were grown by self flux technique as described elsewhere (Kendziora et al. 1996). There is a small amount of yttrium within the crystal to provide phase stabilization. The photolithography and Ar ion beam etching techniques were used to get micron sized mesa arrays; the detailed explanation of the processes can be found in Chapter 3 (Kurter and Ozyuzer 2004). Two different masks (square arrays with the areas 10x10 μm^2 and 20x20 μm^2) were exploited to fabricate different sized mesa structures from optimally doped crystals and measurements were carried out by experimental setup of PCT collecting data in a large range of temperatures. Apart from stacked IJJ arrays, single Josephson junctions were obtained by a break junction method with a blunt gold tip of PCT on the same batch of crystals, for comparison with IJJ. Because the mesa areas are so small, we could not use the other conventional techniques for the electrical characterization such as three or four point contact measurement, hence the contact was done by gold tip of the PCT setup. We could observe more than 1000 mesas over 300x300 μm^2 area.

4.2.1. SIS Break Junctions Obtained by PCT

SIS break junctions can be generated within the body of optimally doped crystals using aforementioned process in an unconventional manner. Figure 4.2 and Figure 4.3 show the single break junction I-V and dI/dV-V characteristics of optimally doped Bi-2212 samples (with T_c= 93 K) at 4.2 K respectively. The inset of Figure 4.2 displays Josephson current at zero bias. Also, from the inset showing expanded subgap region near zero bias, switching nature of Josephson junction can be understood. Because of in-situ creation, SIS break junctions are generally quite stable and demonstrate clear simultaneous Josephson and quasiparticle tunnel currents. The barrier interface is relatively clean and impurity free in SIS break junctions due to the formation without exposing to the air. The junctions were fabricated by a blunt Au tip which breaks the crystal to obtain SIS spectra. These characteristics are presented just before results of IJJ for comparison.

Because the SIS dynamical conductance is a convolution of two SIN tunneling density of states, we can obtain the energy gap, Δ using this characteristic. For SIS junction geometry, the peak to peak separation in the tunneling conductance characteristics corresponds to 4Δ. For this particular junction, an energy gap of 32 meV can be easily obtained from the Figure 4.3, because 2Δ value corresponds to nearly 63 mV in the voltage axis. This value is on the lower side for optimally doped Bi-2212 because of the inhomogeneity of the crystal structure due to the yttrium addition. Enhanced dip and hump structures as well as pronounced quasiparticle peaks can be observed; the locations of reproducible dip and hump structures are ±96 mV, ±128 mV respectively which correspond to exact $\pm 3\Delta$ and $\pm 4\Delta$ values in the spectrum.

Temperature evolution of the tunneling spectra obtained from an SIS break junction on the nearly optimally doped Bi-2212 crystal with T_c= 92 K can be seen from the Figure 4.4. Each curve is shifted 0.4 mS from each other and Josephson current peaks are deleted for clarity. These I-V curves also give well-defined energy gaps indicated by sharp quasiparticle peaks at $eV=2\Delta$ and dip/hump features at higher bias.

.

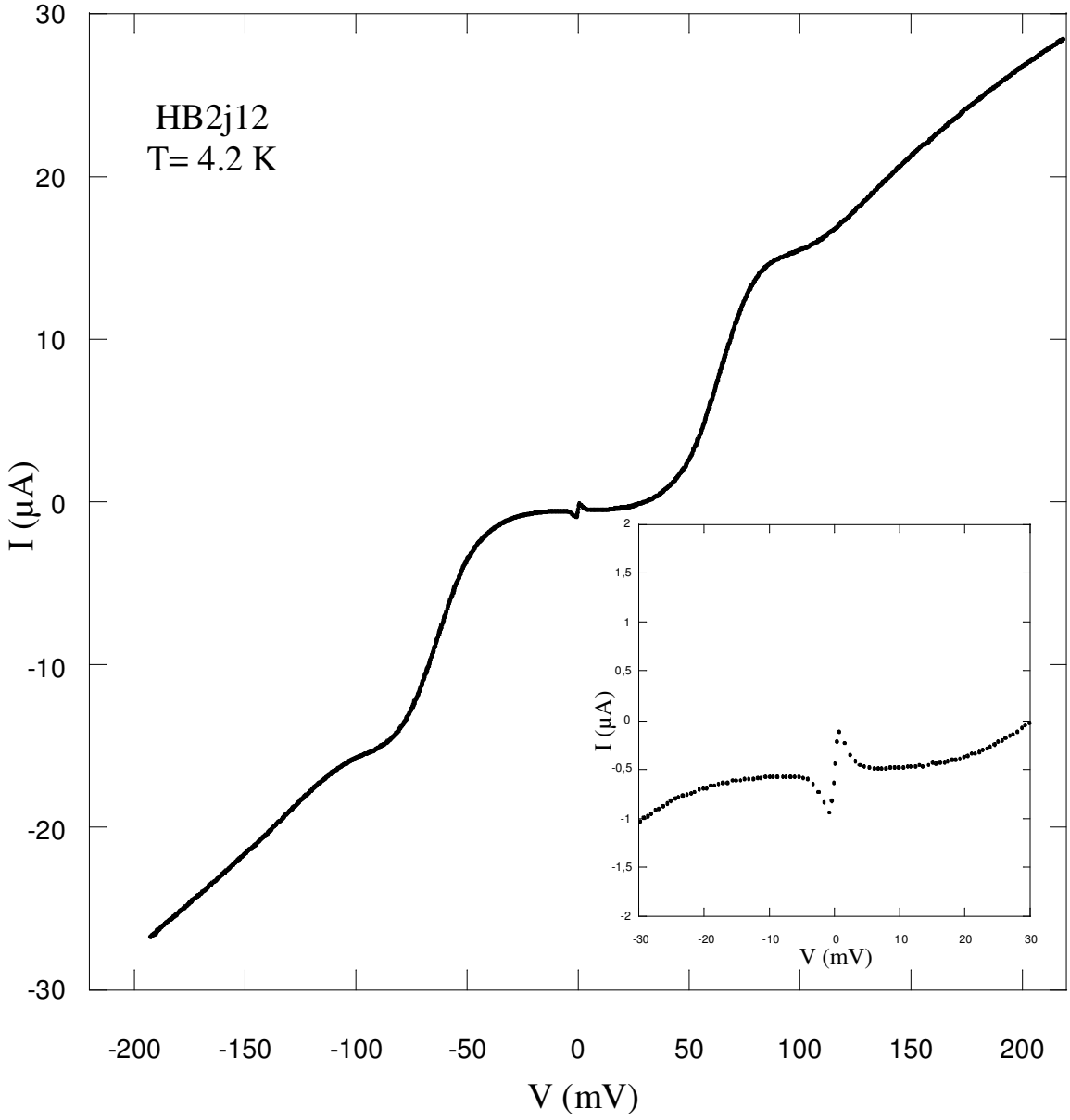

Figure 4.2. Current-voltage characteristic of in-situ formed SIS break junction obtained from optimally doped Bi-2212 single crystal (with T_c=93 K) at 4.2 K. The inset shows the Josephson supercurrent exhibited on a more sensitive scale.

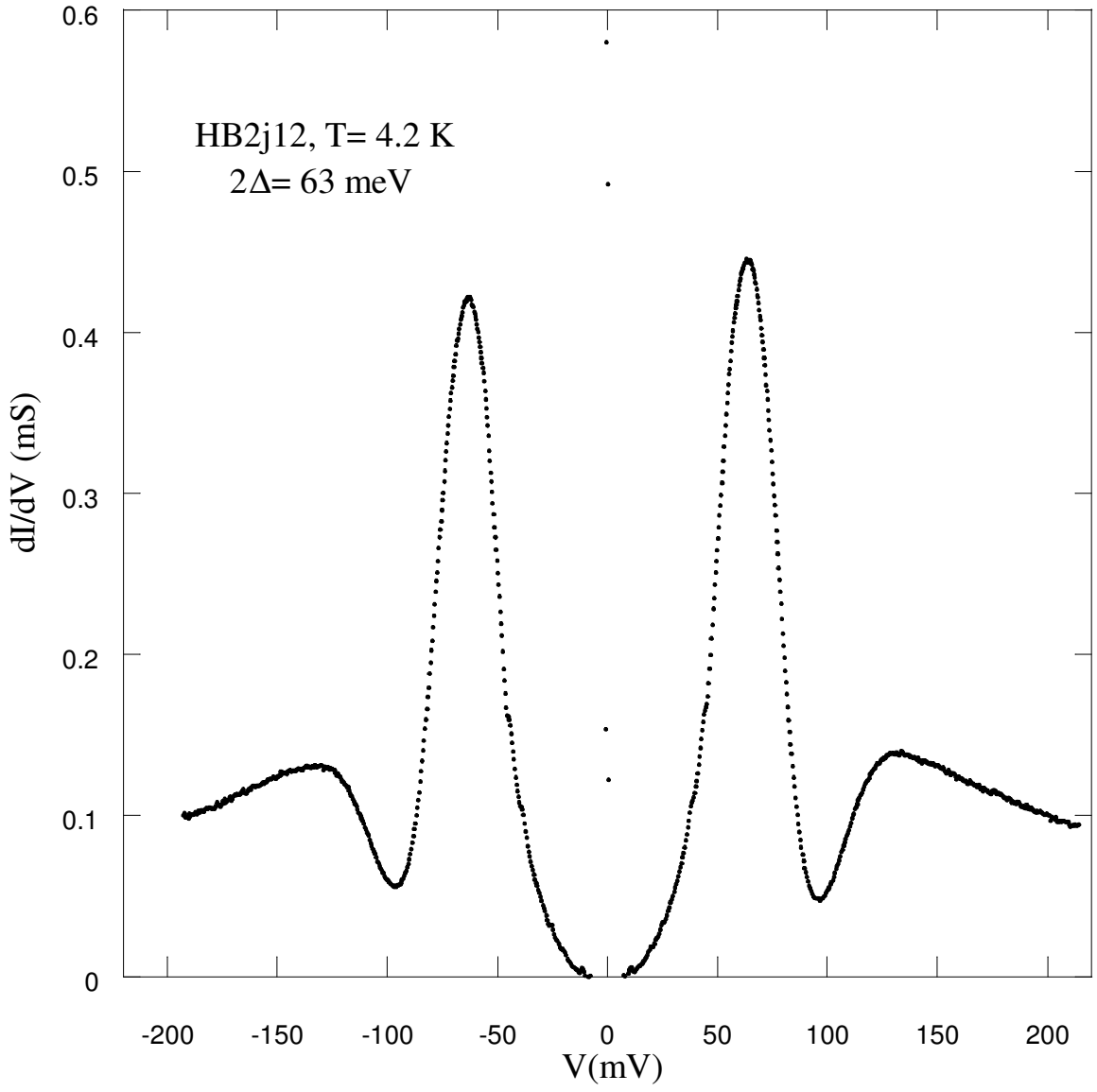

Figure 4.3. Tunneling conductance characteristic of an SIS break junction obtained from optimally doped Bi-2212 single crystal (with T_c= 93 K) at 4.2 K.

Because of the low zero bias conductance and sharp conductance peaks in Figure 4.4, energy gap value can be directly found, which is approximately 2Δ=67 meV. The data also show very strong dip features at ±97 mV and hump features at ±128 mV which correspond a little bit lower than 3Δ and 4Δ values. Tunneling conductance peaks smear when the temperature is raised from 4.2 K to 28 K, however position of the peaks

barely change; which is consistent with a nearly constant superconducting gap as claimed by conventional BCS theory. The details will be discussed later.

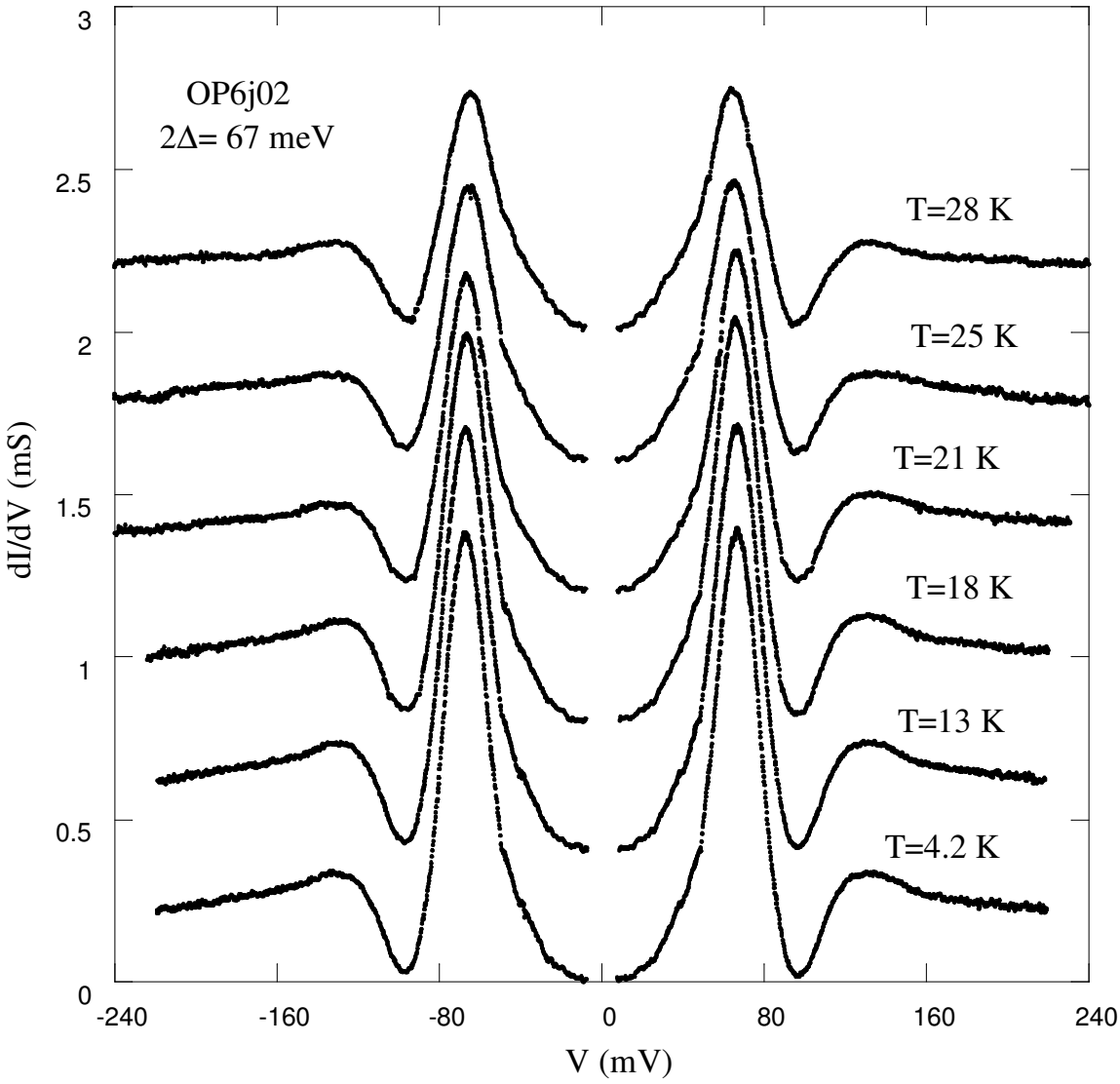

Figure 4.4. Temperature dependence of tunneling conductance characteristics for an SIS junction on nearly optimally doped Bi-2212 (with T_c=92 K).

4.2.2. IJJ within the Optimally Doped Crystals

Many optimally doped Bi-2212 samples with different sized mesas were used for IJJ investigation. These samples with T_c= 93 K were measured by interlayer tunneling exploiting the manner of PCT technique. Here we will present the results of just only two representative samples. In order to prevent the confusion, we named the

optimally doped samples as MC01 (with 20x20 μm^2 mesas, the distance between them is 10 μm) and MC03 (with 10x10 μm^2 mesas, the distance between them is 5 μm).

Figure 4.5 shows an optical micrograph of MC01 containing 20x20 μm^2 mesas on Bi-2212 single crystal; the separation between two squares is 10 μm in the photomask.

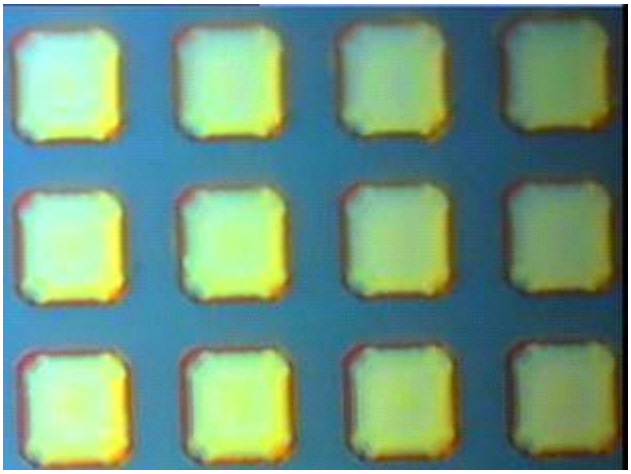

Figure 4.5. Array of squares with the area of 20x20 μm^2 on Bi-2212 single crystal

To examine the obtained structures with optical microscopy is very helpful in terms of having a rough idea about the surfaces of the mesas. This kind of characterization can give information about the quality of the photolithography performed, i.e. the degree of excellence of the images which are supposed to be transferred onto the single crystal surface. In other words, some problems originated from photolithography or etching such as poor contact between mask and crystal surface, undesired reflections because of glass mask, any contamination problem onto the mask surface, remaining of photoresist skin after etching, excess or insufficient milling can be easily understood from optical micrographs. So, this pre-characterization has a useful function at the beginning of investigation for the surfaces of the generated mesas. Figure 4.6 exhibits an optical photograph of MC03 optimally doped sample which is patterned with the 10x10 μm^2 mask (the distance between the squares in the mask is just 5μm). Note that this time the magnification of the microscope is lower.

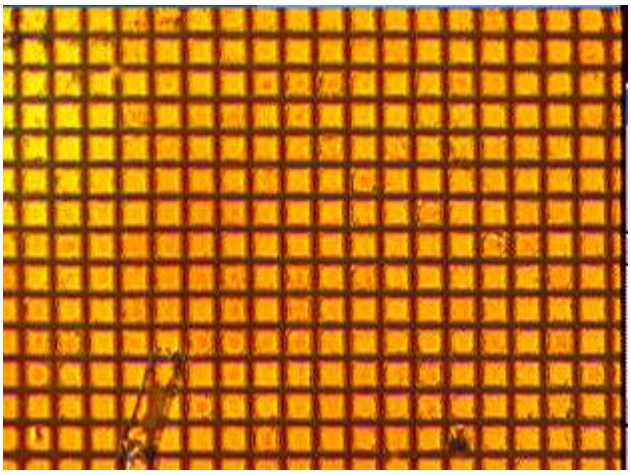

Figure 4.6. An optical image of mesa arrays with the area of 10x10 μm^2

The bright areas in the Figure 4.5 and Figure 4.6 are the deposited gold layers coating the mesa areas while dark regions are Bi-2212 surfaces being illuminated by the microscope light. As the photographs are looked at closely, it can be easily seen that the shapes of the mesas are not proper squares, although they are expected to be so. Alignment problem can be counted as a possible reason for this effect as mentioned before. Besides, the reflections of the UV light from the gold surface onto the mesa or chromium surface onto the glass mask can lead to such kind of change in the size of the images that are wished to be exact squares defined by photomasks.

Since the height of the Bi-2212 unit cell consisting of two Josephson junctions is certain, the number of the IJJ in each mesa can be obtained by measuring the thicknesses of gold film and entire mesa by atomic force microscopy (AFM). In order to reach IJJ number, firstly total height of the IJJ is found at the end of a basic calculation using AFM results and then obtained height value is divided by one SIS junction size in the unit cell which is around 15 A^0 for optimally doped Bi-2212.

The samples checked with optical microscopy coarsely can be investigated by AFM to examine the surface in exceedingly much more detailed way. Three dimensional surface topography of the gold film deposited onto both MC01 and MC03 optimally doped samples obtained by AFM is shown in Figure 4.7.

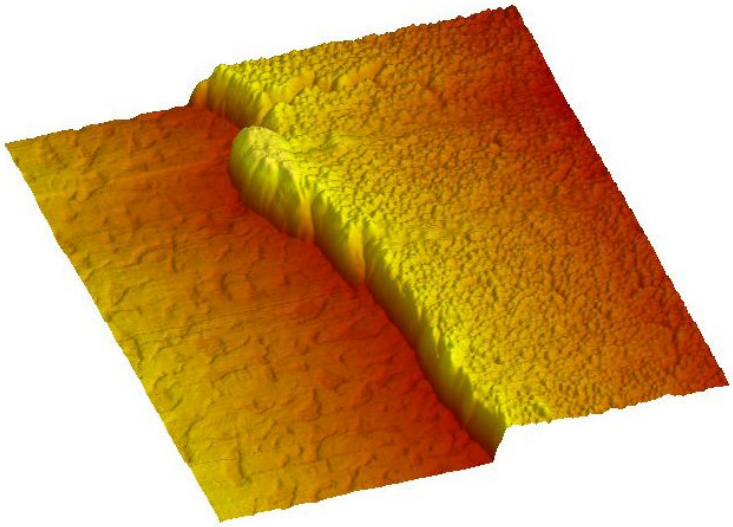

Figure 4.7. 3D surface topography of the gold film deposited onto the mesa surfaces

The measurements done with contact mode of the AFM can reveal the exact height of the gold film evaporated on the crystal surface as well as the mesa height. So, IJJ number in the concerned mesa can be calculated easily by utilizing these values as explained before. In order to determine the Au height, while we are doing evaporation to deposit the gold film onto the crystal surface, a piece of lamella is mounted to the sample holder in addition to Bi-2212 specimen. At the end of the evaporation, the gold film is expected to coat the glass surface with the same degree of quality and of course the same height as the crystal surface. If a very narrow line is created on the Au surface with an aid of extremely thin needle and AFM tip scans the related slit, the gold film thickness can be straightforwardly found. Figure 4.8 illustrates the step height analyses of the gold film from which the height of the gold can be told as nearly 55 nm.

The photographs and graphs shown in Figure 4.9 and Figure 4.10 are the section analyses of MC01 and MC03 optimally doped samples respectively. From the section analyses, it can be seen the total mesa heights. While analyzing the section graphs and determining the related heights, the noise coming from measurements or unsought photoresist skin are not important, what we should take into account are aligned levels in the graphs.

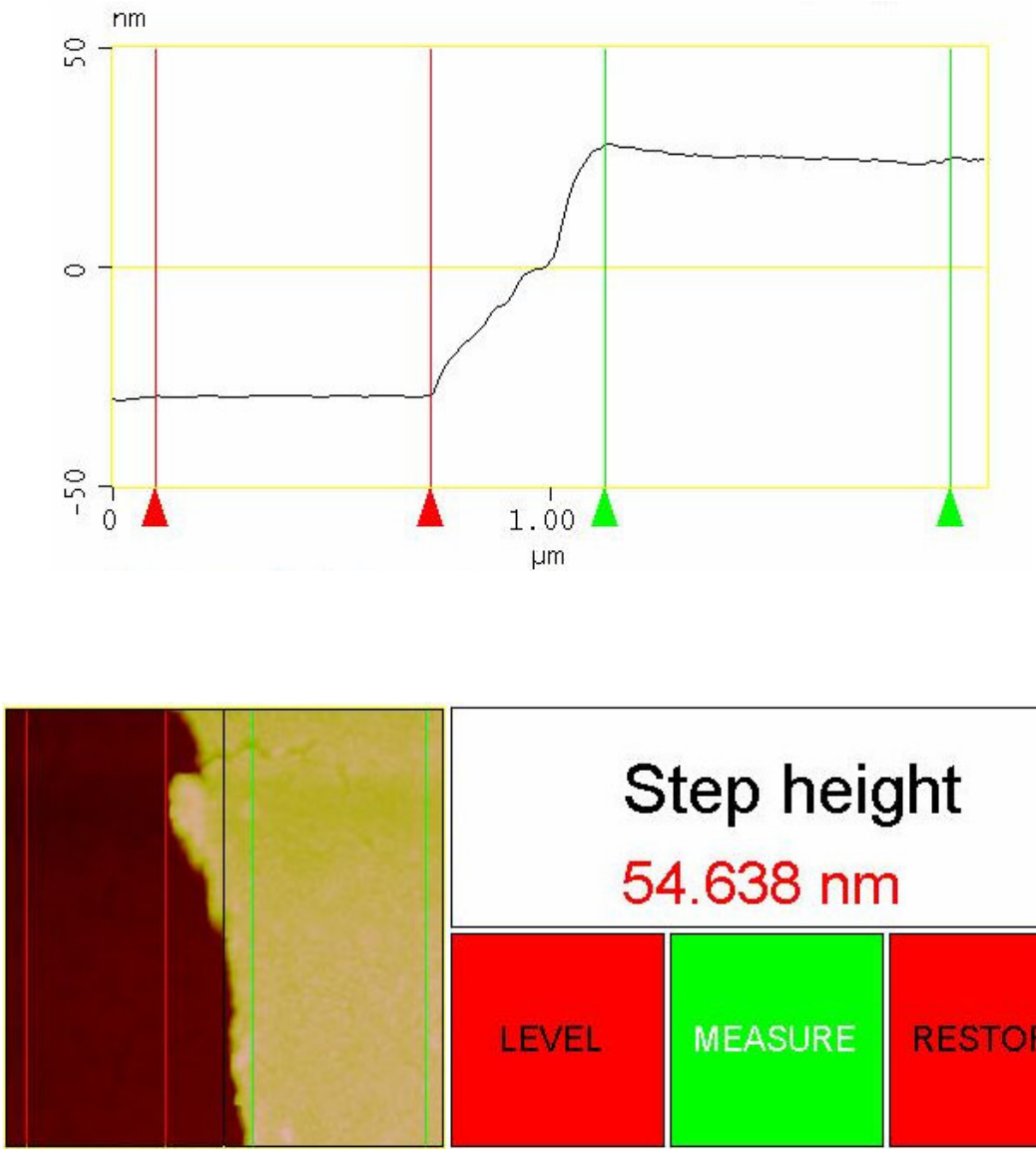

Figure 4.8. The step height analyses of the deposited gold film by AFM

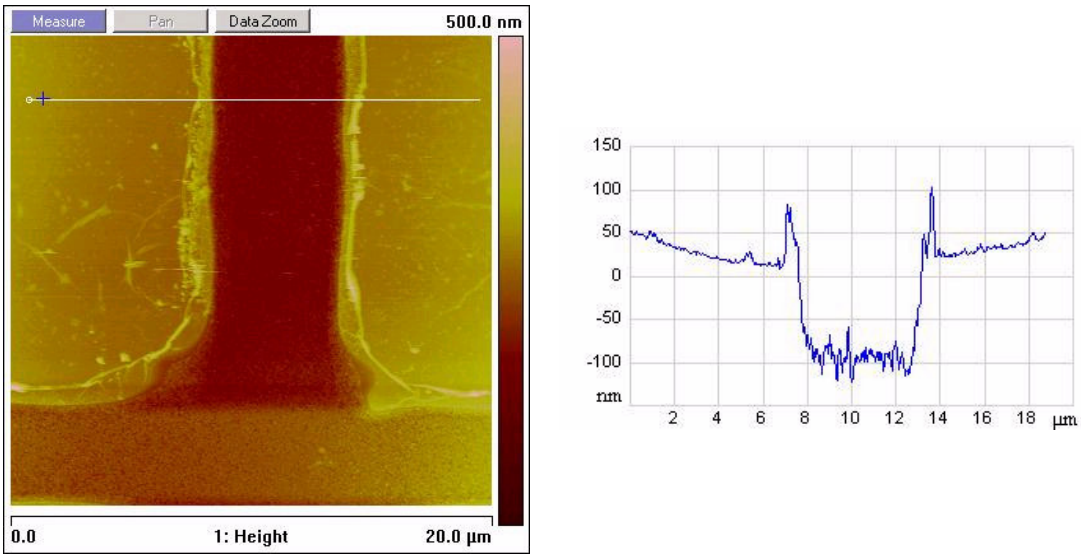

Figure 4.9. Section analyses of 20x20 μm^2 mesas obtained by AFM.

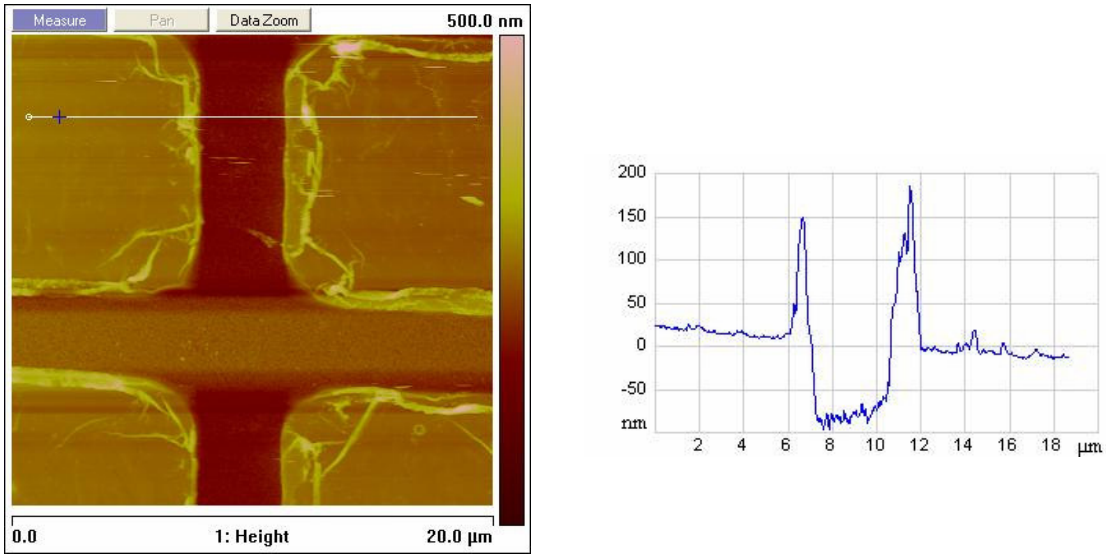

Figure 4.10. Section analyses of 10x10 μm^2 mesas obtained by AFM.

In Figure 4.9, the plot in the right hand side gives the value of approximately 120 nm for the MC01 mesa height while Figure 4.10 gives the MC03 mesa height as approximately 90 nm (The etching parameters for former sample are 700 eV, 22 W, 15 minutes while these parameters for latter one are 700 eV, 22W and 10 minutes-both of them were mounted to the ion beam chamber at a position making an angle of 45^0 with Ar ion beam direction). In order to get the photographs and plots above, AFM tip

scanned 20x20 μm^2 areas onto the crystal surfaces. When Figure 4.9 is examined, the distance between two squares is not exactly 10 μm which is the authentic value of the separation, but approximately 6 μm. Likewise, the distances between 10x10 μm^2 mesas have a reduction as one can easily discern from Figure 4.10. This reduced space is caused by the effects as counted above.

The color differences in the AFM photos indicate the presence of changing heights at different lateral positions, we can say that the surfaces of the obtained mesas are not flat and roughness is pretty high. So, we can deduce from the section analyses, the mesa height alters from point to point onto the surface because of the uneven feature of the mesa faces. It can be reconciled with unequal exposure of the Ar ions during the etching process. Moreover, in many experiments, the photoresist remaining after the Ar ion beam etching forms a thin and partially torn skin; this heterogeneous thickness can create this unequal height. From the photos related to section analyses of MC01 and MC03, one can observe the photoresist skin left after Ar ion beam etching on the mesas. Actually this does not affect the PCT measurements so much because the gold tip can puncture the partially available photoresist layers on the fabricated mesas during the measurements. Mesa structure includes IJJ and the deposited gold film, so if we know the total mesa height and gold film thickness (both of them can be obtained by AFM measurements), we can reach the height of the IJJ within the mesa roughly. Using these heights, the calculation of the IJJ number forming the stacked structure is fairly straightforward. For instance, if the MC03 is taken into account, the number of the IJJ can be found as nearly 23 dividing the IJJ height (350 A^0) by a single SIS size within Bi-2212 (15 A^0).

Figure 4.11 shows the I-V characteristics of MC01 optimally doped sample measured at 4.2 K and a detailed part of this graph is shown in Figure 4.12. In the current-voltage characteristics of the IJJ data, multiple quasiparticle branches and hysteretic behavior can be observed. The quasiparticle branches in the I-V dependence shown in Figure 4.12 can be easily counted. Because each branch observed in the I-V plot indicates a different IJJ within the constructed mesa, the number of the IJJ can be found by just counting the branches.

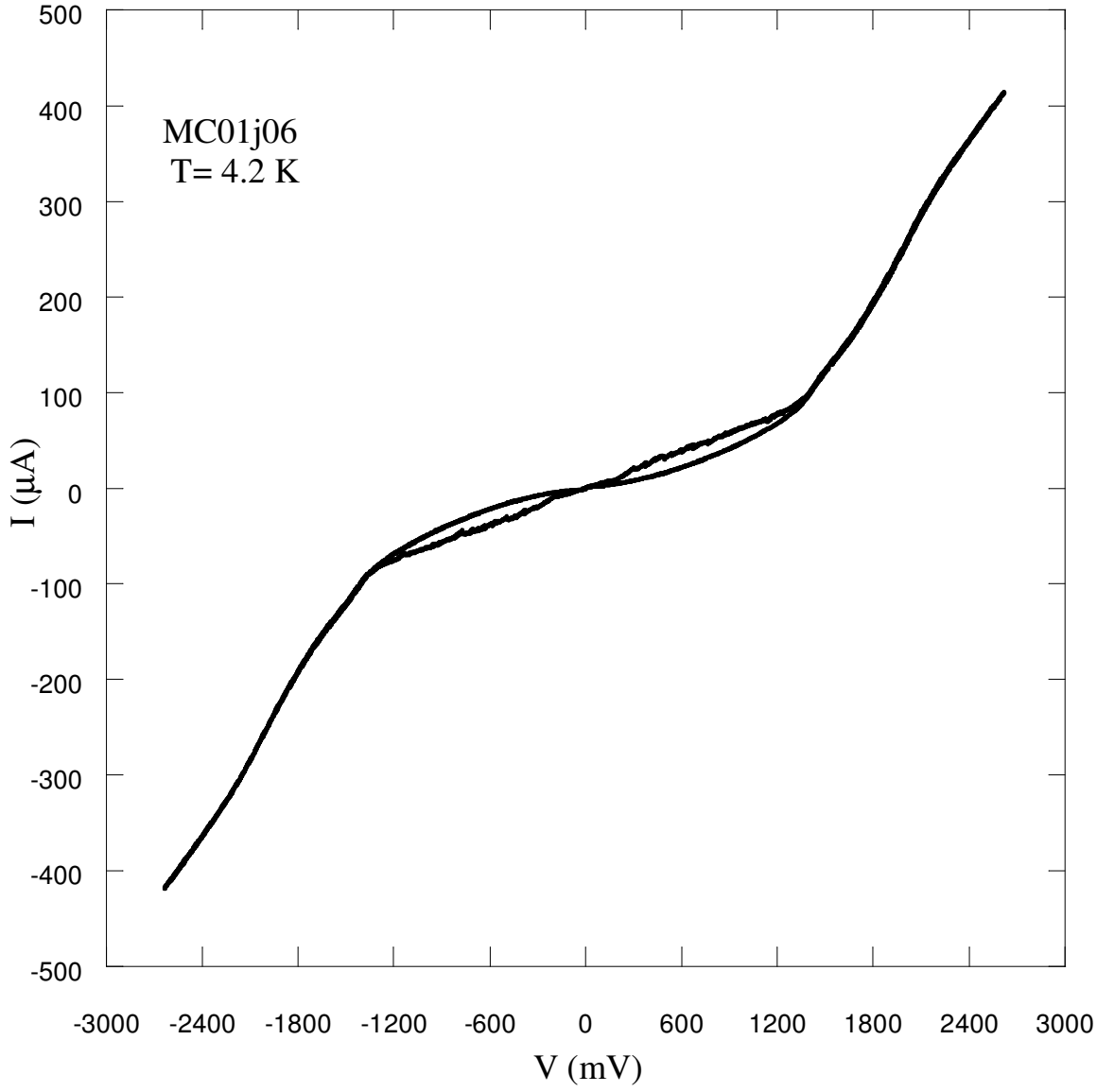

Figure 4.11. Current-voltage characteristics of MC01 at 4.2 K.

.

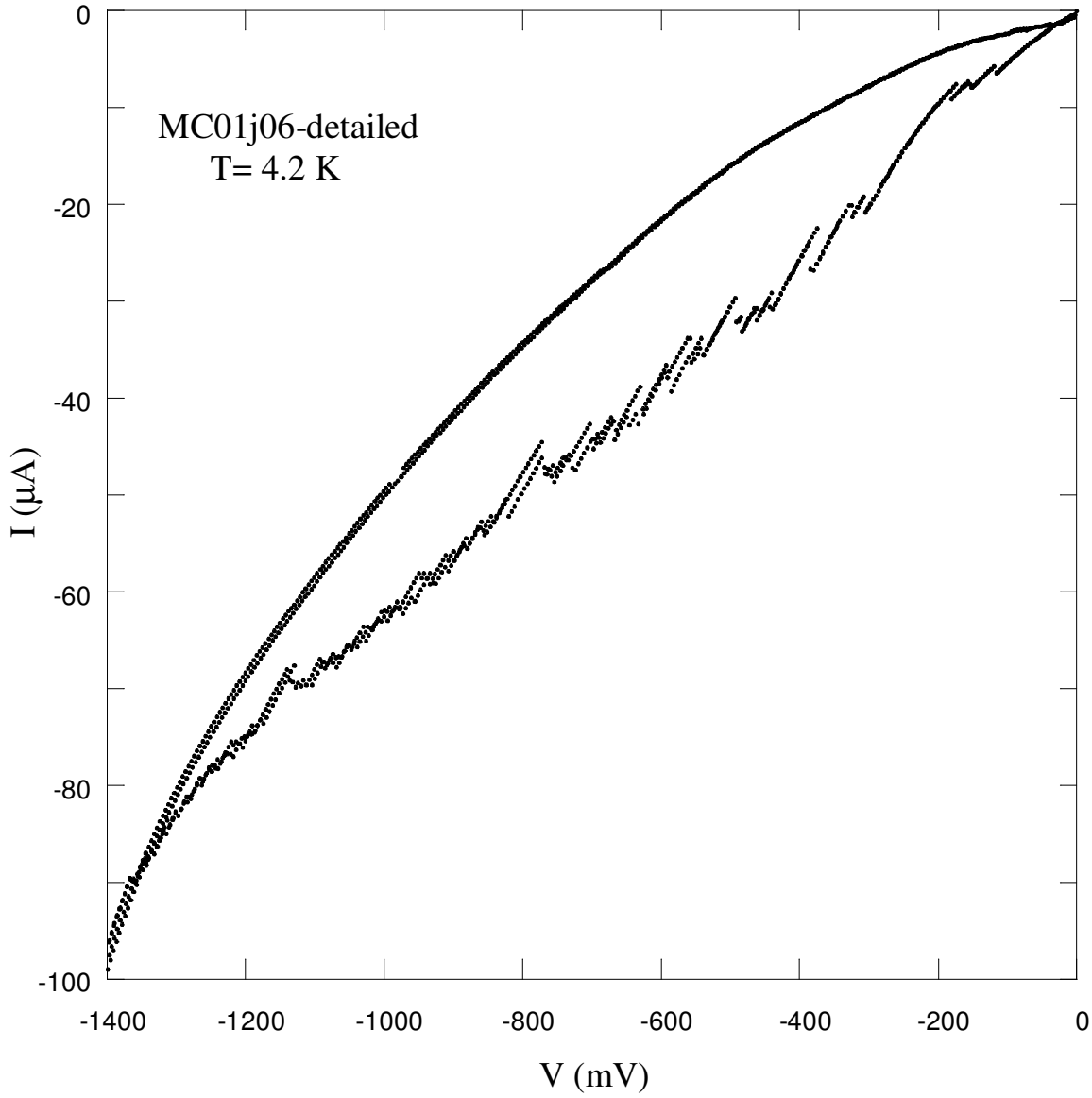

Figure 4.12. Detailed multi-branches and hysteretic behavior in I-V dependence of MC01 at 4.2 K

From the current-voltage characteristics of the MC01, one can identify around 56 quasiparticle branches which can be revealed by means of continuous switching of the bias. However, calculations based on AFM results give the number of the IJJ as 43.

The voltage jumps, i.e. separations between branches should be normally same for all the junctions. If Figure 4.12 is examined, these spaces between quasiparticle branches become smaller as being approached to higher bias values even unclear at the values between -1200 mV and -1400 mV. The reason for decrease in voltage jumps may

be a Joule overheating in the mesa; in this case, inner part of the mesa will be quite warmer than its outer division.

As it is understood from the Figure 4.13, the quasiparticle branches give sharp and narrow peaks for MC01 sample at the almost ±36 mV, which is directly proportional to twice of superconducting energy gap. In the plot obtained from original tunneling conductance data, the dynamical conductance peak corresponds to a voltage value which is proportional to the product of the number of the branches and superconducting energy gap. So, if we would like to obtain dynamical conductance gap voltages with accurate values, the voltage data should be divided by the number of the IJJ in the mesas. Many experimental results associated with optimally doped Bi-2212 single crystals suggest that the value of superconducting energy gap is 30-40 meV. If there are no heating problem or nonequilibrium effects, the value of the energy gap must be in good agreement with the value stated in previous consequences. Here, we found the energy gap approximately 18 meV which is well below even lower limit of predicted value. In the literature, there are reduced gap values as large as 85 % detected and this effect is explained by the collective contribution of heating and quasiparticle injection

There is a striking anomaly in the subgap region of conductance characteristics. If Figure 4.13 is looked at closely, some gap-like features can be seen at ±25 mV values. In fact, these features stem from corresponding I-V characteristics. If Figure 4.11 is examined thoroughly, it can be realized there is a subtle deviation from the normal trend of the graph at the values approximately ±1400 mV, which are the exact positions of the peculiar subgap structures in dI/dV-V plot. The usual SIS conductances show continuous behavior without any features up to quasiparticle peaks as well as dip and hump structures at elevated bias values. The conductance curves shown in Figure 4.13 exhibit cusp-like behavior having an extremely sharp end at zero bias; which can be reconciled with d-wave symmetry. Because of the overheating in the investigated mesa on MC01 optimally doped sample, we could not determine exact locations of dip and hump structures. Note that the conductance curves, although pretty high voltage values are reached, dip features are undeveloped and even hump features are not visible.

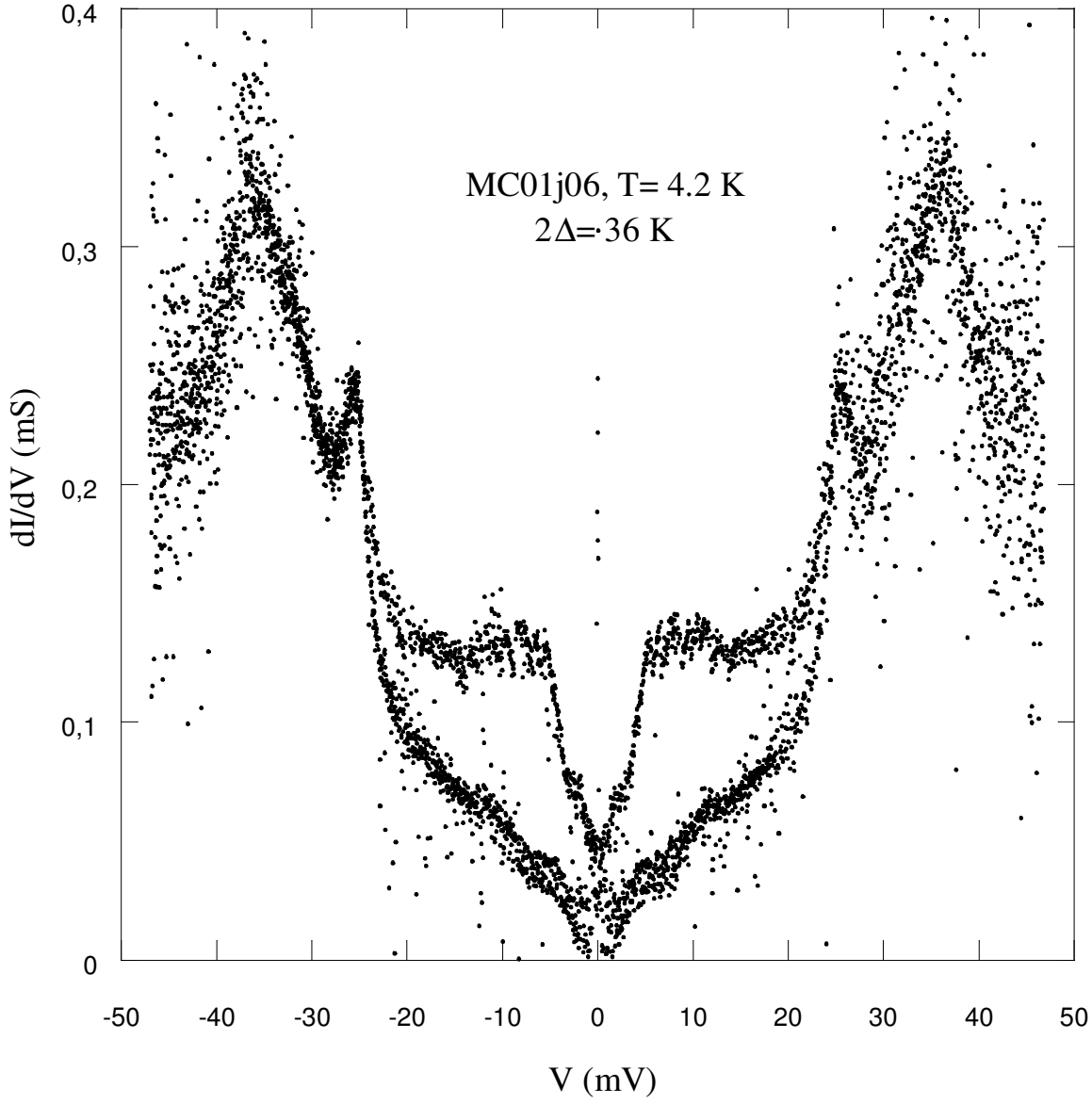

Figure 4.13. Tunneling spectra measured at 4.2 K on MC01.

Figure 4.14 displays I-V characteristics of MC03 at 5.3 K. In order to collect data, the bias voltage is continuously swept positively and negatively many times to obtain different quasiparticle branches. The sweep rate is 5 mHz for MC03, while that of MC01 is 3 mHz. Sweep generator produces triangle waveform which varies periodically between a minimum and maximum value. The I-V curves do not follow the same way while going from positive bias to negative bias as going from negative bias to

positive bias, which leads to hysteresis in the I-V characteristics. If there is a small contact resistance between the gold tip and the surface of Bi-2212 single crystal, Cooper pairs tunnel at zero bias and a Josephson current can be seen. If Figure 4.14 is examined, it can be realized that there is no Josephson current at zero voltage, which reflects the comparatively high resistance between the Au layer and the Bi-2212 crystal relative to the resistance of the entire mesa. This situation suggests that the first junction is SIN junction created by Au and Bi-2212. The hysteretic behavior of the I-V curves and multi-branches can be seen in Figure 4.15 in details. There are 26 quasiparticle branches in the I-V characteristics. Due to the high contact resistance, the authentic number of IJJ in MC03 optimally doped sample can not be obtained by counting the present quasiparticle branches. Note that the I-V dependence shown in Figure 4.15 does not exhibit any branch up to ±390 mV, which indicates there are available invisible branches apart from ones that we can count easily using tunneling characteristics.

In some PCT measurements on MC03, we encountered backbending as a signature of nonequilibrium or heating effects (Tanabe et al. 1996). Figure 4.16 exhibits I-V characteristics of another mesa on MC03 with backbending. If the thickness of stacked Josephson junctions is less than the quasiparticle diffusion length, the quasiparticles created in one junction can easily pass neighboring junction diminishing their superconducting features. The effect of nonequilibrium current injection in coupled arrays of tunnel junctions is usually manifested in a heavy backbending of the I-V curves in the region of the sumgap (Yurgens et al. 1996b). The total dissipated power was around 2.4 mW during the experiment. It is a noticeable value, due to the fact that this is by far larger than the value which can be observed in a single Josephson junction. The nonequilibrium quasiparticle injection leading to backbending can also result in the gap value to decrease. Because the thickness of each double CuO_2 layers is around 3 A^0 in the structure, the quasiparticles generated in single Josephson junction can move into the other junctions without difficulty and after arrival, they can alter the the quasiparticle population there. The competition between the rate of quasiparticle generation and their recombination rate determines the steady concentration of quasiparticles and the operational gap parameter (Yurgens 2000).

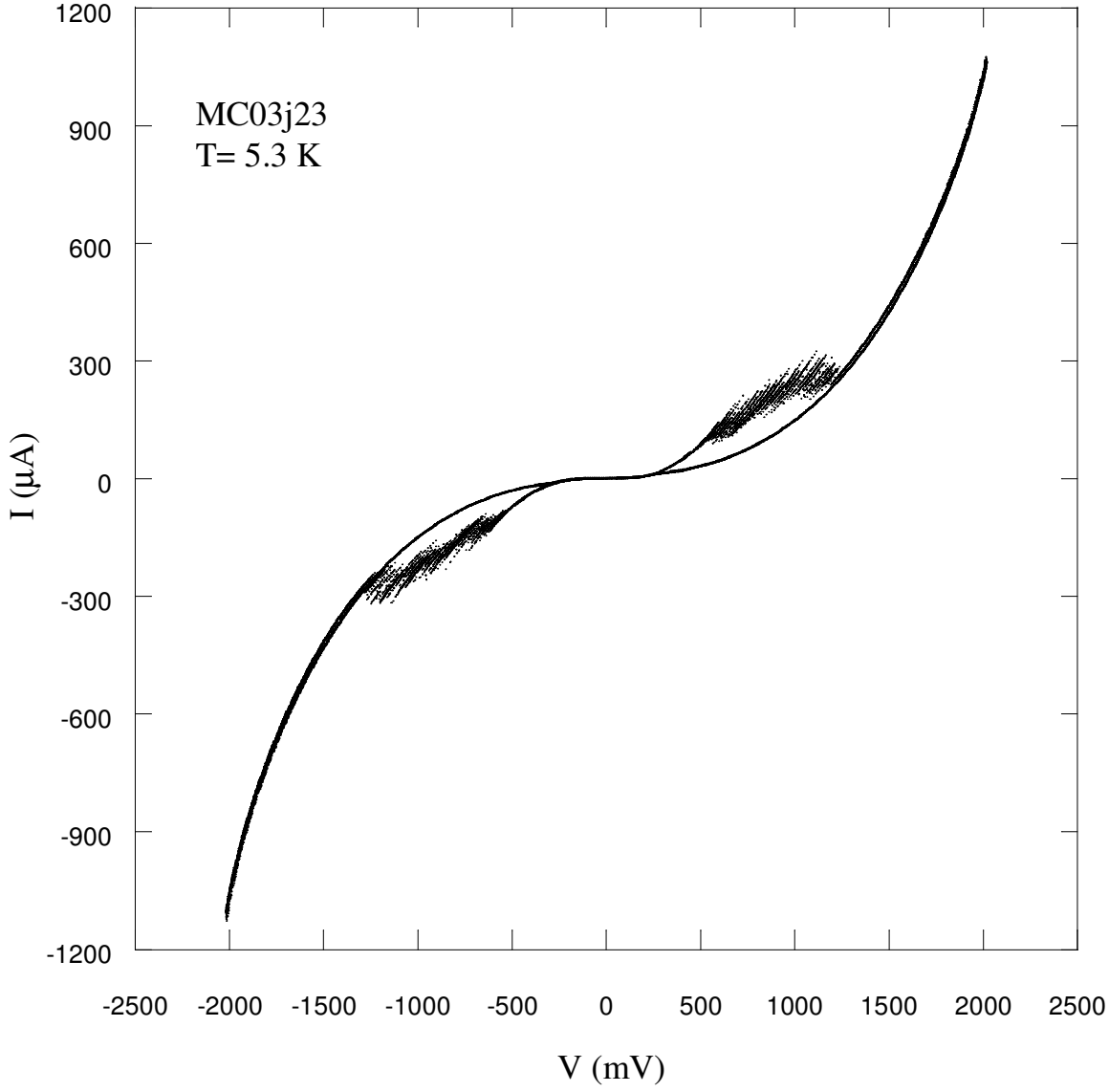

Figure 4.14. I-V characteristics and multi-branches of MC03 at 5.3 K

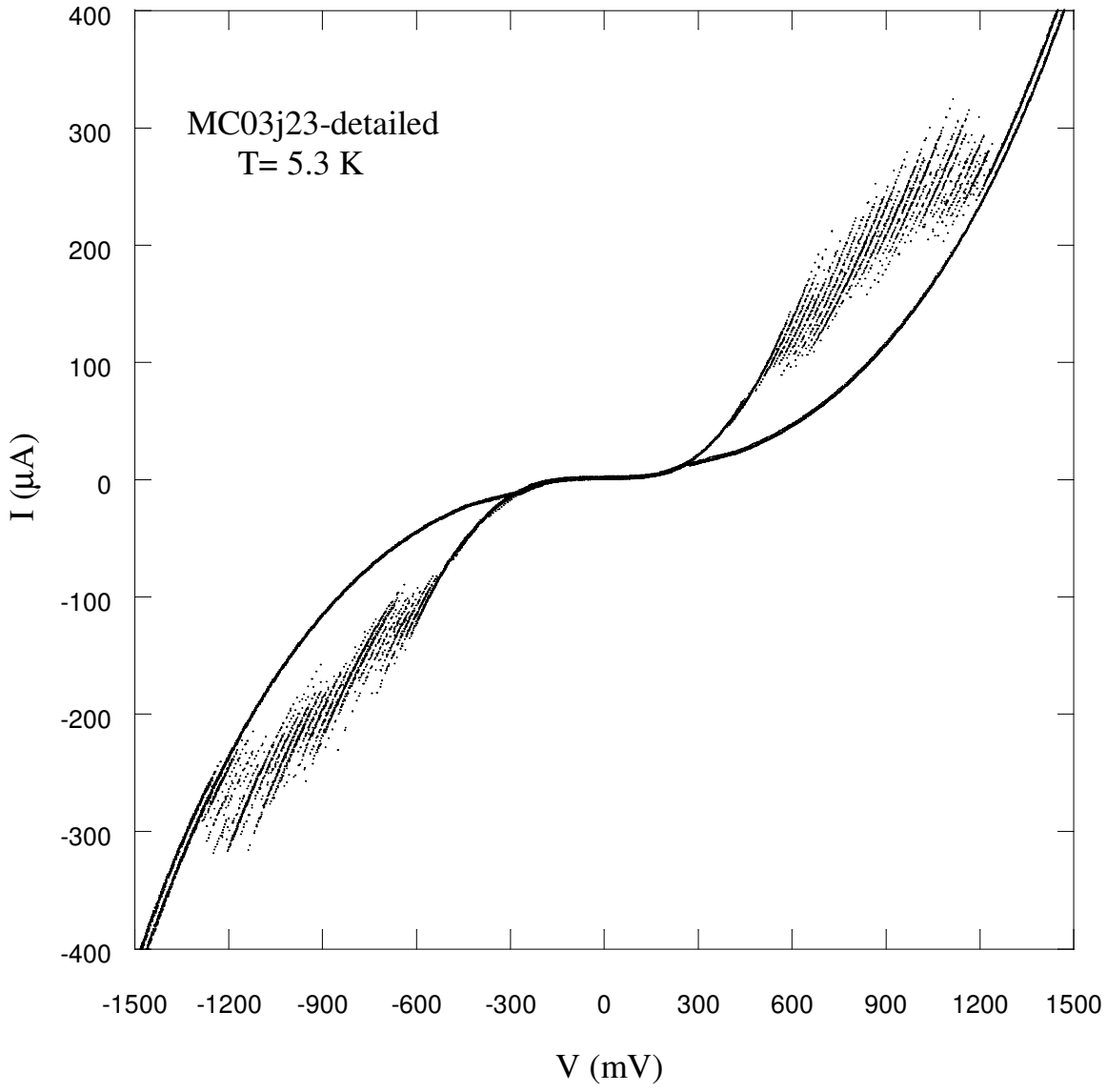

Figure 4.15. Multiple branches within the MC03 in detail

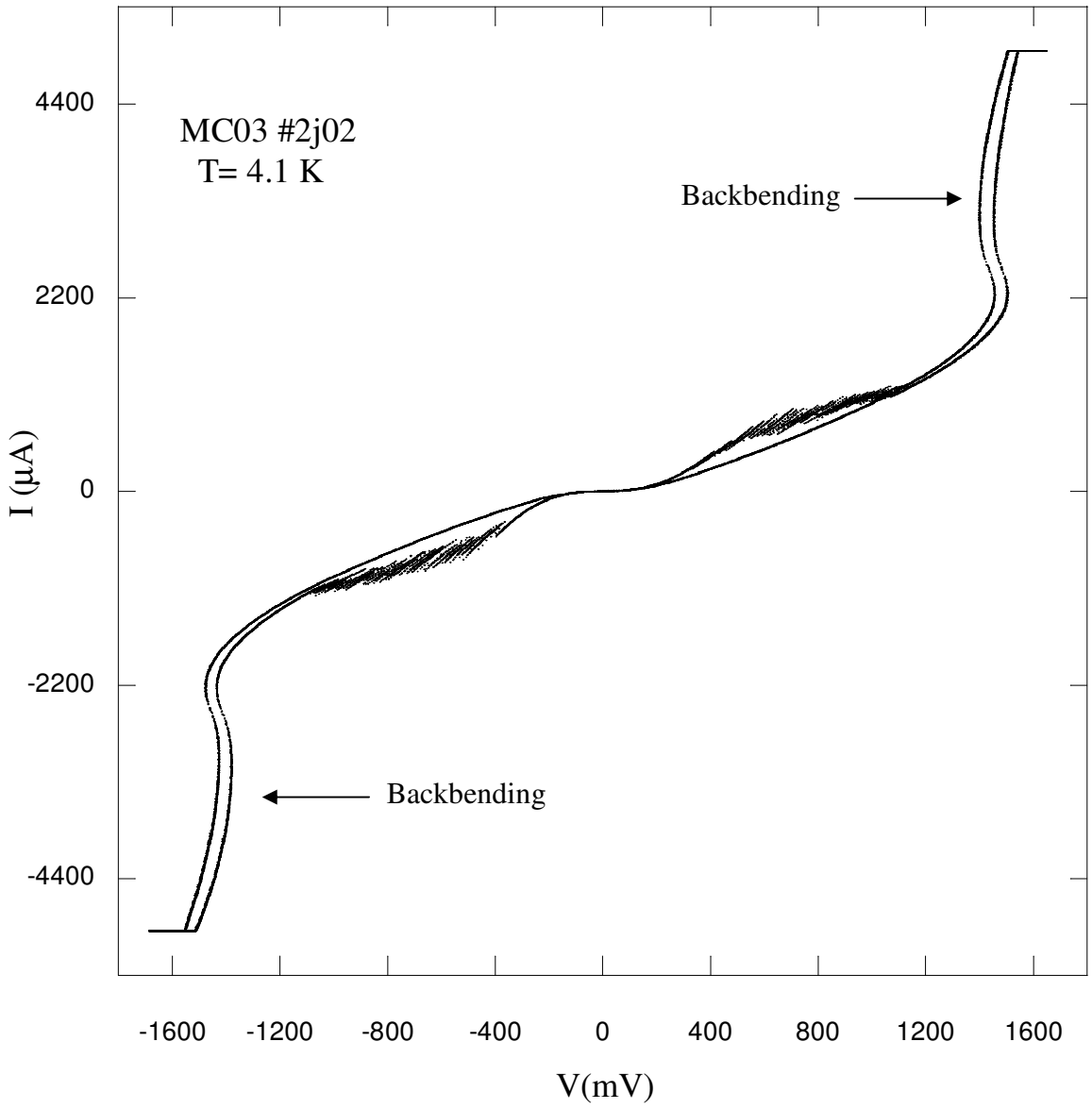

Figure 4.16. I-V characteristics of MC03 with backbending

Note that the interesting features at elevated voltage values in concerned I-V characteristics of MC03 with backbending. The curves follow a trend of straight line approaching to the maximum bias values, because PCT tip is affected by high bias.

In Figure 4.17, some quasiparticle branches in the I-V characteristics shown in Figure 4.14 can be seen in detail. Each interval in the voltage axis is interrupted by approximately 4 quasiparticle branches. As it can be understood from the graph, the separation between the branches is approximately 17 mV, which corresponds to 2Δ value. The same reason as discussed before can be given for the reduction in

superconducting energy gap. It can be deduced that the heating problem is relatively more exacerbated in MC03 if compared with MC01 because of the considerable deviation from the expected value of the energy gap for Bi-2212.

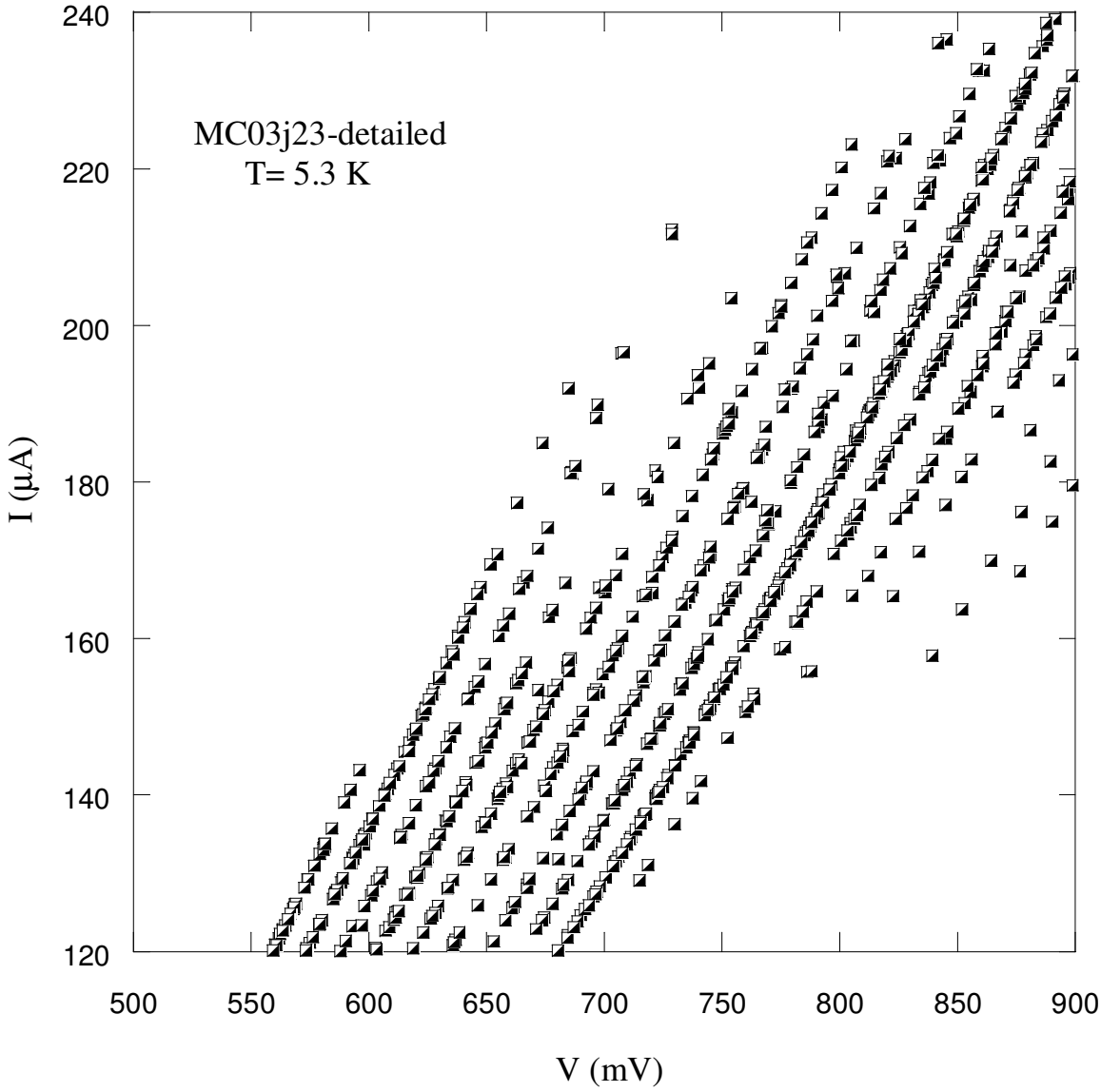

Figure 4.17. The high resolution representation of quasiparticle branches of MC03.

Tunneling conductance characteristics of MC03 obtained by PCT can be seen from Figure 4.18. The number of the IJJ in the mesa can also be found as 26 from the dI/dV-V characteristics. We can not observe any spectral features reconciled with SIS junctions such as quasiparticle peaks, dip and hump structures from this plot, although high bias voltages are reached. The problem can be linked again overheating.

Figure 4.19 and Figure 4.20 show I-V dependences and c-axis dynamical tunneling conductances of MC01 at different certain temperatures respectively. From both of them, it can be discerned that there is a strong relationship between the energy gap and temperature. If Figure 4.19 is looked at, it can be observed that the curved character of the I-V dependence becomes nearly linear beyond 100 K. According to BCS model, the energy gap is totally destroyed, when the temperature reaches the critical temperature value. From the Figure 4.20, it can be seen that the conductance peak voltages dramatically decrease with increasing temperature. Besides, it can be observed rapid decrease of quasiparticle peak heights with temperature. But there is no straight line in the temperature dependent conductance curves; which indicates presence of superconducting gap even at the temperatures quite above T_c. The availability of energy gap above transition temperature in cuprates might be a precursor of pseudogap.

Some deviations from the usual continuity of the curves can be realized in Figure 4.19. Especially from the left part of the I-V curve, it can be seen there is a changing in regular way of curves at 100 K and 160 K; which can be linked that tip pressure alters with temperature. As one can infer from Figure 4.20, energy gap shows a decreasing tendency with increasing temperature. After 40 K, the aberrant picture of the I-V curves (with strange subgap features) begins to enhance and subgap region is much closer to the curve which is supposed to be. The cusp-like feature associated with d-wave symmetry can be seen in each conductance curve. It is observed that the superconducting gap is very hard to determine above 100 K, because of the absence of sharp and clear quasiparticle peaks.

The temperature dependence of the energy gap magnitude,$\Delta(T)$, is well understood both theoretically and experimentally for conventional superconductors. $\Delta(T)$ is almost constant up to $T \sim T_c/4$, while it begins to approach zero in the vicinity of T_c, where it is proportional to $(1-T/T_c)^{1/2}$. Due to the presence of some special properties such as pseudogap, the energy gap in high T_c superconductors does not depend on temperature in the same way as observed in s-wave superconductors.

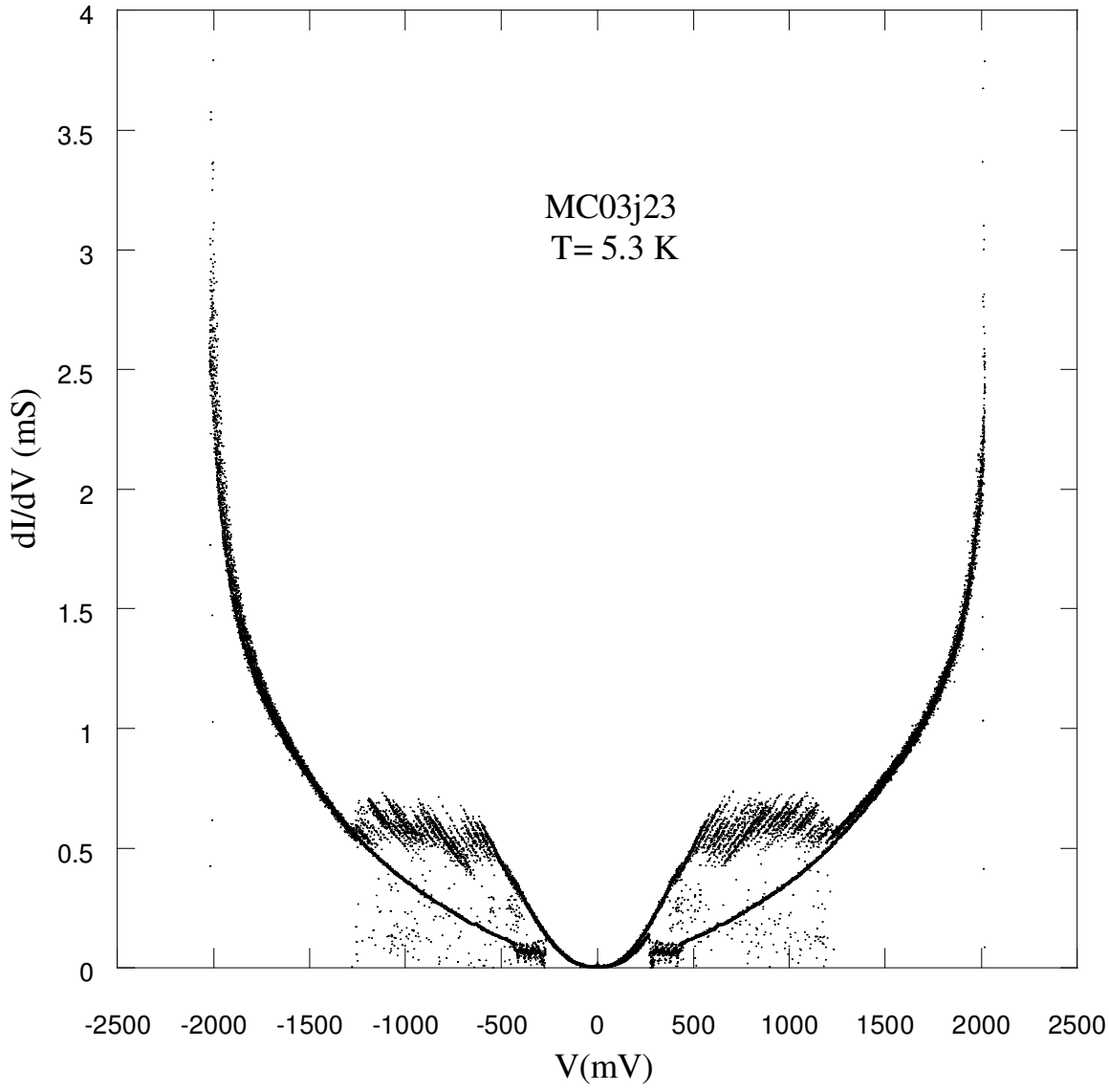

Figure 4.18. Tunneling conductance characteristics of MC03 at 5.3 K

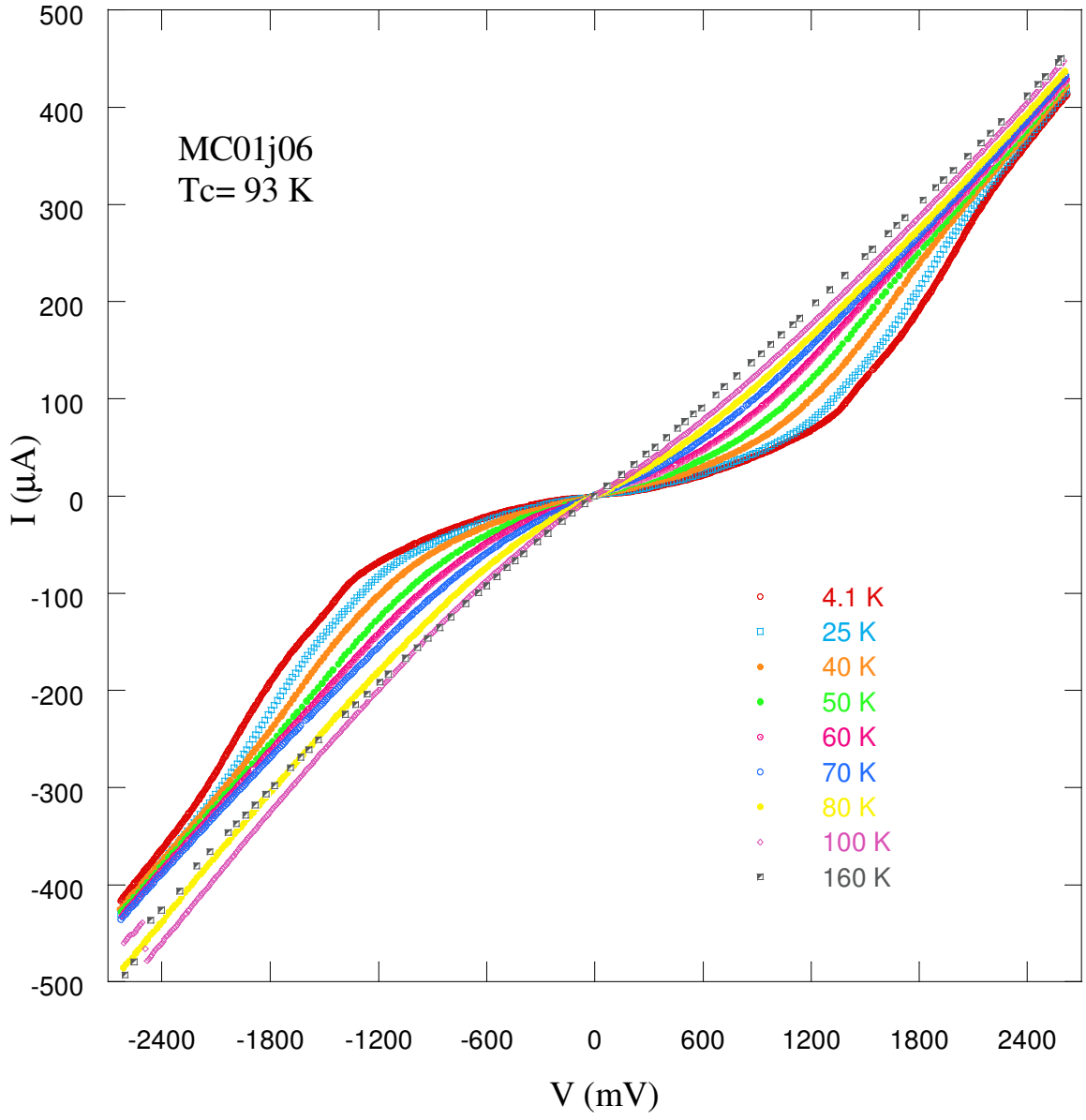

Figure 4.19. Current-voltage characteristics of MC01 at different temperatures. From the figure a set of I-V curves measured by PCT at the temperatures between 4.1 K to 160 K can be seen.

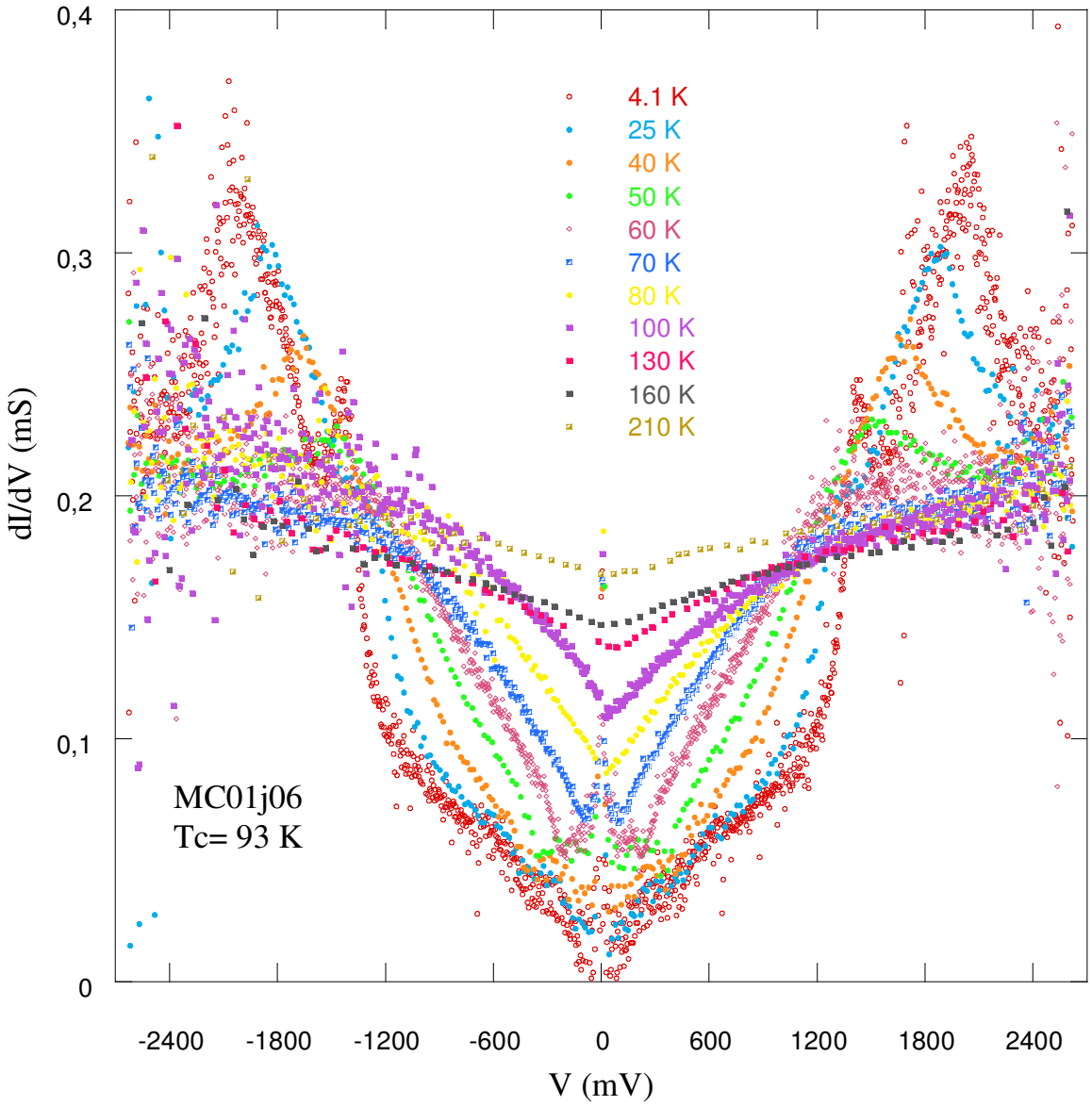

Figure 4.20. Tunneling conductances of MC01 at different temperatures

Figure 4.21 exhibits the normalized gap voltage versus normalized temperature graph of MC01 optimally doped sample. In terms of BCS model, the energy gap should be zero at 93 K which is the transition temperature of the MC01. As one can understand from the Figure 4.21, the Bi-2212 gap voltages directly proportional to the energy gap are not suppressed at the critical temperature as expected.

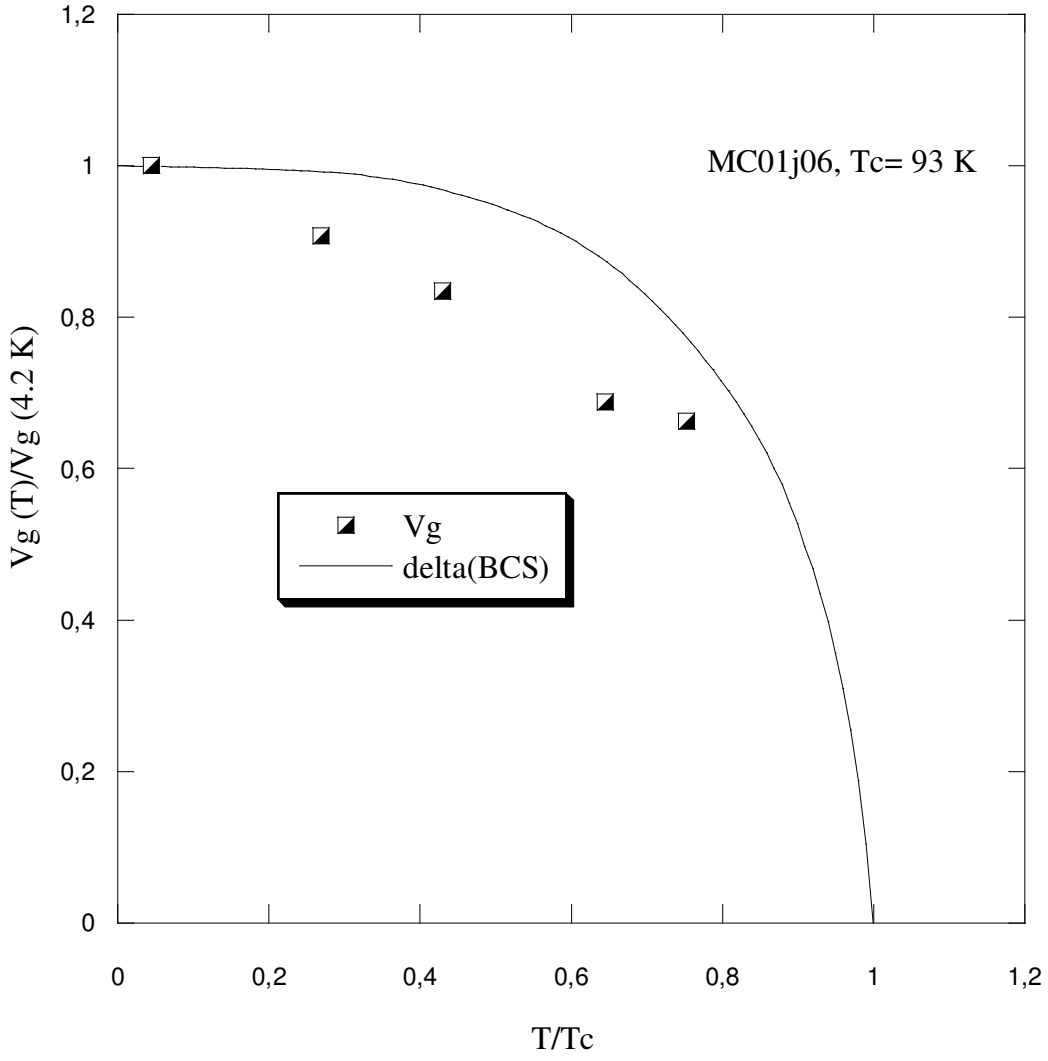

Figure 4.21. Normalized gap voltage versus normalized temperature plot of MC01

Figure 4.22 displays the zero bias conductance (ZBC) plotted against temperature for MC01. The conductance values at zero bias show a rising with increasing temperature and different from zero. Up to critical temperature, the increment of the ZBC is pretty regular, after the 100 K this increase shows a different fashion. From this plot, the existence of pseudogap for MC01 can be understood due to the absence of anticipated point at 0.2 mS corresponding to 210 K which is well above transition temperature.

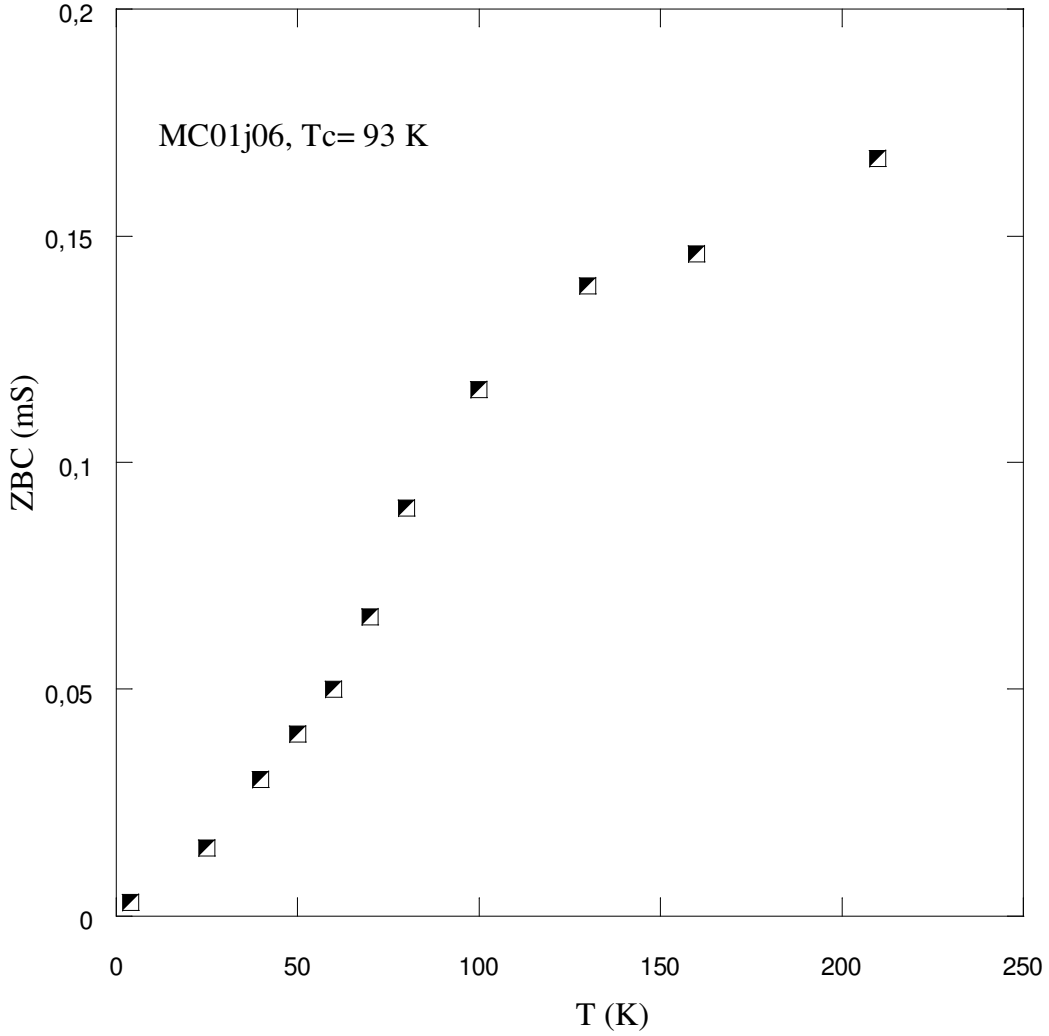

Figure 4.22. Zero bias conductance versus temperature plot of MC01

4.3. Results of $HgBr_2$ Intercalated Bi-2212 Single Crystals

$HgBr_2$ intercalated Bi-2212 single crystals were synthesized by vapor transport reaction between host and guest in vacuum sealed tube. These samples were obtained by heating the pure compounds with excess $HgBr_2$ at 230 ^{0}C for 16 hours. For intercalation, before this process the pristine Bi-2212 single crystals with Tc=77 K were grown by floating zone technique. Various $HgBr_2$ intercalated Bi-2212 samples with different mesa heights were measured by means of PCT technique, in certain cases SIN and SIS single junctions were obtained between the tip and a piece of sample as well as separate pieces of the crystal. In this thesis, we present the results of just only 4

intercalated single crystals whose critical temperatures are approximately 74 K and the sample codes are BH3e, BH4d, BH5b and BH8 (without mesa structures). Photolithography and Ar-ion beam etching techniques were used to fabricate stacked IJJ but the processes such as amount of gold deposition, UV exposure time, or etching parameters were changed from sample to sample.

4.3.1. SIS Break and SIN Single Junctions Obtained by PCT

Some measurements were done by touching the surfaces of the bulk intercalated crystals with a blunt Au tip as described before and at the end of these measurements some SIN and SIS characteristics were obtained. Figure 4.23 and Figure 4.24 exhibit I-V and dI/dV-V characteristics of an SIN junction obtained by PCT on BH8 single crystal respectively. From SIN conductance, the superconducting energy gap can be seen as 24 meV. For negative bias corresponding the electron removal from the superconductor, a well-defined dip feature can be observed at -46 mV (matching with nearly -2Δ) followed by a hump structure at -72 mV which is proportional to exactly -3Δ. In the positive bias part of the graph, there is no sharp dip feature but quite a rapid change of slope and the hump is hardly discernible. This asymetry can be encountered in most spectra obtained by PCT. Some of the I-V curves demonstrate nonlinearity at high bias voltages as the right part of the I-V curve shown in Figure 4.23, which is believed to come into existence due to the barrier effect (Ozyuzer et al. 1999b). If the tip penetrates into the crystal sufficiently, then SIS break junctions can be generated. The reproducible I-V and dI/dV-V characteristics are given in Figure 4.25 and Figure 4.26 which belong to SIS break junction within BH8 sample. SIS current-voltage characteristics also display a deviation from linearity at higher bias values. The SIS conductance gives sharp quasiparticle peaks at ±48 mV values, which are convenient with SIN single junction results obtained on the same crystal. One can also see from Figure 4.26 well-defined and clear dip/hump features at ±80 mV and ±115 mV which are slightly more than expected values. The comparison of two SIS conductances obtained by different junctions within the same crystal is shown in Figure 4.27. Their subgap regions are relatively in a good agreement while PHB ratios show pretty high diffrence. The quasiparticle peaks cut the voltage axis at almost the same values (±48 mV). Besides dip and hump structures exhibit close features in both of them. The

locations of these features are also nearly same: dip features at ±3Δ and hump features at a little bit greater than ±4Δ as determined for BH8j11 above.

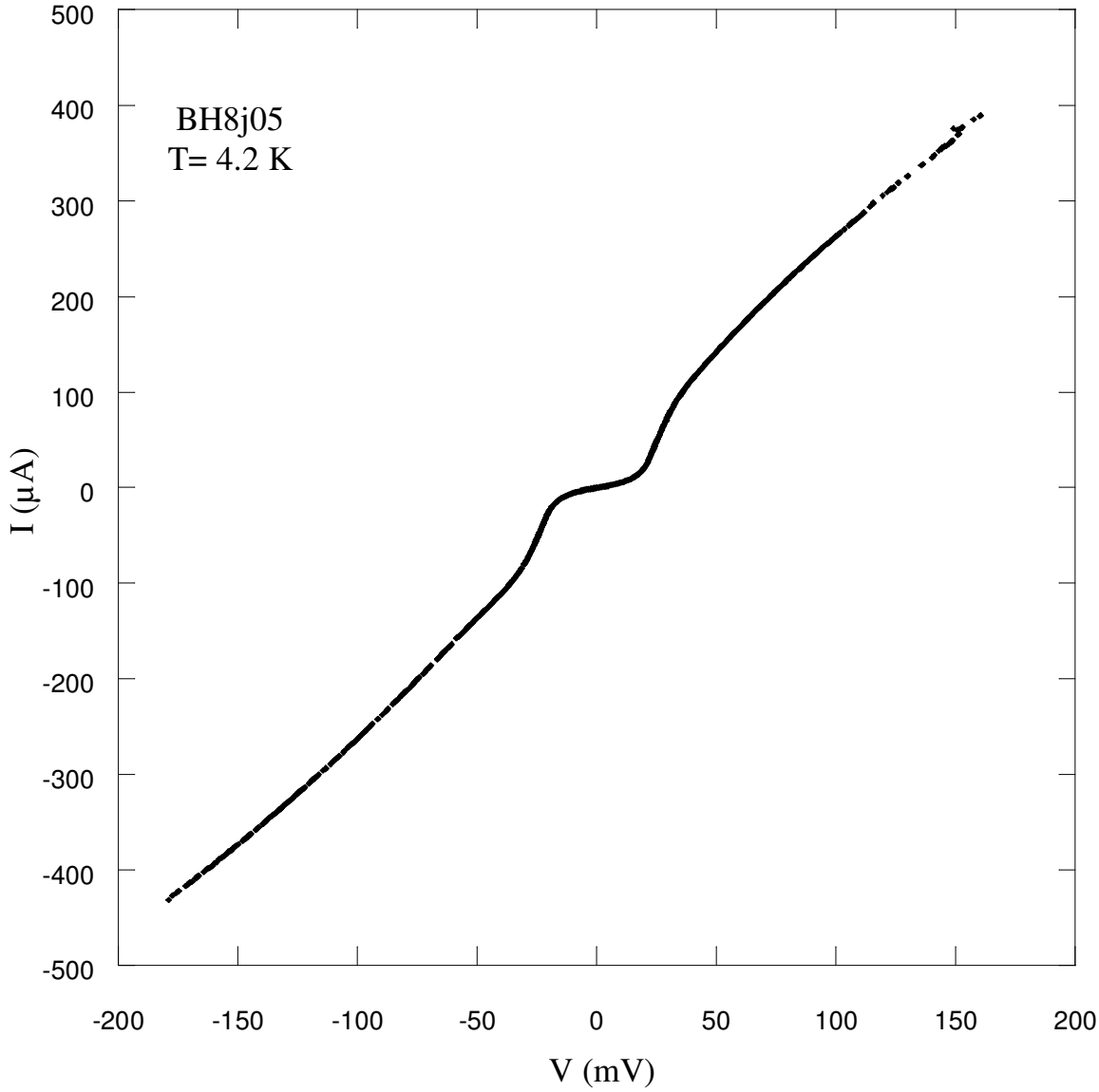

Figure 4.23. I-V characteristic of an SIN junction on BH8 at 4.2 K

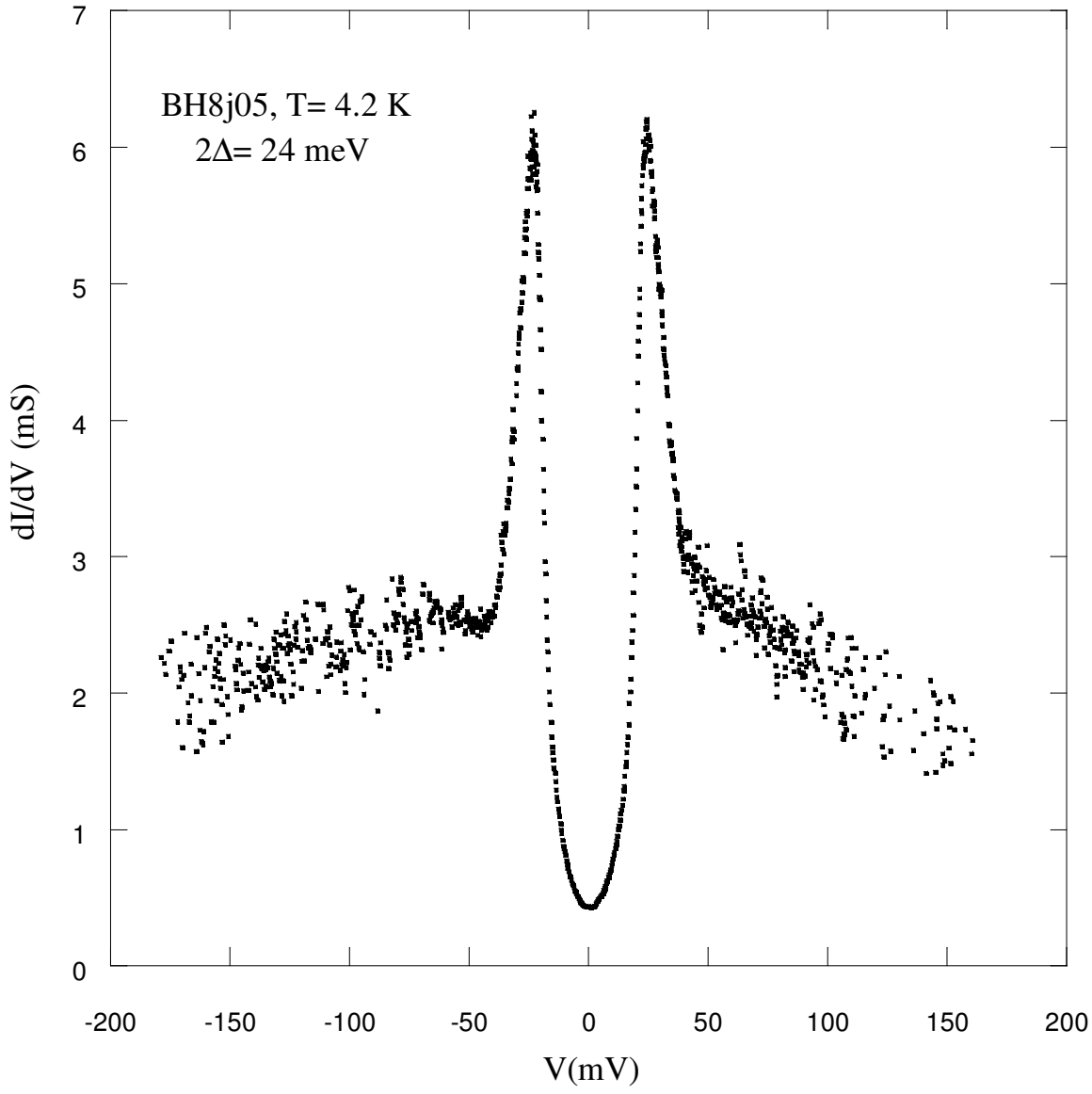

Figure 4.24. dI/dV-V characteristic of an SIN junction on BH8 at 4.2 K

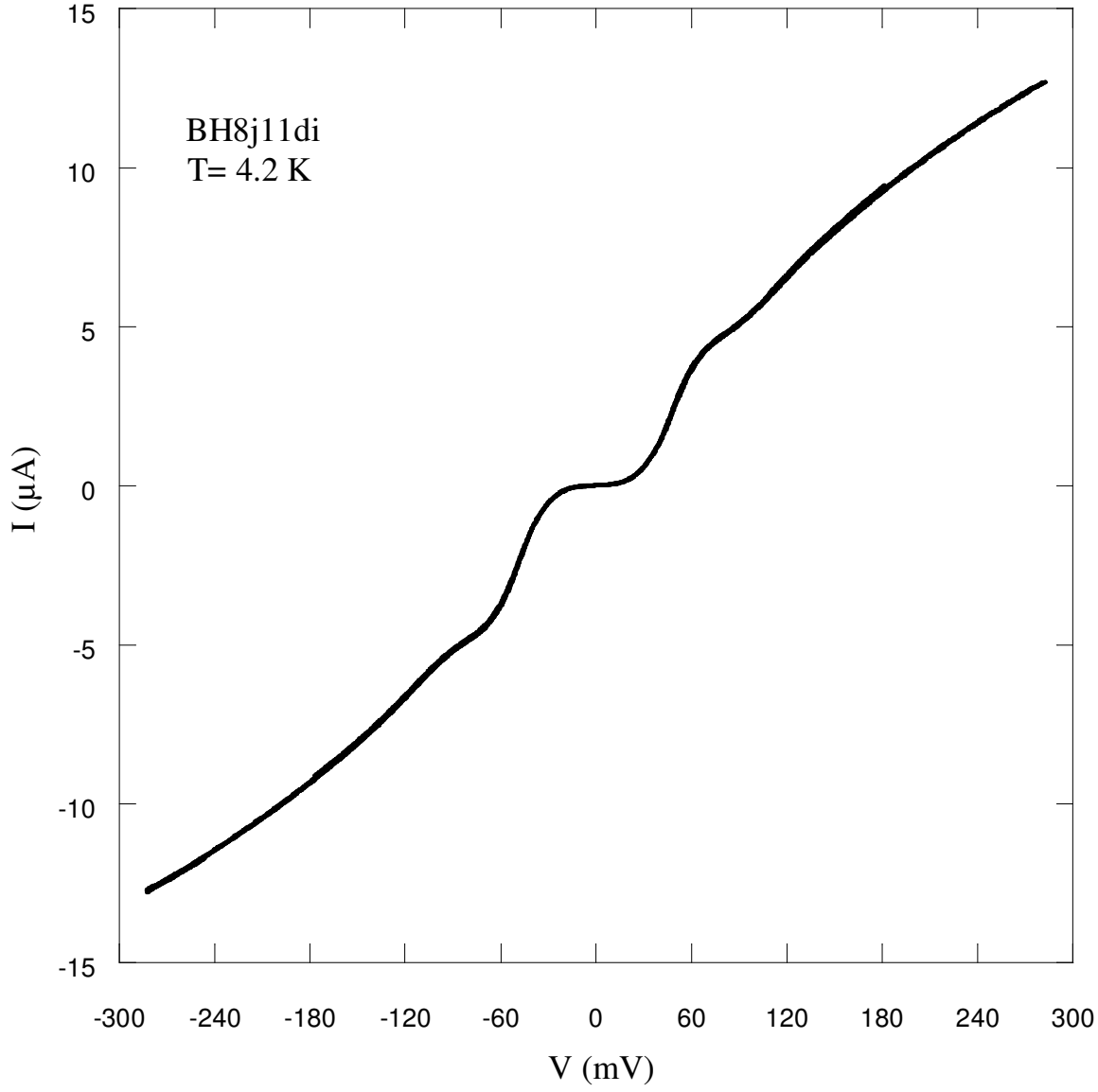

Figure 4.25. Current-voltage characteristic of an SIS break junction between two pieces of BH8 single crystal at 4.2 K

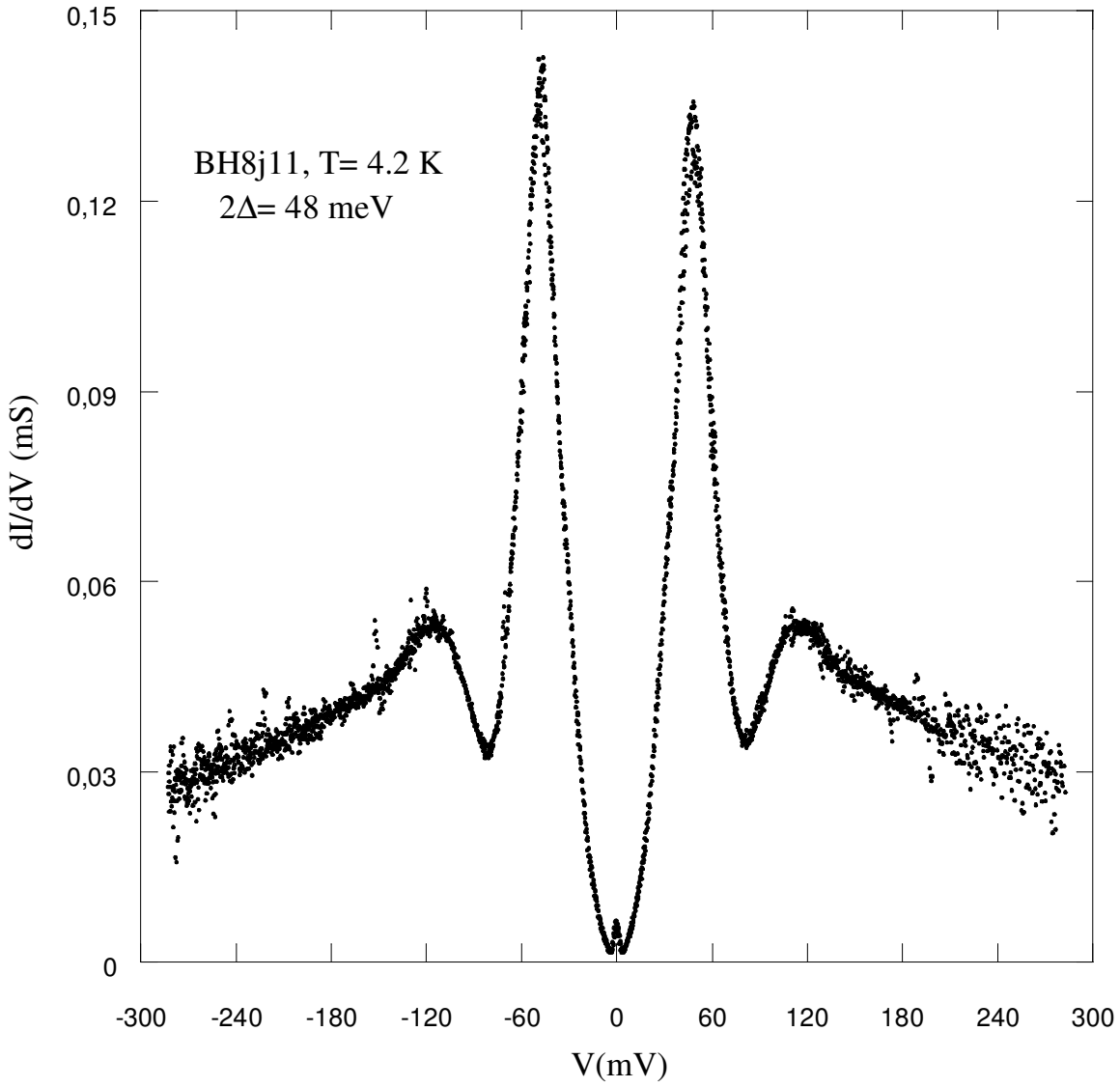

Figure 4.26. dI/dV-V characteristic of an SIS junction within BH8 at 4.2 K

From Figure 4.27, one can discern the difference between 2 junctions in terms of Josephson current. Gold curve exhibits supercurrent at zero bias while the blue curve does not (actually it is barely discerned), which points the junction resistance is much more in junction12 than junction11.

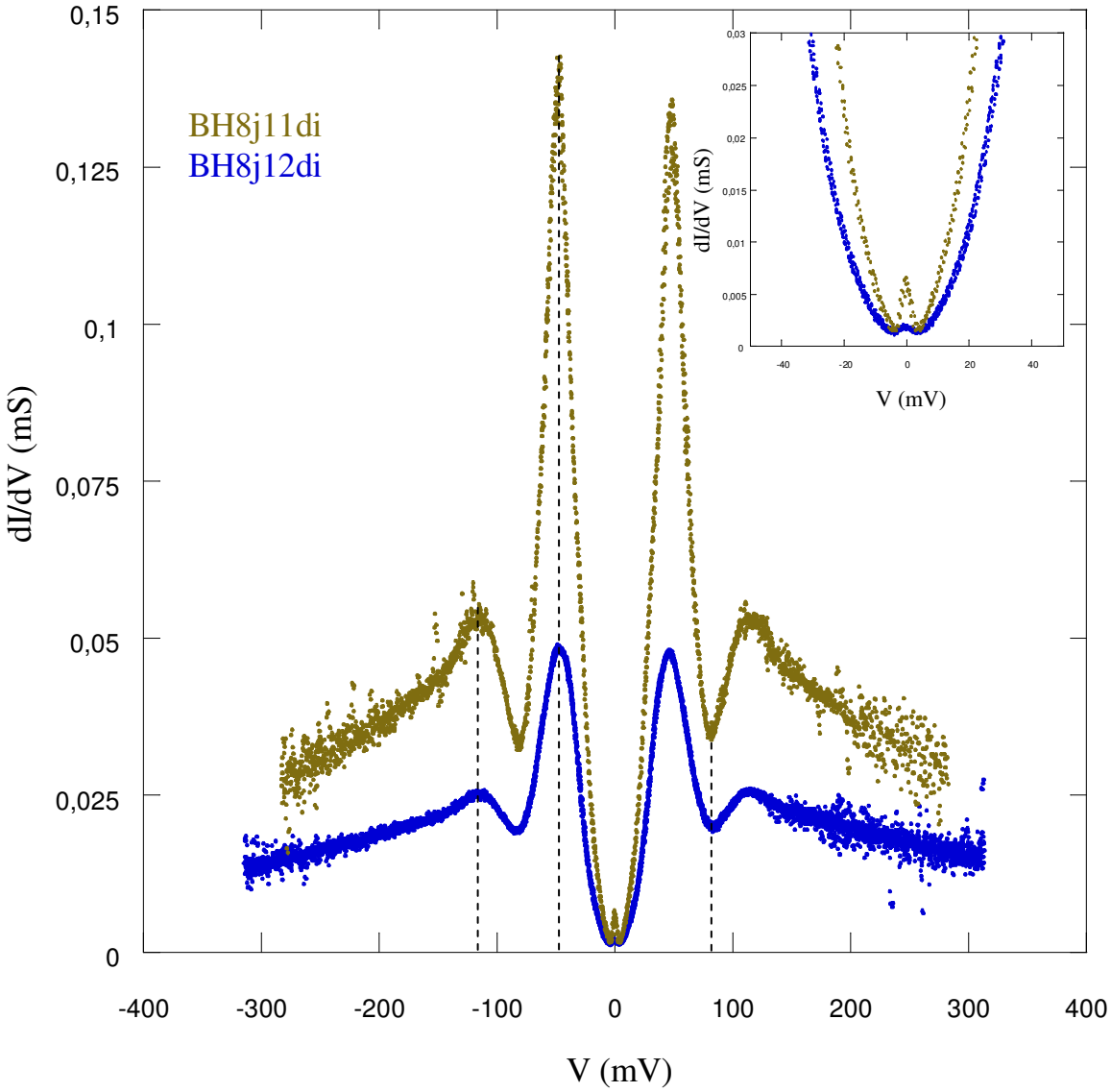

Figure 4.27. Comparison of two SIS break junctions within BH8 in terms of their tunneling conductances. The locations of the quasiparticle peaks, dip and hump structures are nearly same.

4.3.2. IJJ within the $HgBr_2$ Intercalated Crystals

Tunneling experiments were carried out on 3 different $HgBr_2$ intercalated samples for IJJ investigation: BH3e, BH4d, BH5b. All of them were patterned by using aforementioned special techniques. BH3e single crystal with T_c=74 K includes 20x20 μm^2 mesas on the crystal and the separation between mesas is 5 µm. Figure 4.28 shows the photograph of these mesas obtained by optical microscopy. The photoresist skin can be distinguished easily from the photograph. To get rid of this undesired remaining, etching in oxygen plasma can be done.

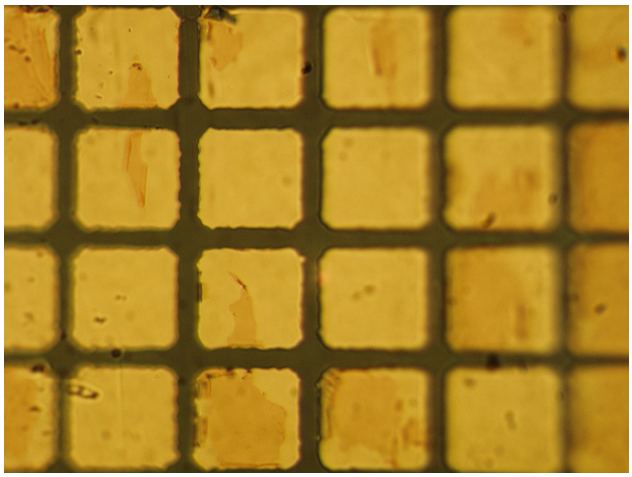

Figure 4.28. Optical micrograph of the mesas on BH3e

The section analyses of the same sample are given in Figure 4.29. The left image shows the intersection of four mesas on the BH3e surface. The height of one mesa on BH3e is approximately 80 nm as shown on the right plot. Also using AFM, the height of the deposited gold film was found as 40 nm. So, we can get the thickness of the stacked IJJ as 40 nm, from this information the number of the IJJ within the mesa can be calculated as 19. Here the unit size of the SIS junction is taken as 21 A^0 instead of 15 A^0 because of the expansion in the unit cell due to the intercalation.

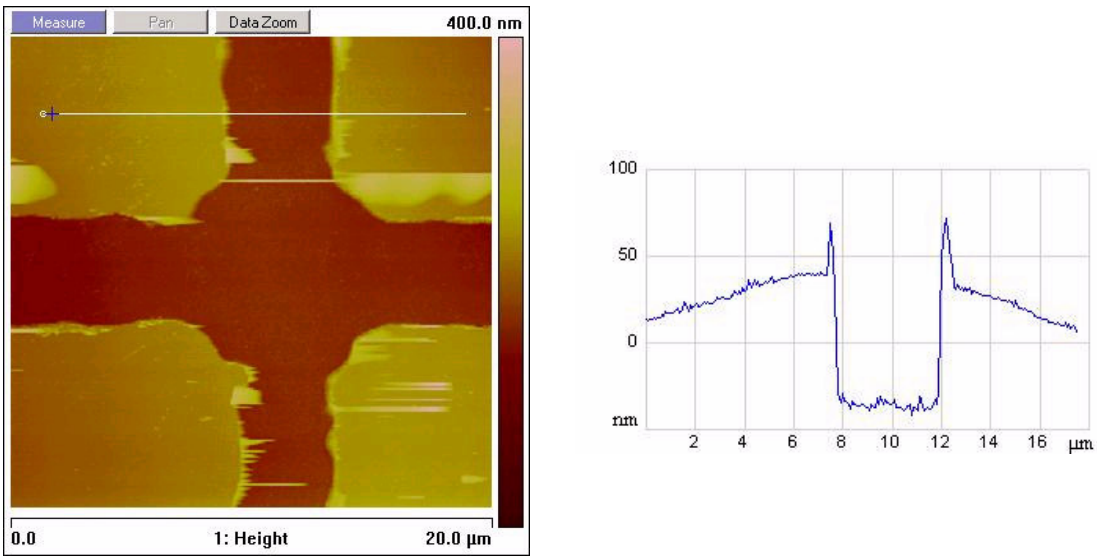

Figure 4.29. The section analyses of the mesas on BH3e

Figure 4.30 exhibits I-V dependence for an array of 14 junctions within BH3e. As it can be seen, the branches are fairly clear, which facilitates to count them and provides to determine the number of the branches with a great accuracy. Each of the branches was traced one by one in multiple runs with a small bias current sweep in a similar way done in optimally doped sample measurements.

From Figure 4.31, one can easily verify that there are 14 different quasiparticle branches in the plot. The value for the IJJ number obtained from I-V curve is quite close to AFM results. This indicates that while doing PCT measuments, all the problems related to heating were relatively minimized, which is maybe the most important consequence of the intercalation. If I-V characteristics are examined closely, the sharp current jumps can be seen at ±480 mV values, which determine the locations of quasiparticle peaks in the tunneling conductance plot. The value of 2Δ is around 32 meV as shown in Figure 4.32. The weak dip and hump structures at ±36 mV and ±40 mV respectively are signatures of the superconducting phase and both of them can been easily seen from the graph.

How I-V characteristics change with temperature can be seen from Figure 4.33 while dependence of tunneling conductance on temperature is shown in Figure 4.34. As going further temperatures, the I-V characteristics display a linear tendency. Although the feature of the I-V dependence changes with rising temperature values, we can not observe exact linearity in the experimental data even at higher temperatures. This property is generic for all high Tc cuprates. The IJJ spectra exhibit a rapid decrease in conductance peaks with increasing temperature.

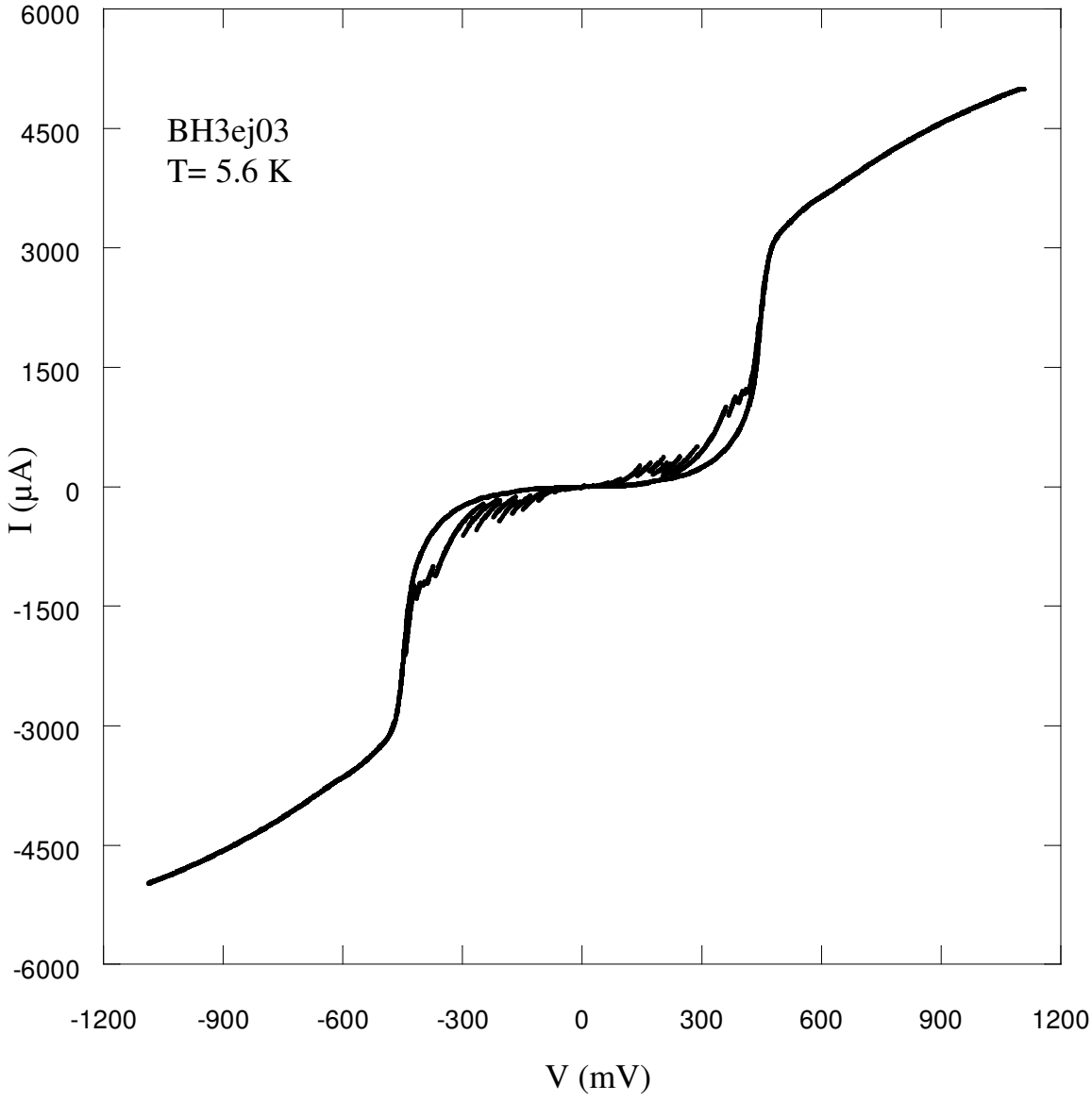

Figure 4.30. I-V charactersitics of BH3e at 5.6 K, which show pronounced quasiparticle current jumps at eV= 2Δ as well as weak Josephson current at zero bias.

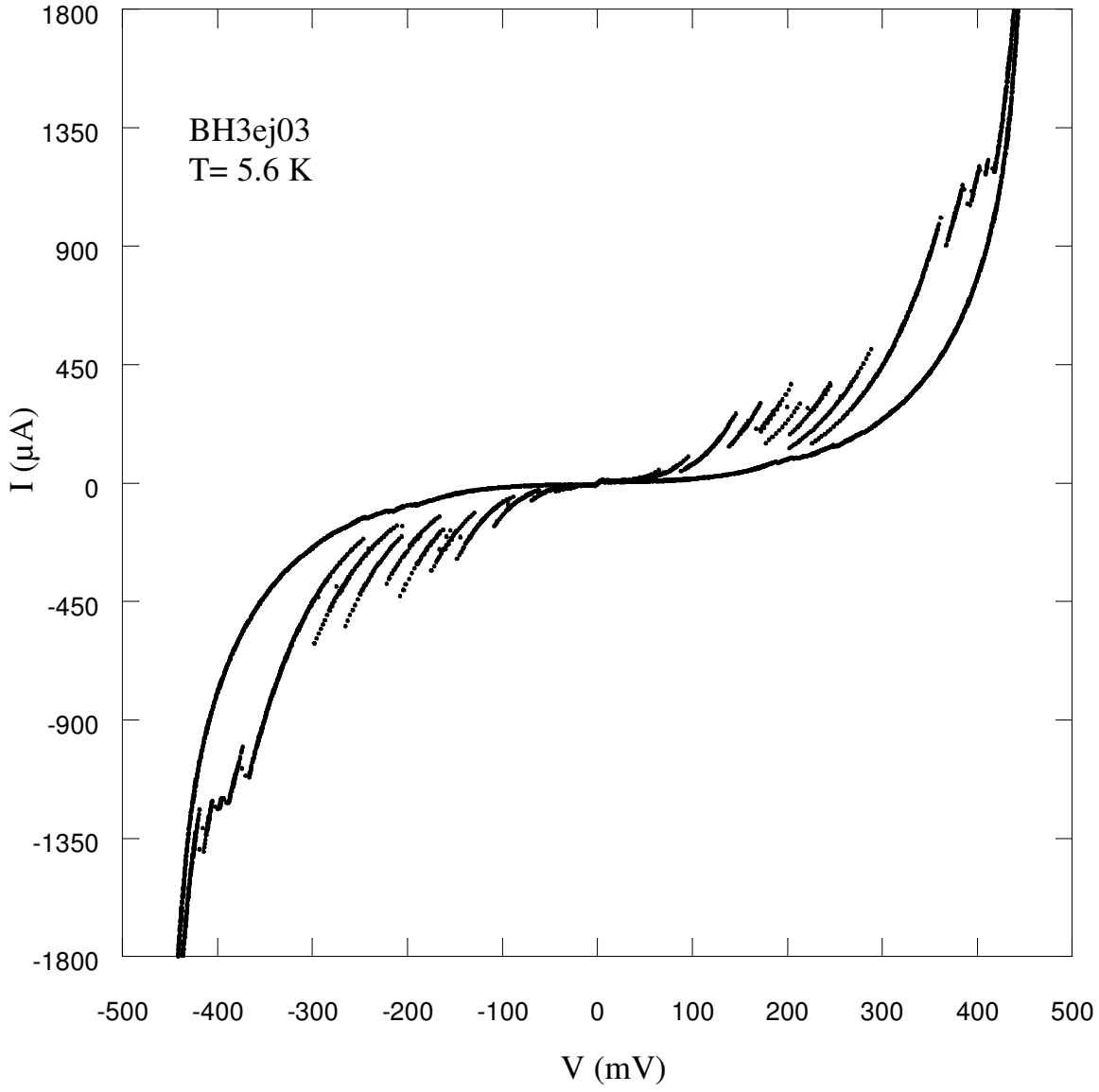

Figure 4.31. The I-V characteristics of BH3e at 5.6 K in detail

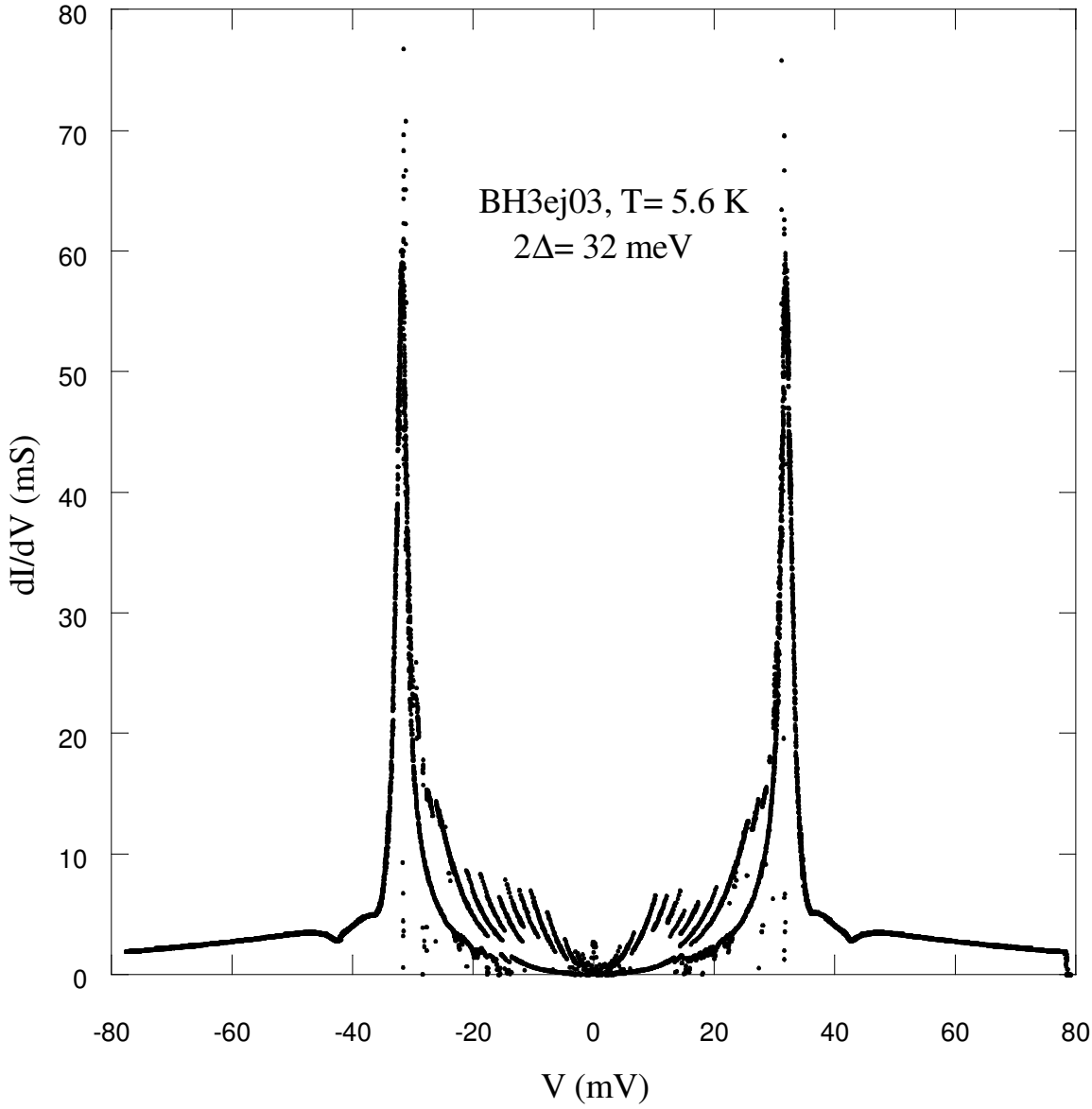

Figure 4.32. Tunneling conductance of BH3e at 5.6 K

When Figure 4.34 is examined, dip and hump structures can be observed between 5.6 K and 71 K values in the tunneling conductances. The dip feature in the dI/dV-V dependences which is the best defined at lowest temperature, 5.6 K, begins to disappear gradually while going further values of temperatures. At 99 K, we could not see any dip or hump characteristics in the dI/dV-V curves. Up to 150 K, normal state conductances have a rising tendency but above 150 K, curves begin to go down.

Actually IJJ spectra of intercalated samples are pretty similar to that of optimally doped ones. However, insertion of the inert $HgBr_2$ molecules causes to decrease of the c-axis critical current density. In turn, the heat release during I-V sweeps to reach the normal state part of the curves and nonequilibrium effects from a high density of injected quasiparticles are decreased, resulting in a disappearance of the common backbending of I-V at large bias (Yurgens and Claeson, 2001).

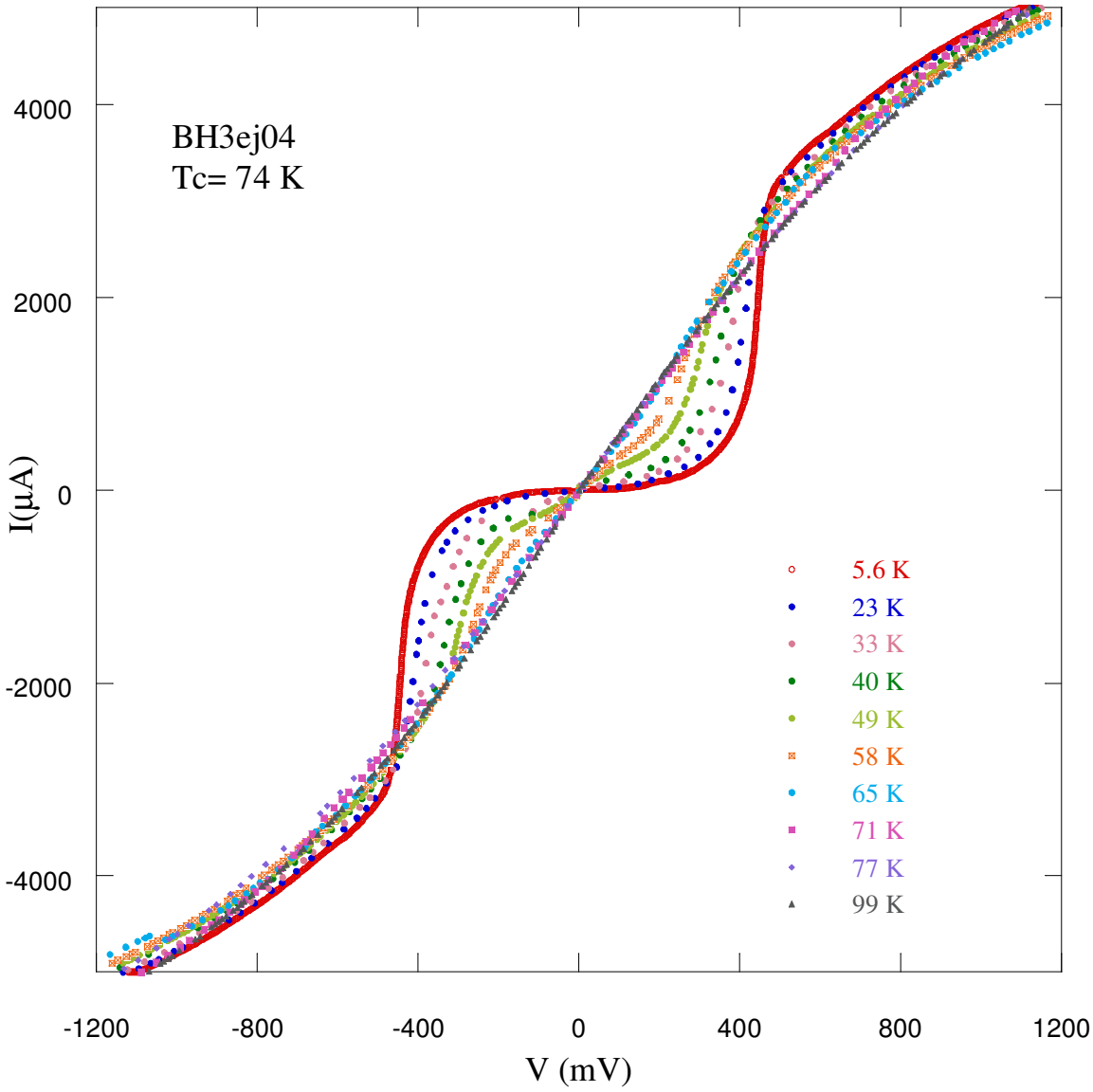

Figure 4.33. I-V characteristics of BH3e at different temperatures

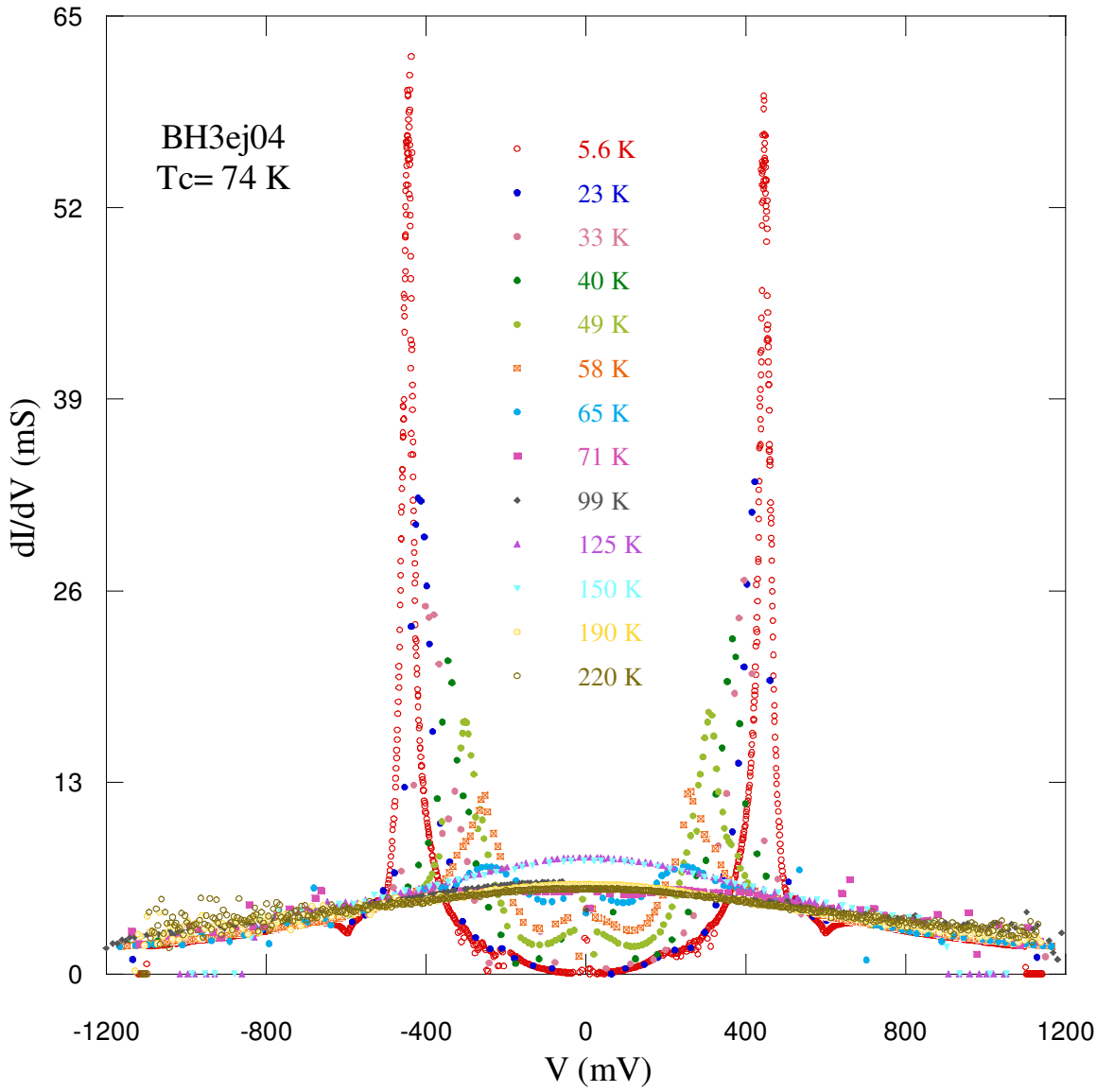

Figure 4.34. Evolution of dynamical conductances of BH3e with temperature

Figure 4.35 shows normalized gap voltage versus normalized temperature for BH3e. The voltage values corresponding peak positions in dI/dV-V characteristics decrease with temperature. To probe the suitability of the experimental results with BCS prediction, both voltage and temperature data were normalized by maximum constant values (These constants are the peak voltage value at the lowest temperature for voltage axis normalization and critical temperature for temperature axis normalization).

According to BCS model, at the critical temperature, there is no energy gap in the spectra, while experimental data still indicate the presence of a gap-like feature. From the figure, one can see the considerable deviation from the BCS prediction. Experimental data suggest that the superconducting energy gap does not go to zero at transition temperature (Yurgens et al. 1996b).

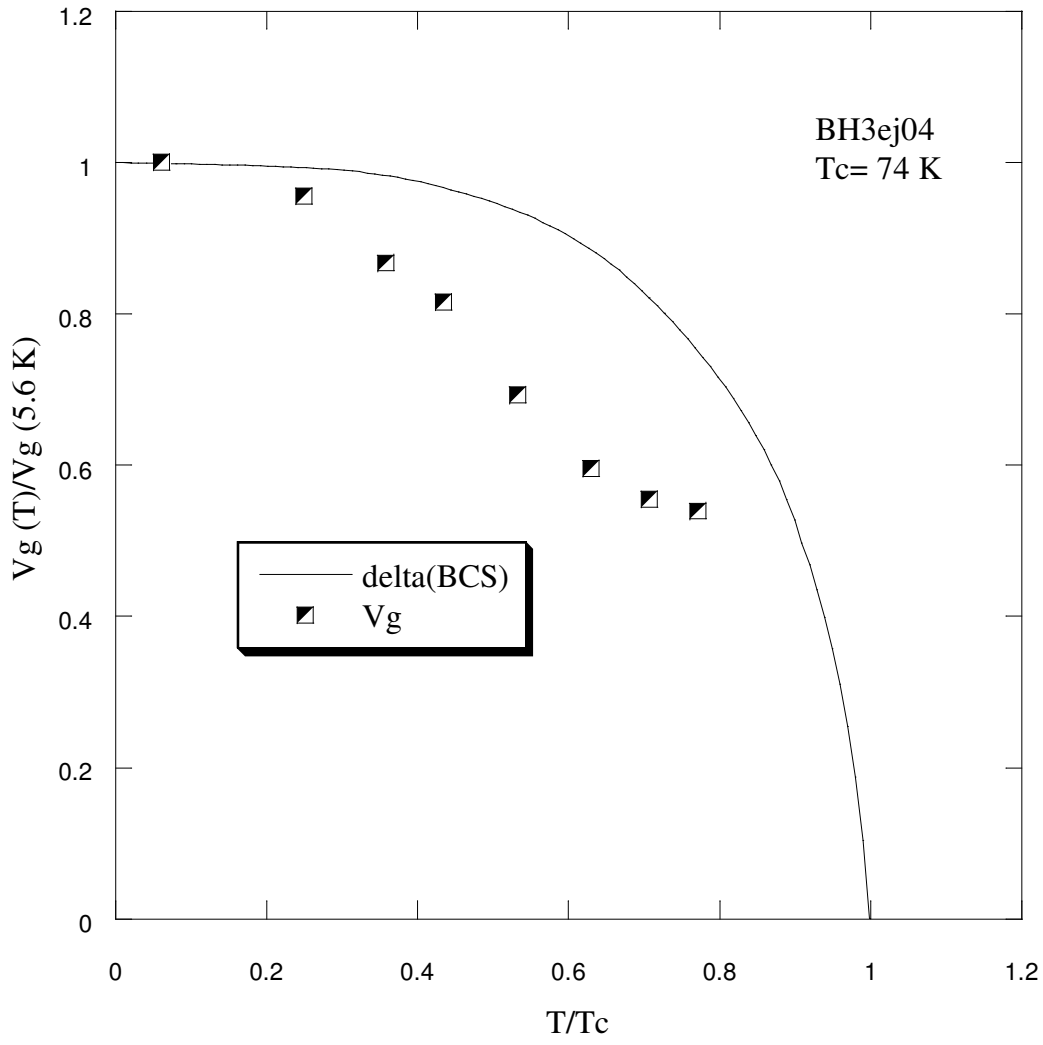

Figure 4.35. Normalized gap voltage-normalized temperature dependence for BH3e

Figure 4.36 exhibits zero bias conductance dependence on temperature for BH3e. There is an increasing trend in ZBC with temperature up to 125 K. After 150 K, ZBC begins to drop dramatically.

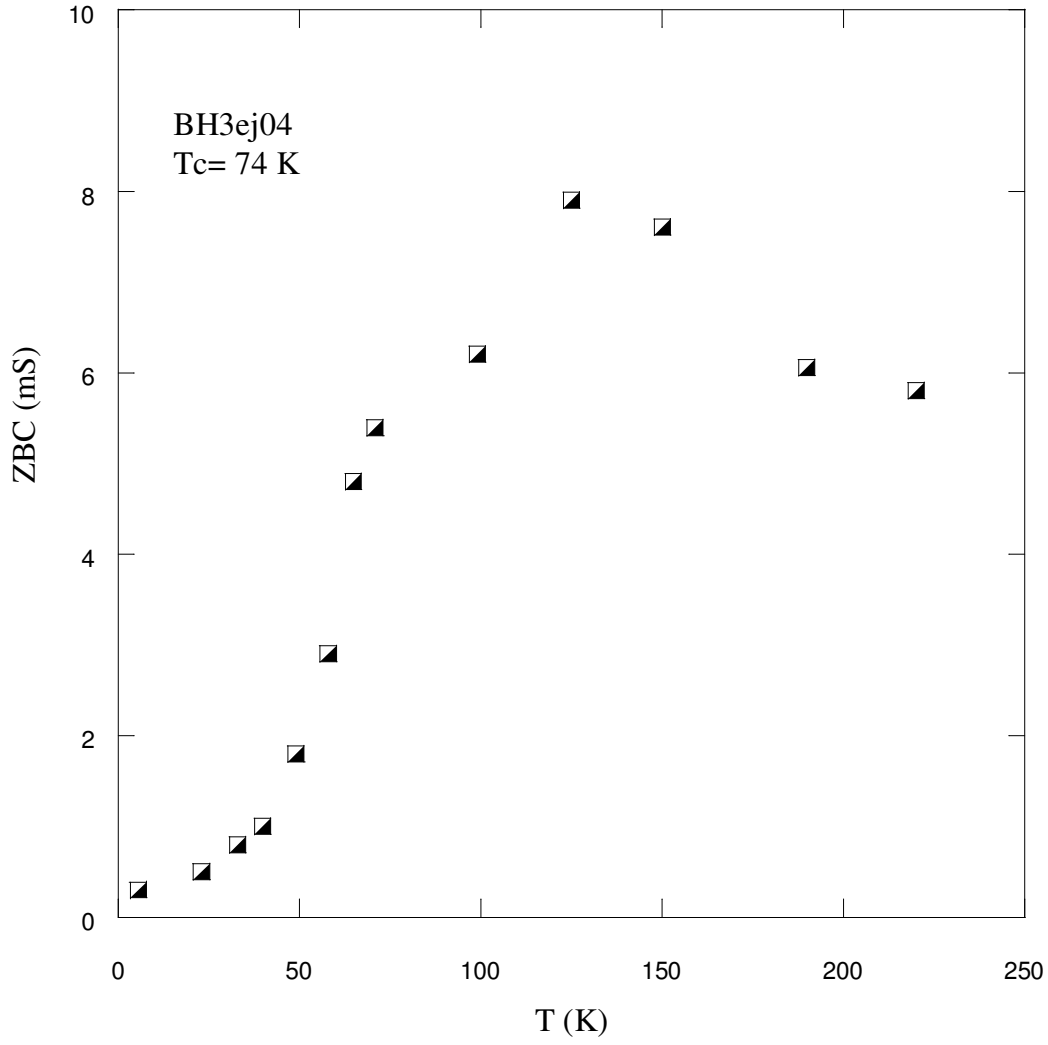

Figure 4.36. Zero bias conductance versus temperature of BH3e

Other investigated specimens are BH4d and BH5b, whose crystal stoichiometries differ from previous ones in that especially rich calcium content. In order to prepare BH4d and BH5b samples, $10x10\mu m^2$ sized mesas were fabricated on intercalated Bi-2212 single crystals with T_c= 74K using aforesaid techniques. The mesa height of the BH4d is approximately 65 nm, while that of BH5b is 119 nm. The gold film thicknesses are different for two crystals: former has 35 nm gold film layer and this value is 74 nm for the latter one. Figure 4.37 shows multi-branches in the I-V

characteristics of a mesa on BH4d sample while Figure 3.38 exhibits the tunneling conductance of the same mesa.

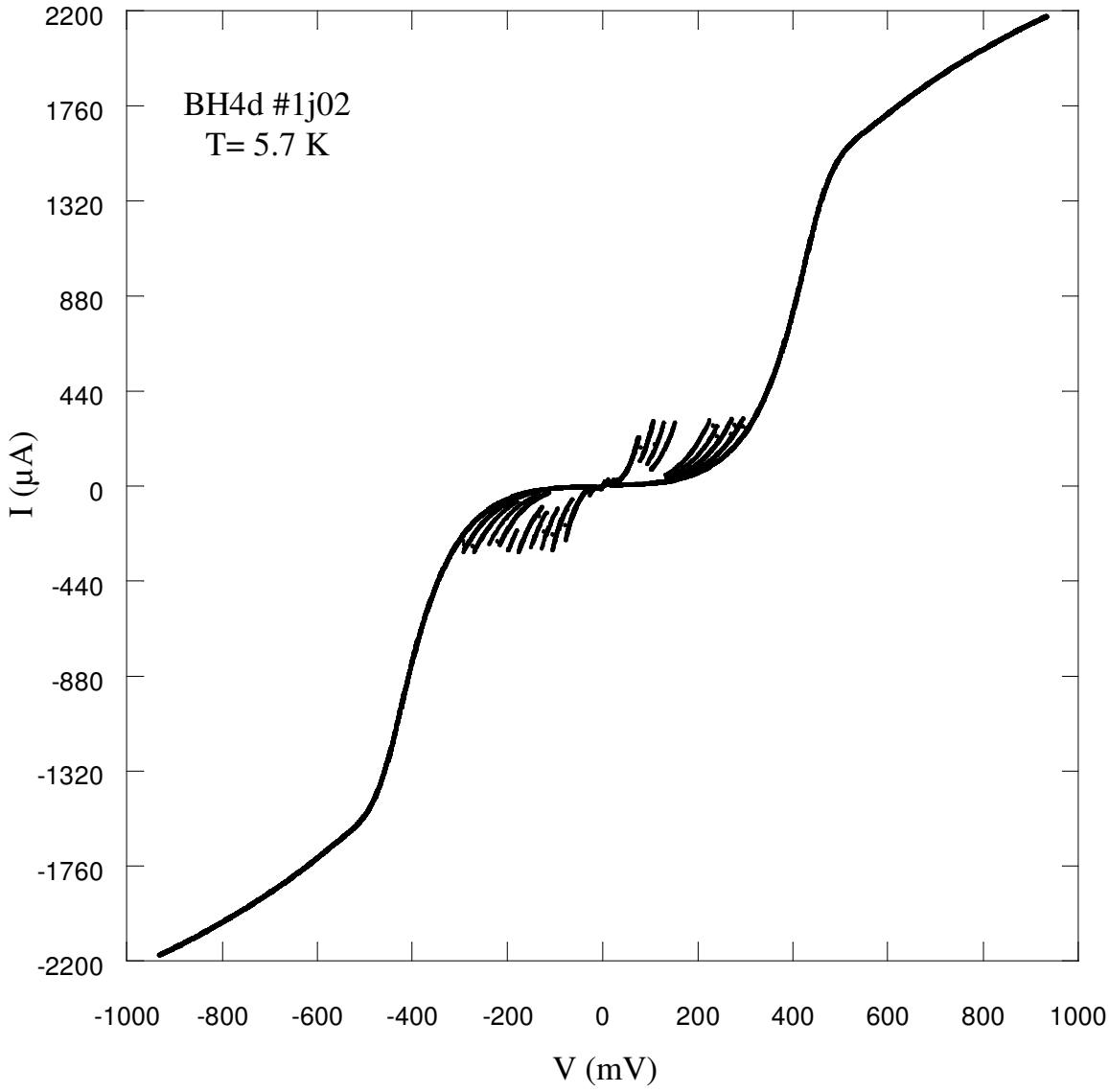

Figure 4.37. I-V characteristics of a mesa on BH4d at 5.7 K

12 quasiparticle branches can be observed from Figure 4.37 for concerned mesa on BH4d. The peak positions of the tunneling conductance characteristics match ± 427 mV in the quasiparticle spectra. These curves can be generated by using the original data. If genuine value of the energy gap is wished to obtain, the gap voltage values should be divided by number of the IJJ. This value can be found as 36 meV by dividing 427 by 12.

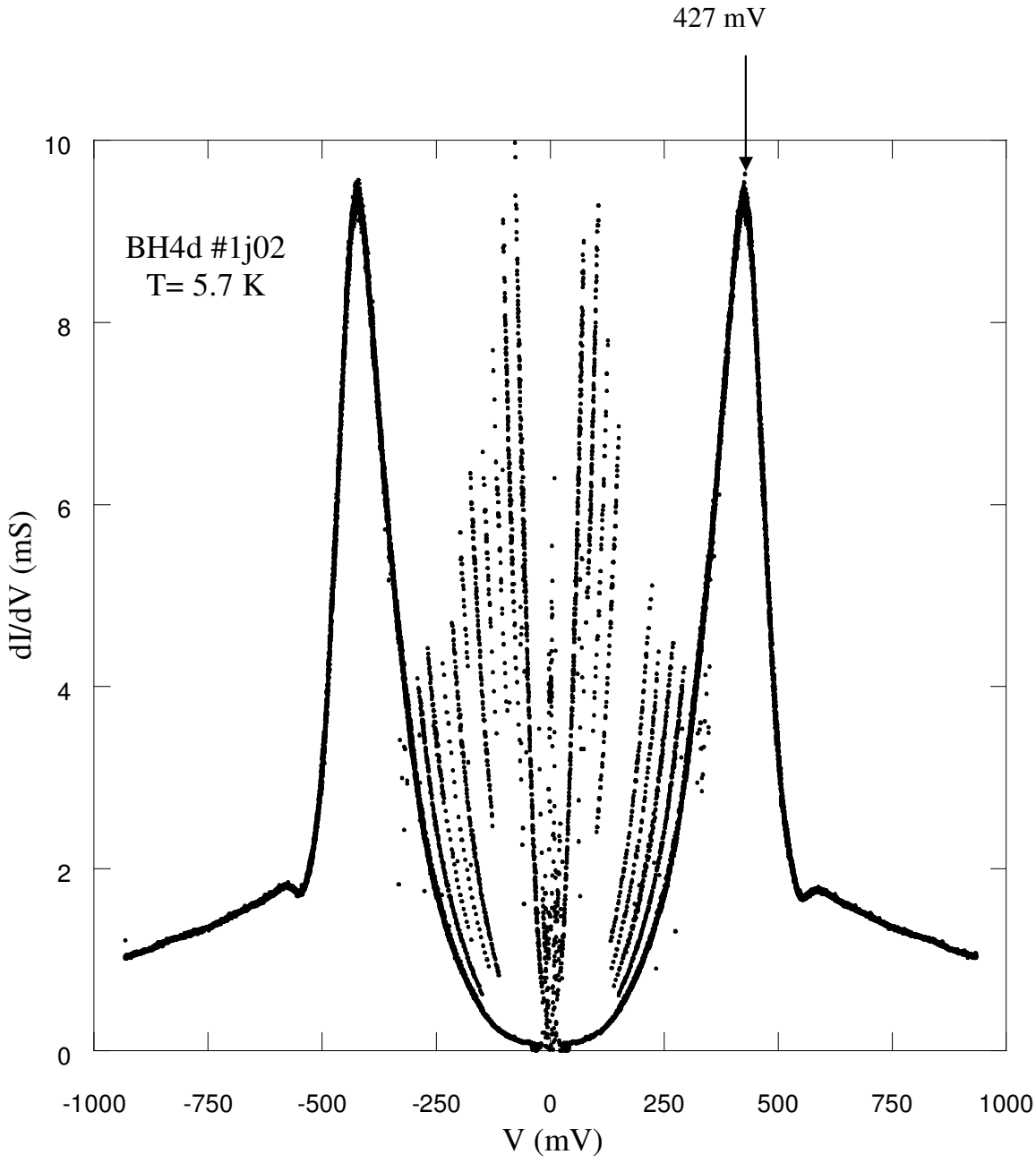

Figure 4.38. Tunneling conductances of a mesa on BH4d at 5.7 K

Another mesa on BH4d gives a little bit different style of I-V dependence and conductance characteristics shown in Figure 4.39 and Figure 4.40 respectively. Note that there is no dip/hump features in conductance curves as encountered in the previous mesa on BH4d (BH4d#1). Another difference is the number of the branches obtained by I-V characteristics. From Figure 4.39, one can see 21 quasiparticle branches which give the IJJ number in BH4d#2.

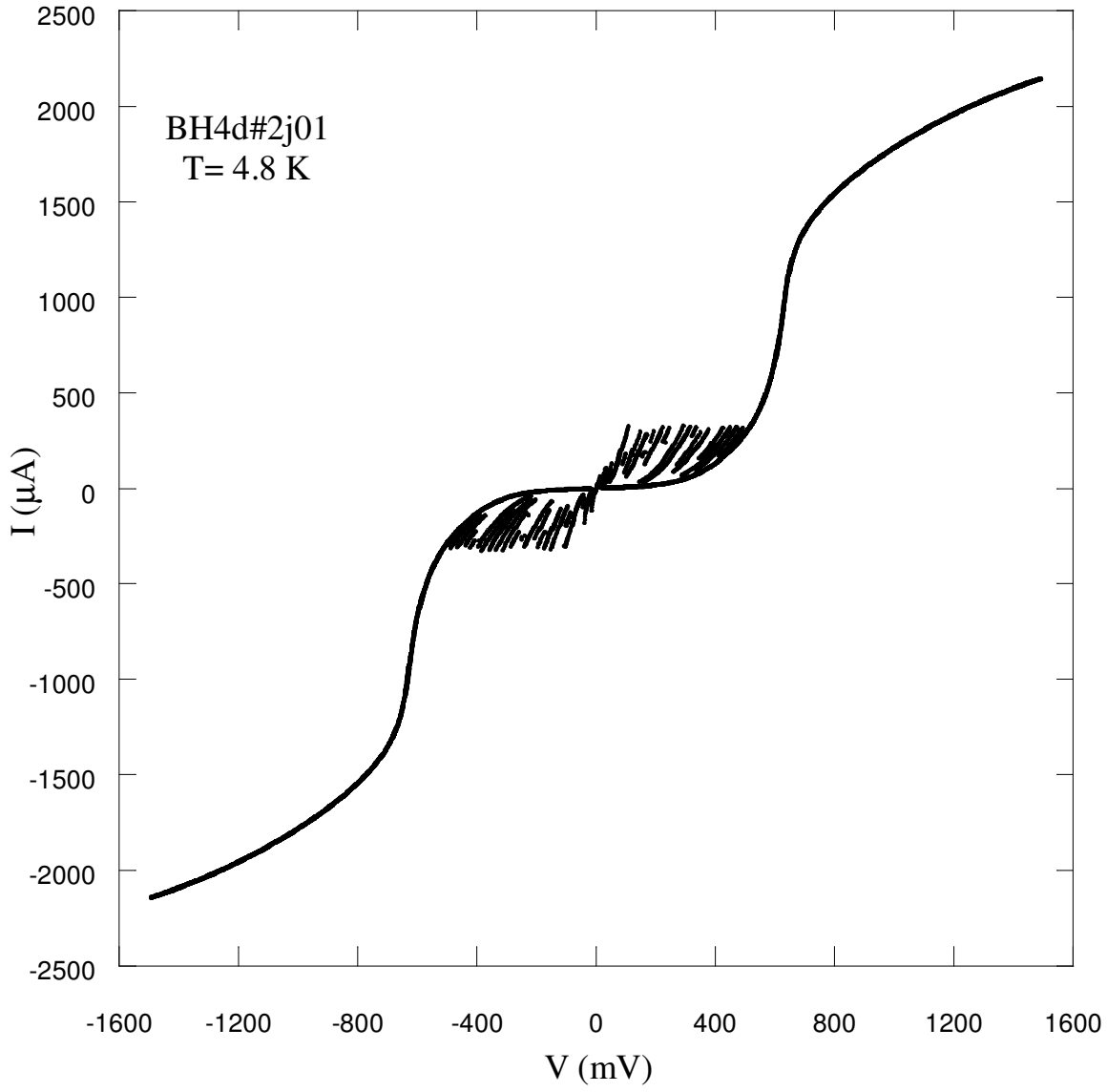

Figure 4.39. I-V characteristics of a second mesa measured on BH4d

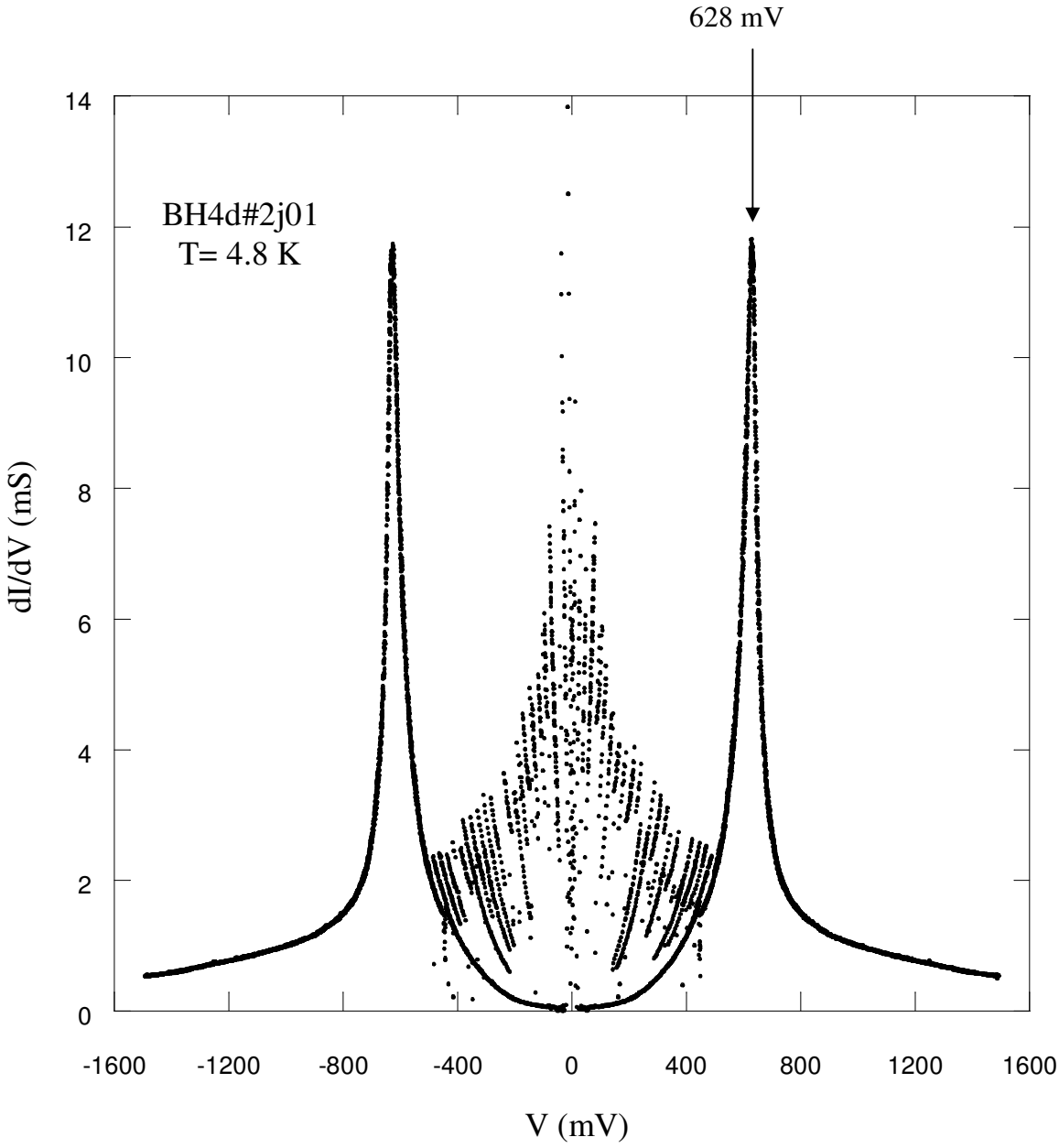

Figure 4.40. Tunneling conductances of a second mesa measured on BH4d

The results of the last mesa measured on BH4d are shown in Figure 4.41 and Figure 4.42. The IJJ characteristics on this mesa also do not exhibit peculiar spectral features (dip and hump structures). One can count 19 quasiparticle branches in the I-V characteristics of BH4d#3. The quasiparticle peak positions are different in each mesa due to the various number of the IJJ along the c-axis. The difference can be a result of inhomogeneous exposure of Ar ion beam etching of crystal or rough surface due to the poor quality of photolithography as mentioned before.

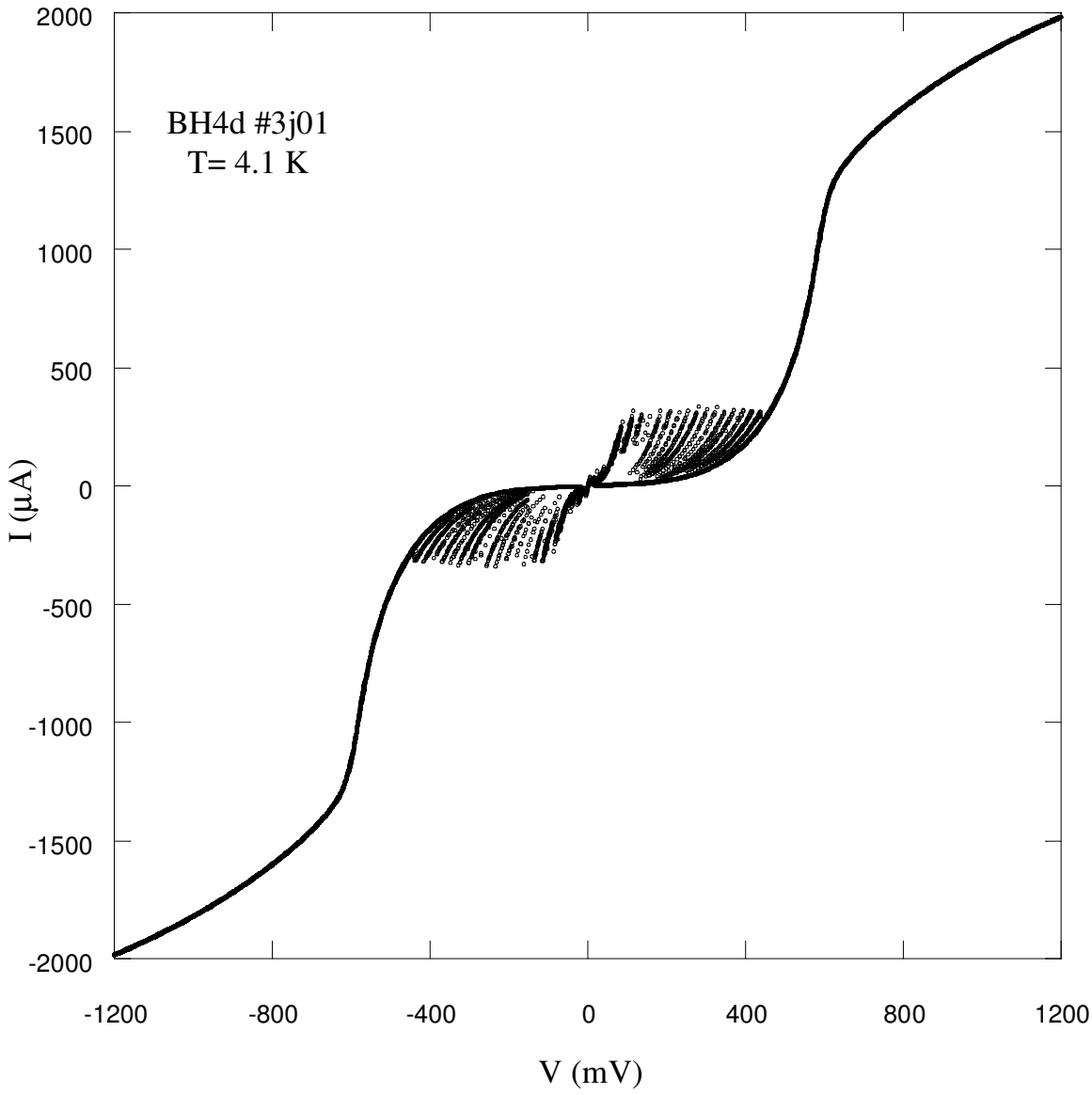

Figure 4.41. I-V characteristics of a third mesa measured on BH4d at 4.1 K

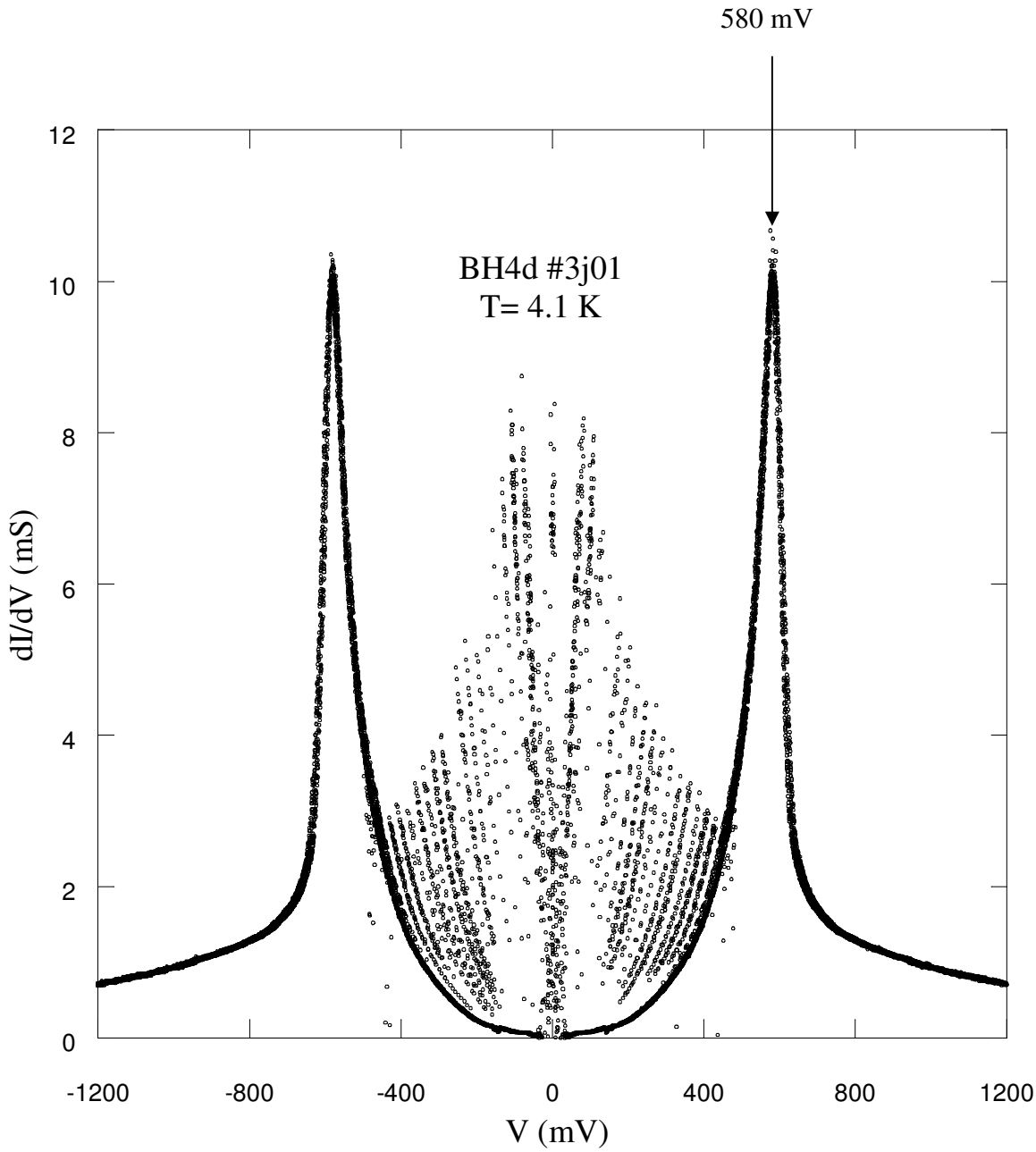

Figure 4.42. Tunneling conductances of a third mesa measured on BH4d

The temperature dependence of current-voltage characteristics of BH4d sample is shown in Figure 4.43. Because of the change in tip pressure on the mesa surface while doing measurement, some data obtained at higher bias do not give a good result to create a plot. So after 62 K, we could not get pronounced I-V characteristics for BH4d#1. Figure 4.44 shows dynamical conductances at various temperatures for BH4d#1.

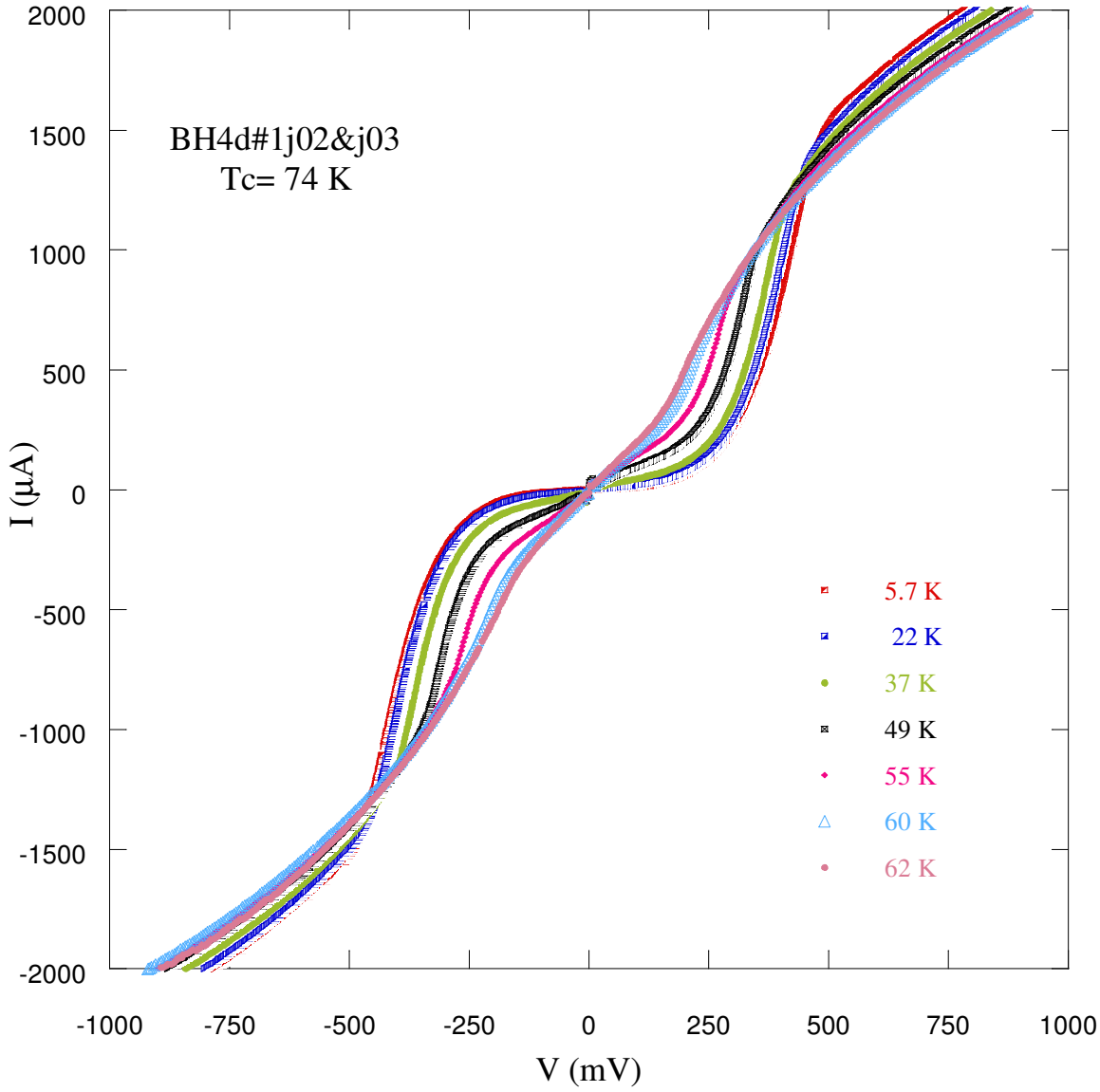

Figure 4.43. I-V curves at various temperatures belonging to BH4d#1

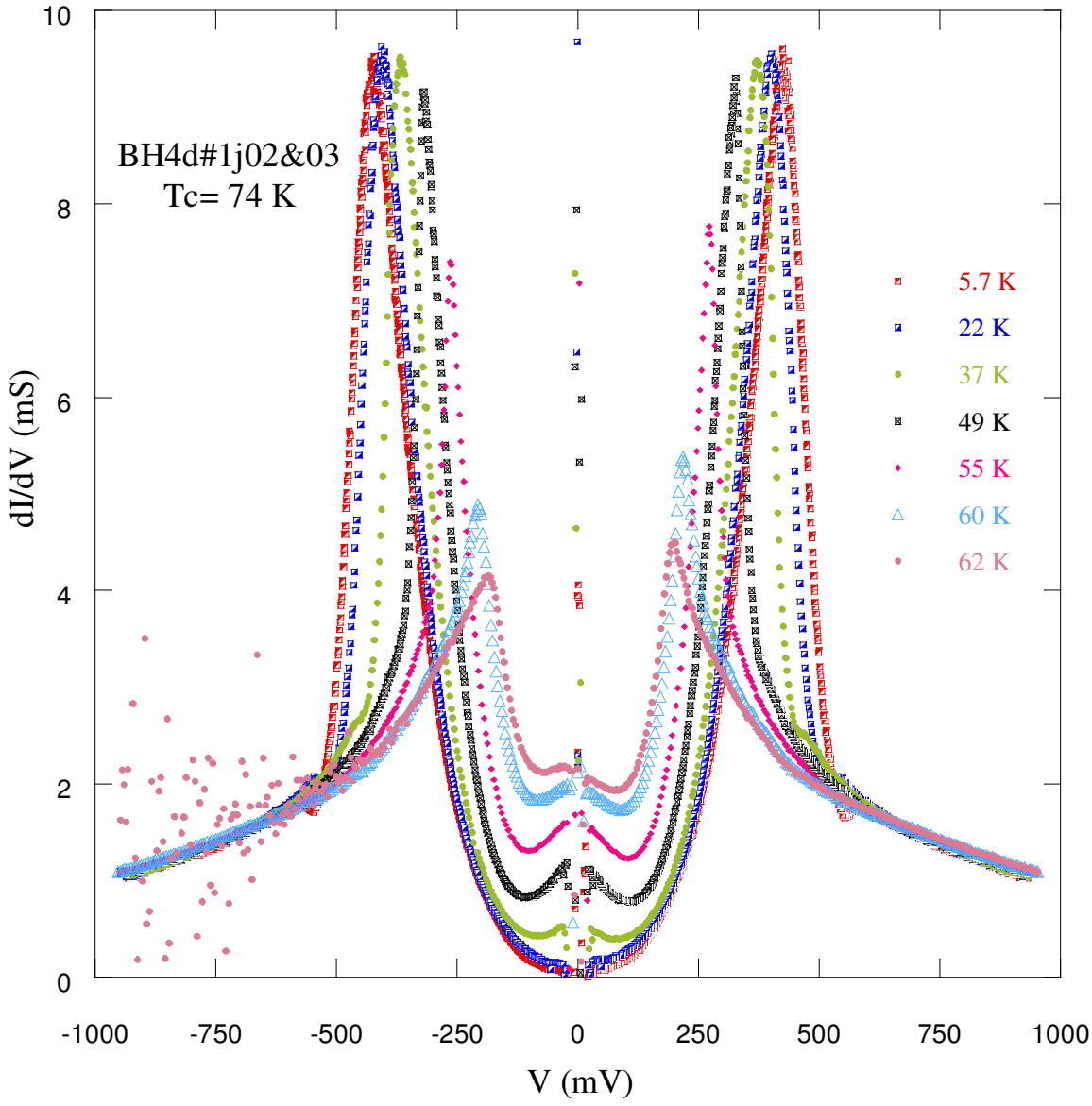

Figure 4.44. Dynamical conductances of BH4d#1 dependent on temperature

Figure 4.45 shows the low temperature conductance curves of BH4d#1 exhibiting dip and hump structures. The detailed parts of these curves are shown in Figure 4.46(a) and Figure 4.46(b). The temperature dependence of the I-V curves and c-axis conductances for BH4d#2 are shown in Figure 4.47 and Figure 4.49 respectively. Also the detailed features of the I-V characteristics for this mesa can be seen from Figure 4.48. Some striking deviations in tunneling conductances which belong to examined second mesa on BH4d can be observed from Figure 4.49. Note that tunneling

conductance curves at 4.8 K, 26 K and 36 K. According to literature and previous results, the quasiparticle peaks will be lower with increasing temperature. The first three curves do not follow expected trend of tunneling data dependent on temperature. Beyond 36 K, tunneling conductances display usual behaviors.

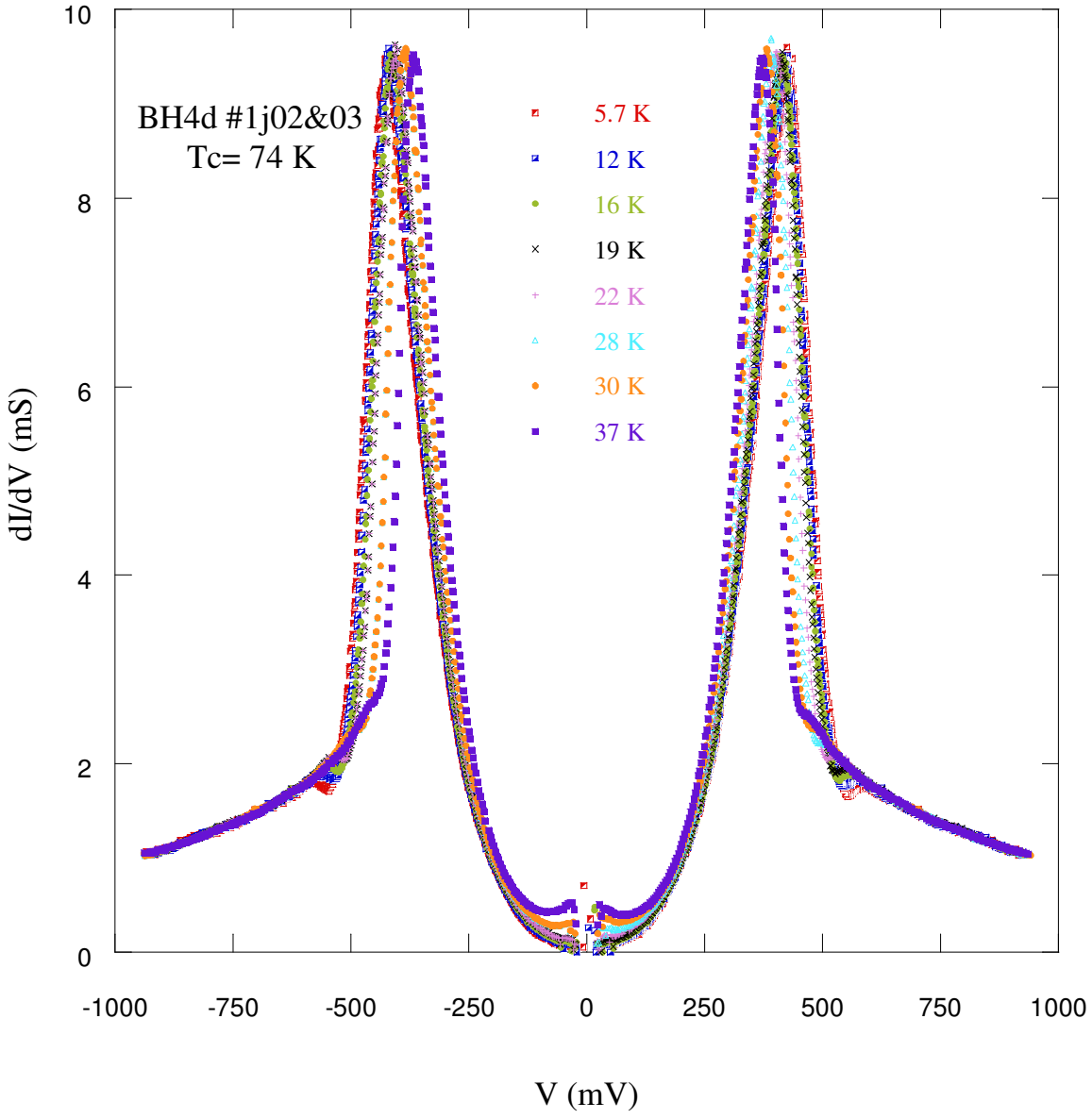

Figure 4.45. The dip structures of BH4d#1 at low temperatures

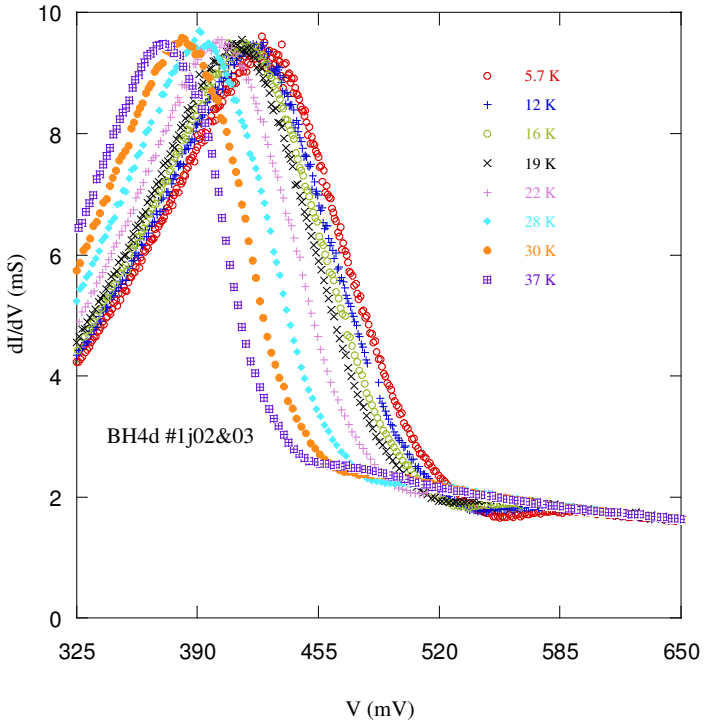

Figure 4.46(a). Gap voltages in BH4d#1 conductances at low temperatures

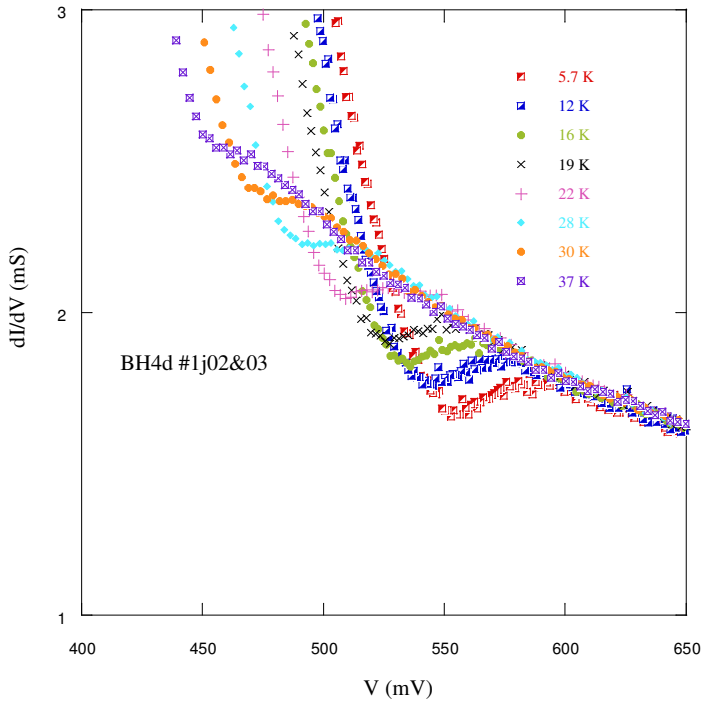

Figure 4.46(b). Dip/hump structures in BH4d#1 conductances at low temperatures

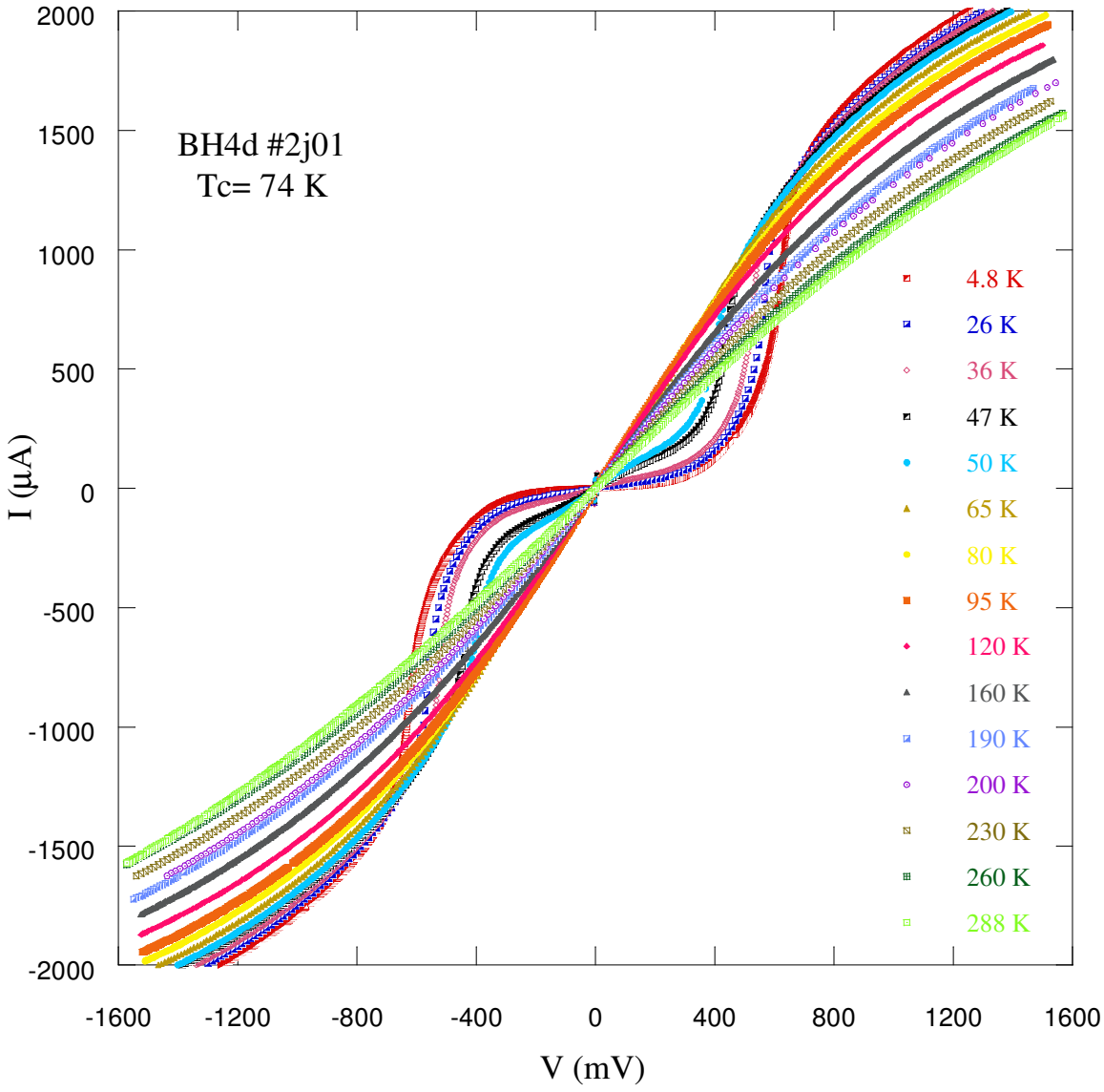

Figure 4.47. I-V dependence on temperature for BH4d#2

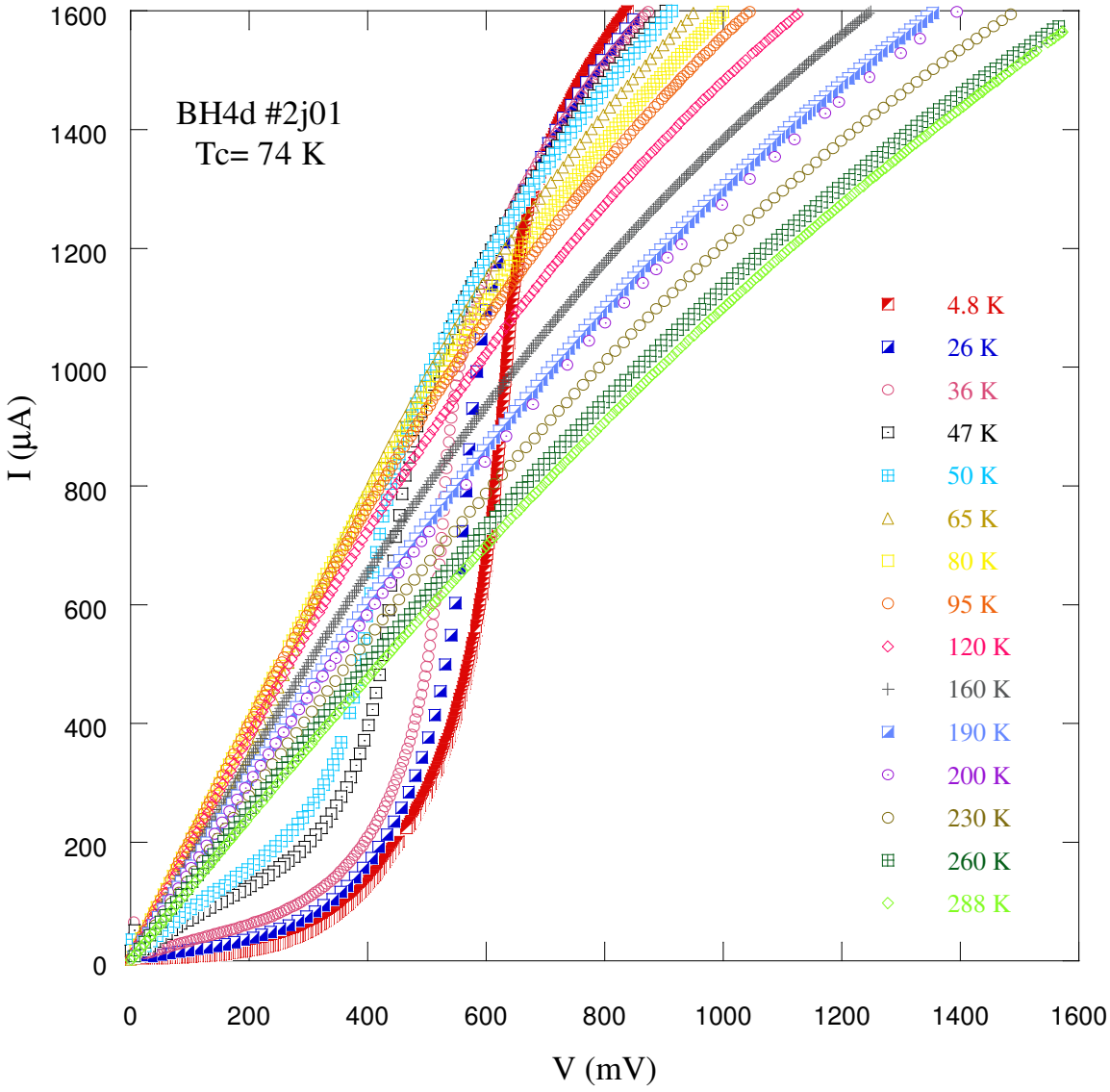

Figure 4.48. Detailed I-V curves at certain different temperatures for BH4d#2

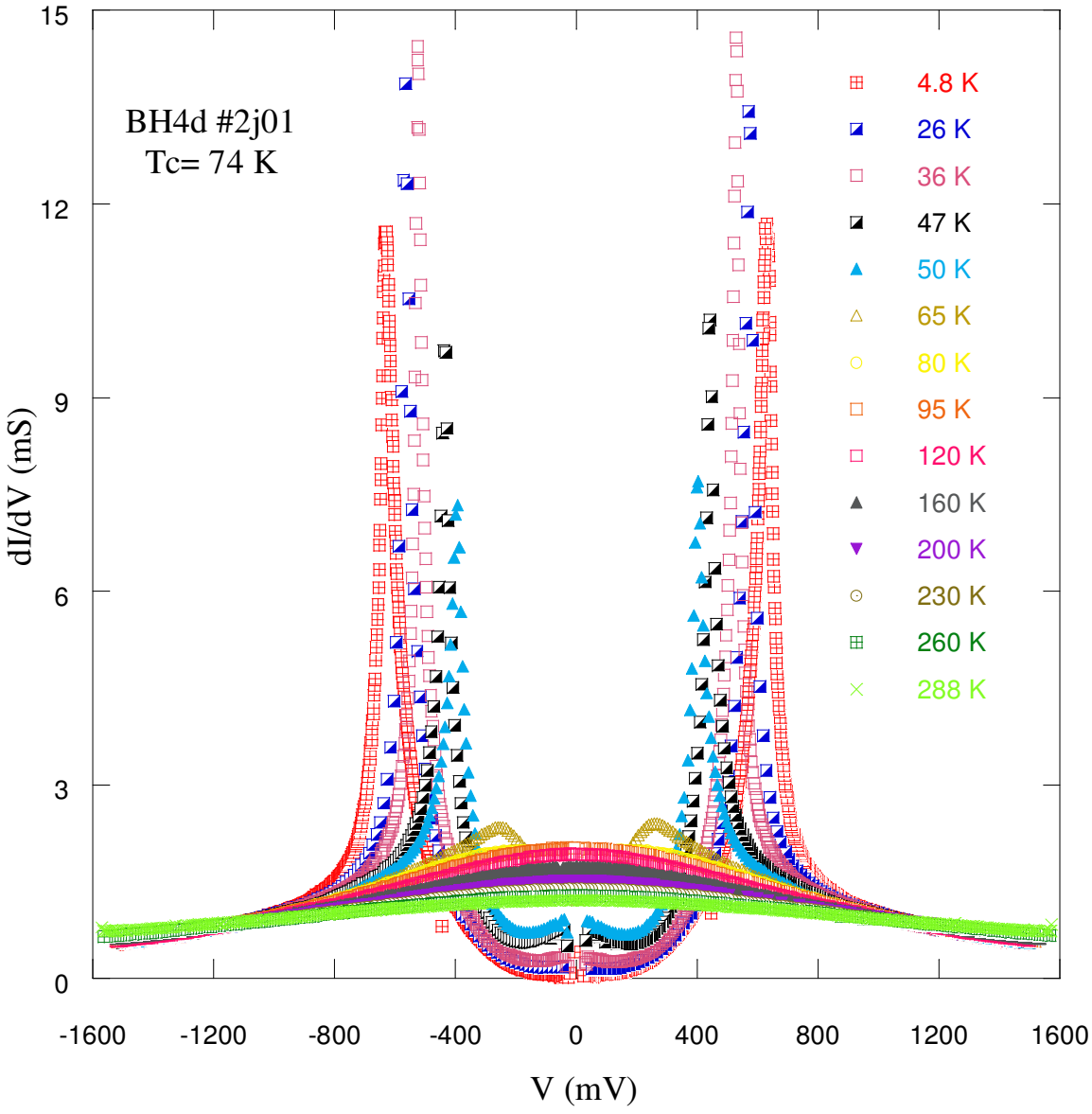

Figure 4.49. Dynamical conductances of BH4d#2 at different temperatures

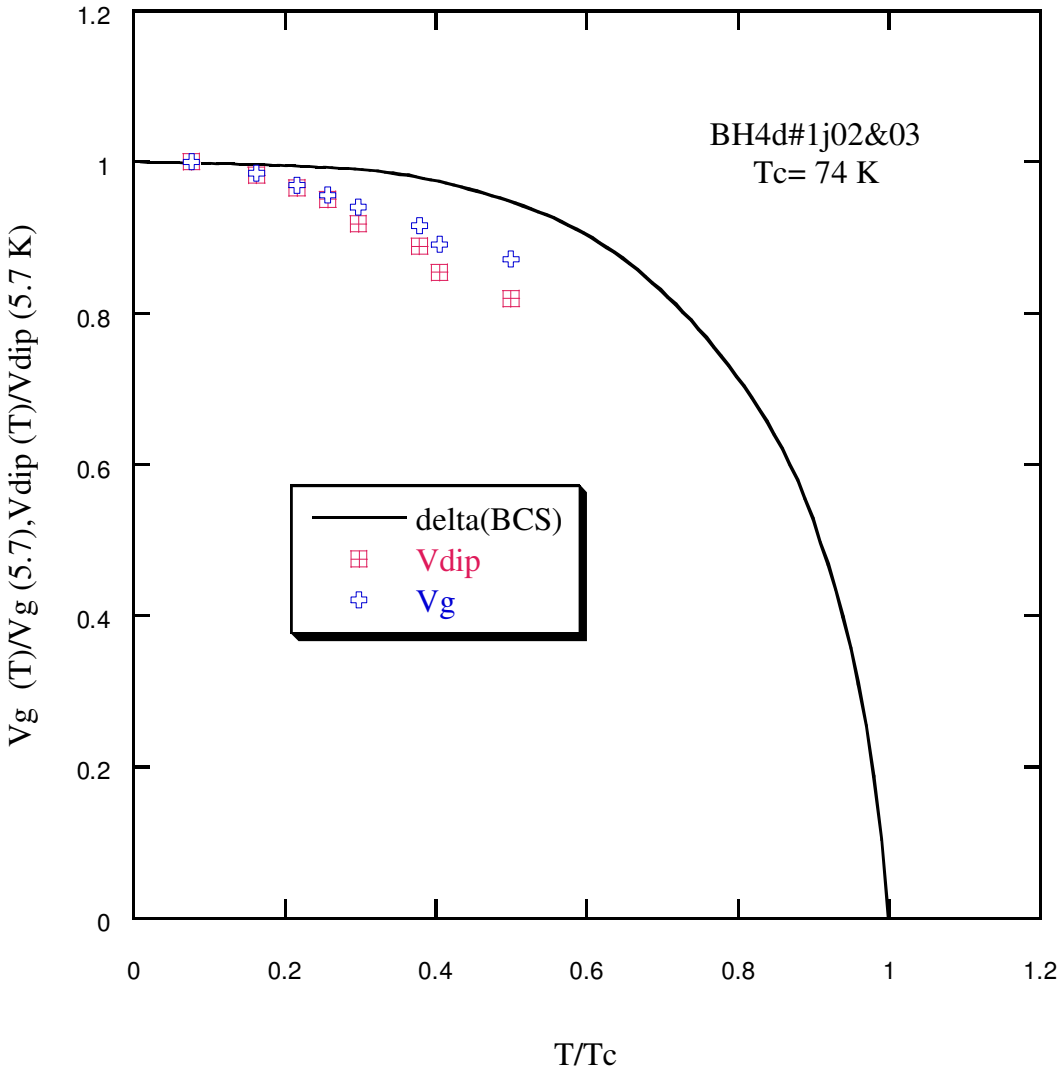

Figure 4.50. Normalized gap and dip voltages dependent on normalized temperature

Using the data of Figure 46(a) and Figure 46(b), normalized gap voltage and normalized dip voltage can be compared in same plot as shown in Figure 4.50. Figure 4.51 exhibits normalized gap voltage by the voltage value at the lowest temperature vs. normalized temperature by critical temperature of material (almost 74 K). The BCS prediction dependent on temperature can be observed from the same plot; which gives a insight about the suitability of theoretical and experimental data. The gap voltage decreases much more rapidly with increasing temperature than that predicted by BCS theory. The experimental data show that the gap voltage never becomes zero at the vicinity of critical temperature. Zero bias conductance vs. temperature plot can be seen from the Figure 4.52

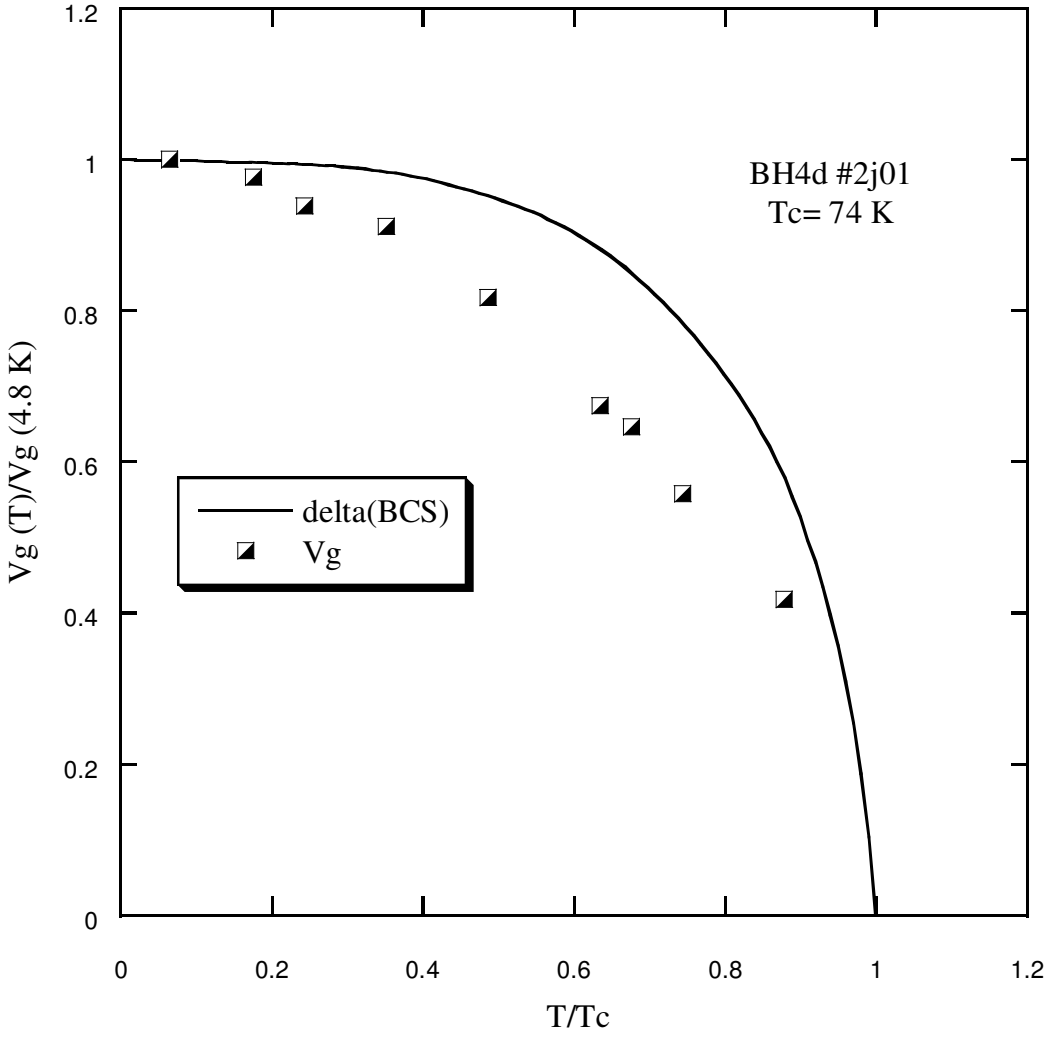

Figure 4.51. Normalized gap voltage versus normalized temperature for BH4d#2

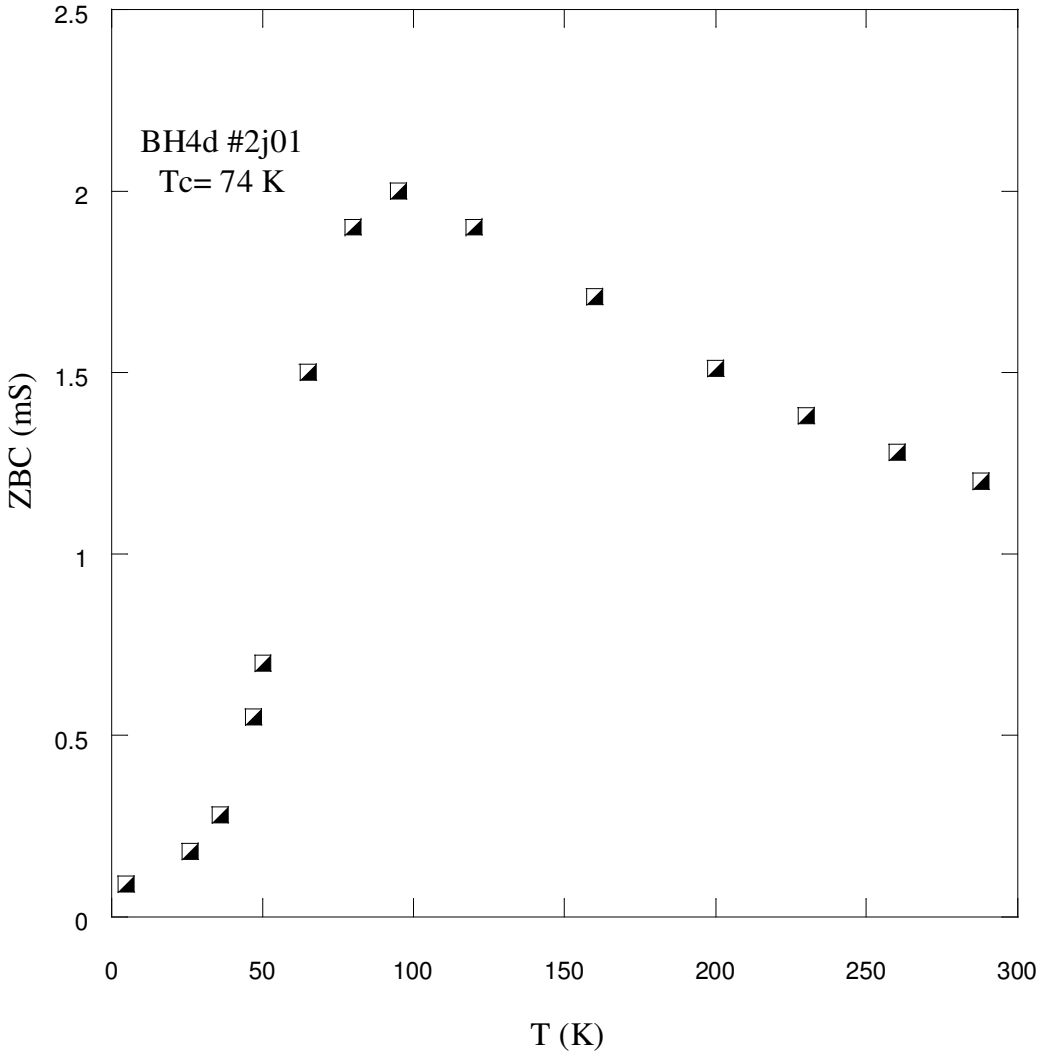

Figure 4.52. Zero bias conductance versus temperature of BH4d#2

Figure 4.53 illustrates the I-V characteristics obtained from BH5b while the tunneling conductance of this sample is shown in Figure 4.54. Nearly 30 quasiparticle branches can be distinguished from the current-voltage characteristics as shown in Figure 4.53.

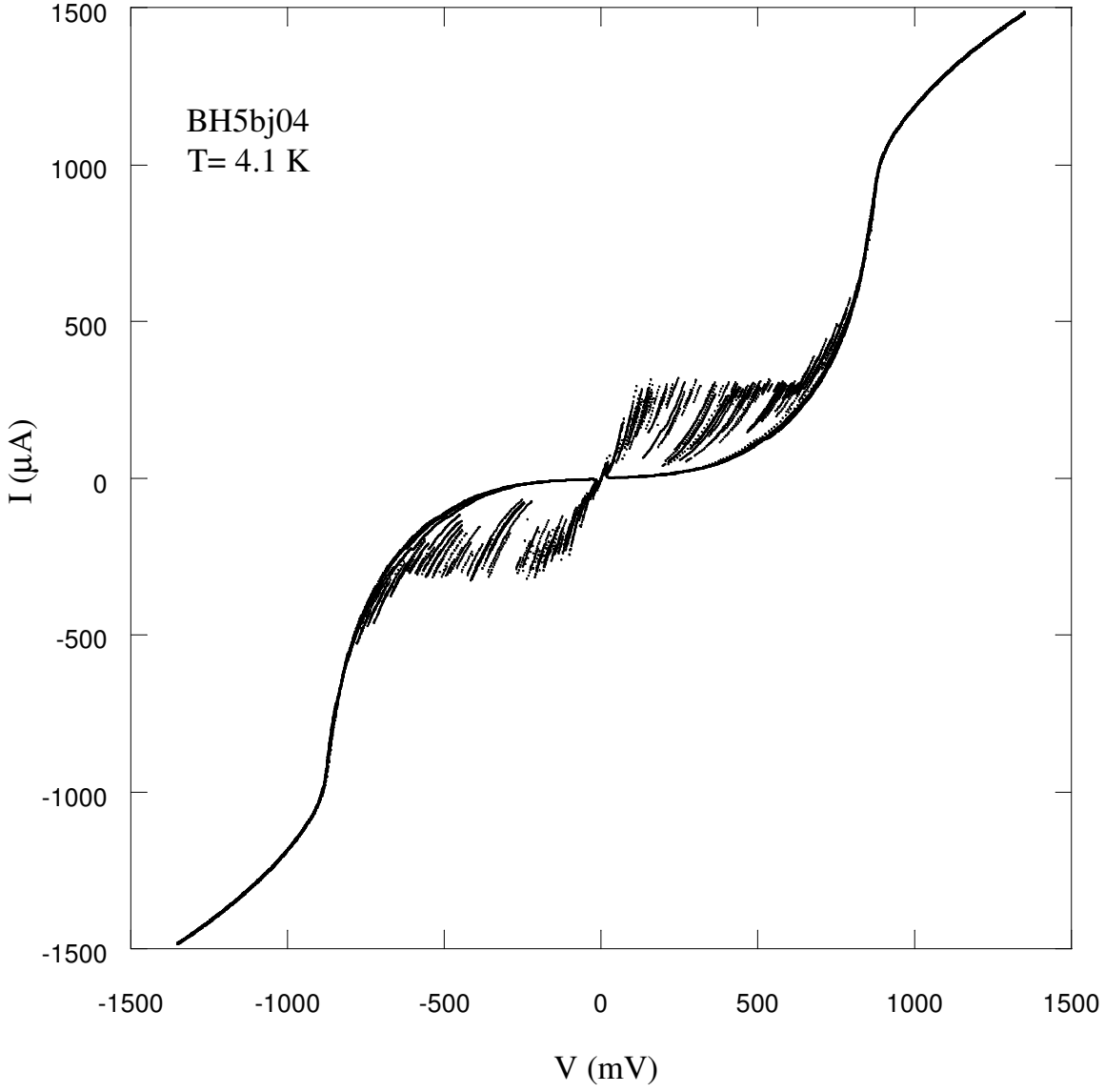

Figure 4.53. I-V characteristics obtained from BH5b mesas at 4.1 K

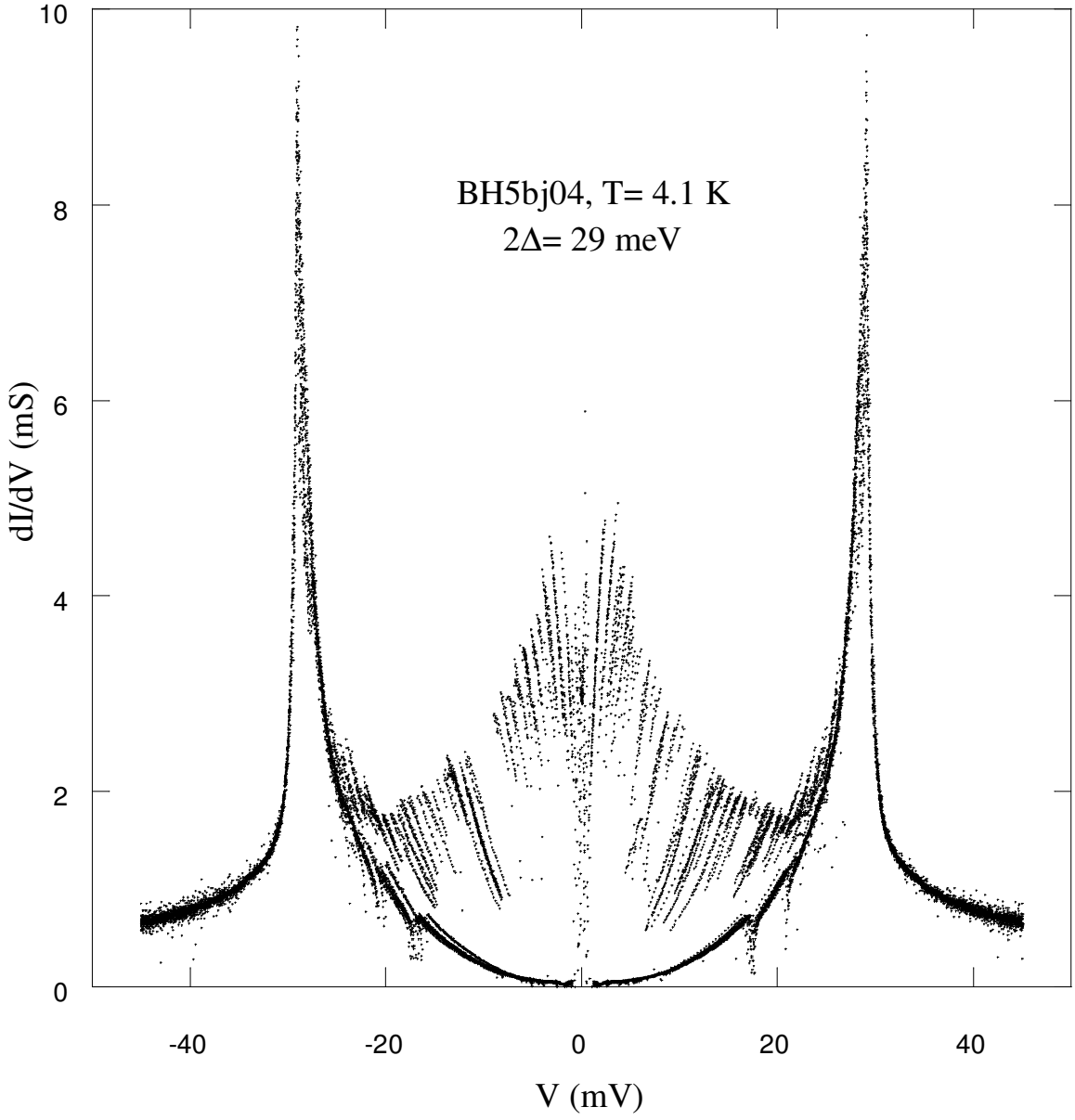

Figure 4.54. The c-axis tunneling conductance of BH5b at 4.1 K

The temperature dependent I-V characteristics and tunneling conductances are shown in Figure 4.55 and Figure 4.57 respectively. With increasing temperature the features of the I-V curves begin to be smooth but there is no exact linearity for the temperature values even well above critical temperature. The detailed information about the I-V characteristics of BH5b can be taken from Figure 4.56.

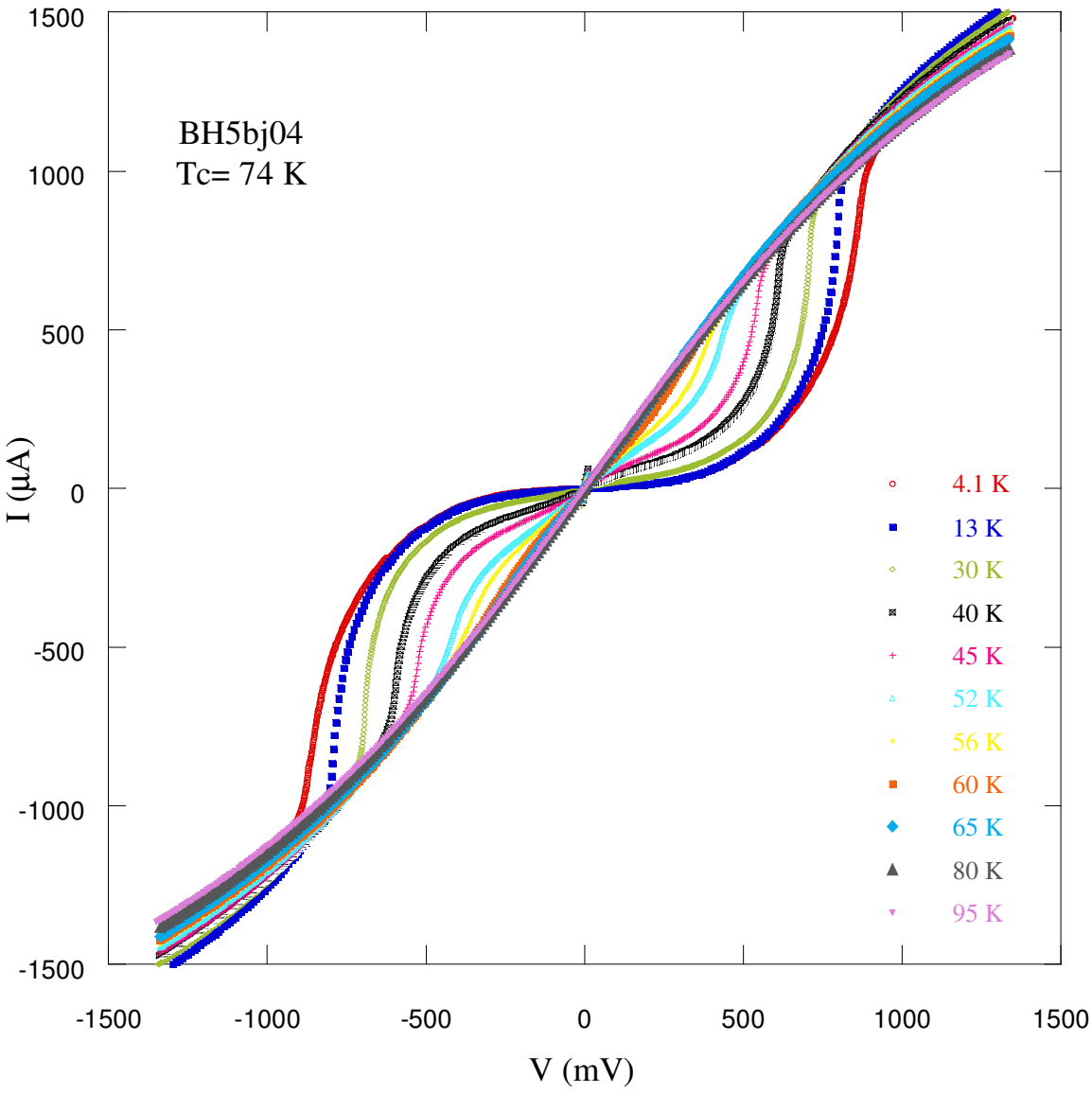

Figure 4.55. Tunneling conductances of BH5b with changing temperatures

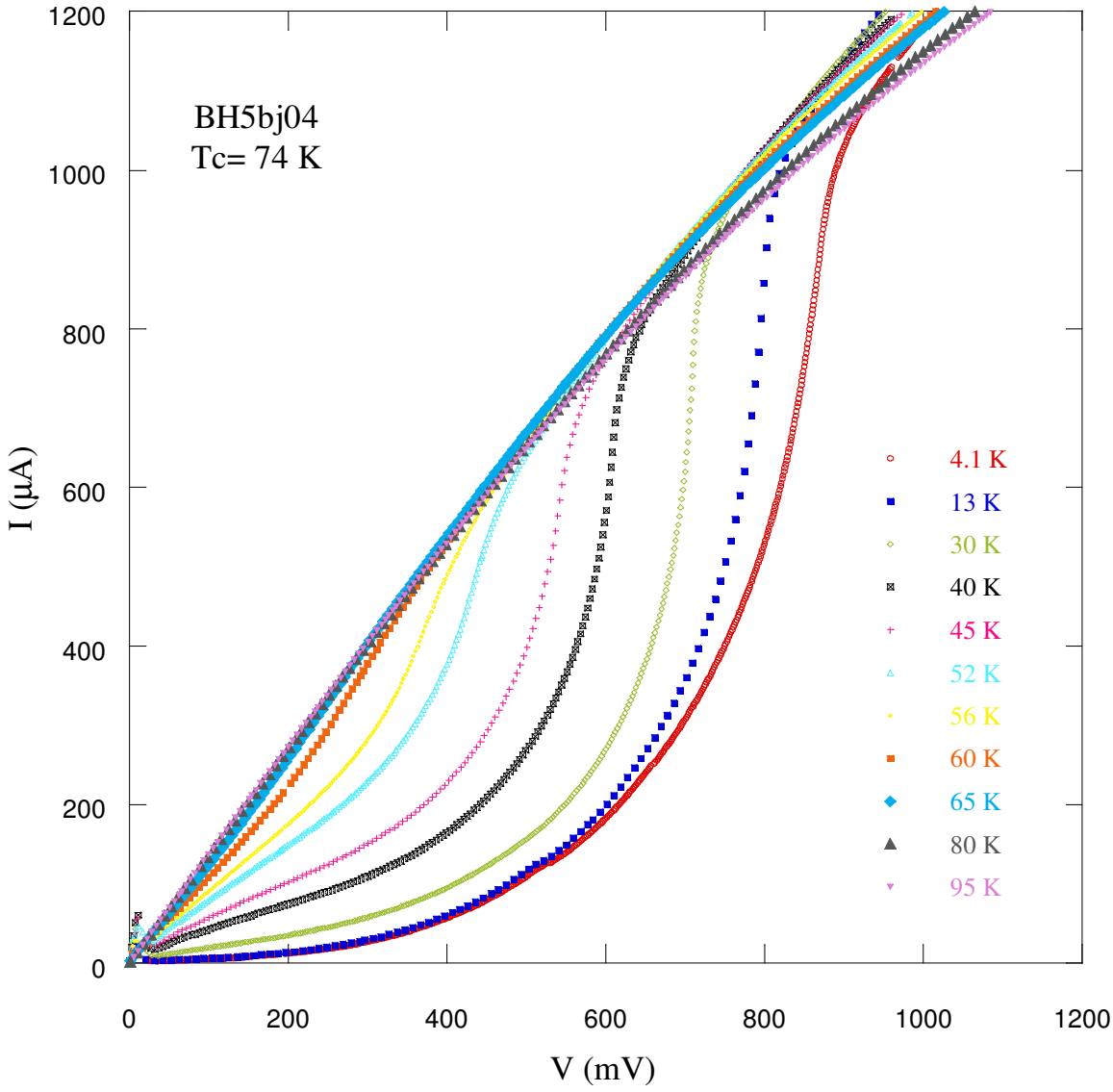

Figure 4.56. The more detailed representation of Figure 4.55

There is an eccentric behavior observed in the subgap regions of the tunneling conductances which belong to BH5b as shown in Figure 4.57. Note that two conductances corresponding to lowest temperatures do not demonstrate dip and hump structures which are associated with superconducting properties. Besides some quasiparticle peaks break the regular trend, e.g. the peak height at 13 K is higher than that at 4.1 K. The detailed part of the dI/dV-V plot can be seen from Figure 4.58.

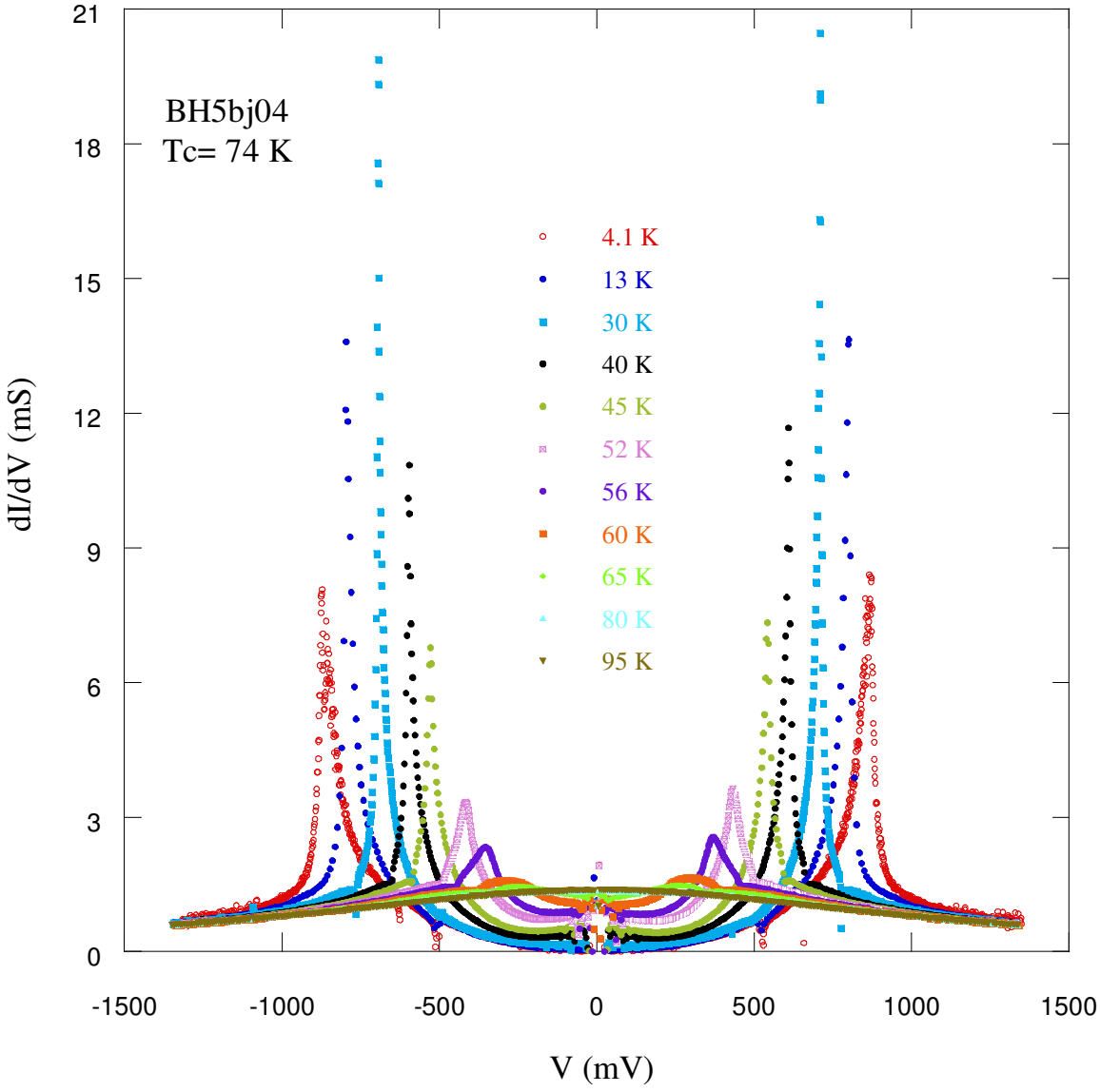

Figure 4.57. dI/dV versus V characteristics with various temperatures for BH5b

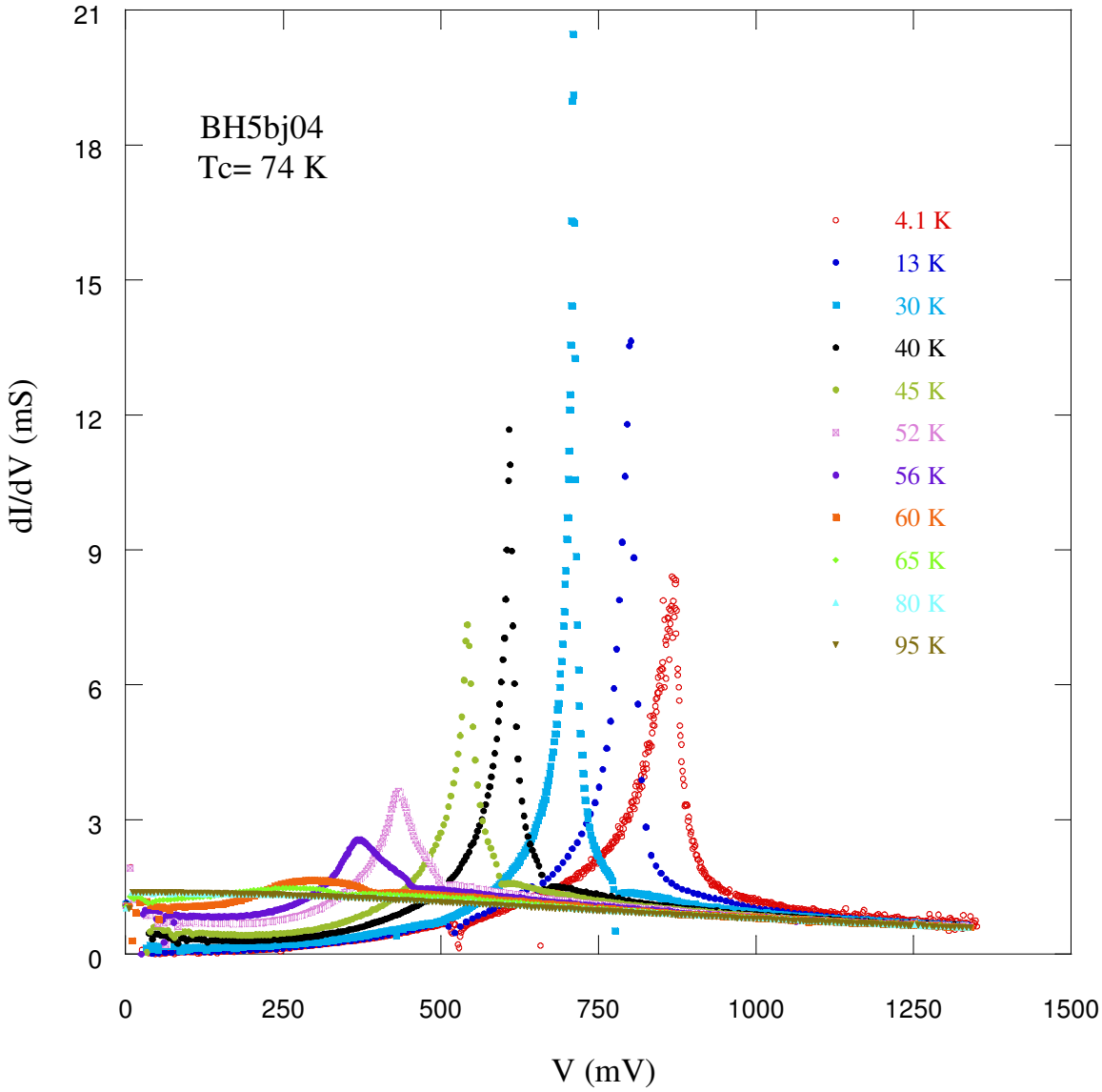

Figure 4.58. Temperature dependence of tunneling conductance of BH5b in detail

Figure 4.59 can be created by the data obtained by Figure 4.57. The locations of the voltages of gap and dip structures are determined and then normalized to compare with BCS prediction. Note that the curve of dip feature follows superconducting gap fashion. Both curves show much more rapid decrease with increasing temperature if compared with BCS dependence. The features of the tunneling conductances including dip and hump structures are not depend on the sort of the material and can be attributed to the superconducting gap. Some studies showed the dip structures have the role of

phonons in conventional superconductors. The doping and temperature dependences of the dip feature link it to the resonance spin excitation and point that the quasiparticles are robustly coupled to this mode.

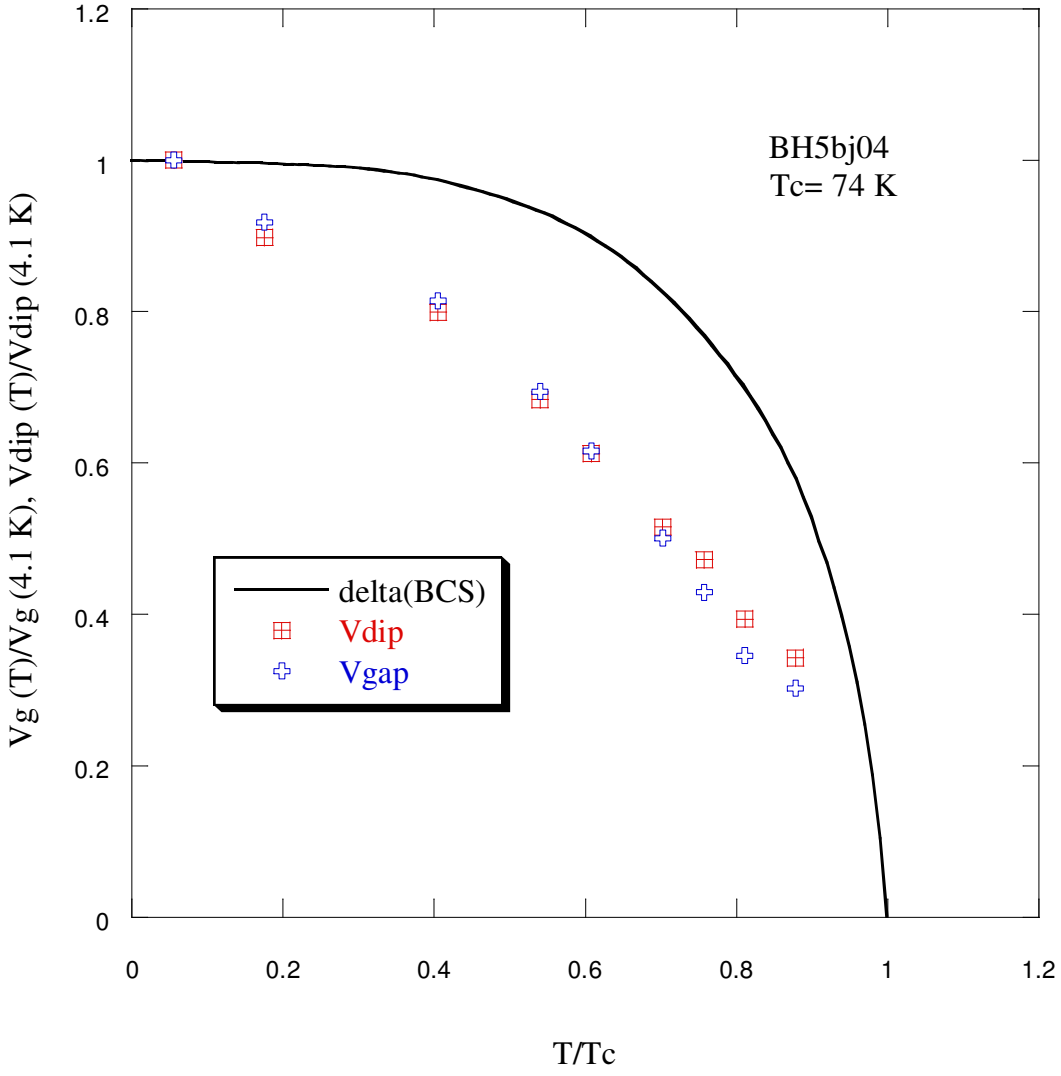

Figure 4.59. Normalized gap voltage vs. normalized temperature and normalized dip voltage vs. normalized temperature

CHAPTER 5

SUMMARY AND CONCLUSION

We performed conventional and interlayer tunneling measurements on both nearly-optimally doped (T_c= 93 K) pristine and $HgBr_2$ intercalated (T_c= 74 K) Bi-2212 single crystals. A novel method, PCT, is developed to get contact from mesa surfaces and to generate tunnel junctions. Using this versatile technique, IJJ tunneling characteristics can be obtained to compare with SIN and SIS junction characteristics and to investigate striking features of high T_c superconductors.

The PCT results of IJJ differ from those obtained from SIN single junction and SIS break junctions in that the IJJ spectra do not show well-defined dip and hump structures at higher bias, which is consistent with the loss of superconductivity in the IJJ at high voltages due to a combination of heating and quasiparticle injection effects. For nearly optimally doped Bi-2212, the energy gap is around 32 meV according to data obtained from SIS break junction measurements; this value is just only 18 meV if IJJ tunneling characteristics of sample MC01 are referred. In other words, IJJ exhibits 56% of the energy gap. The huge difference is due to the heating of the mesa structure during the measurement. We observed a cusp like feature at zero bias in tunneling conductances of the same nearly optimally doped sample (MC01) which is linked to d-wave symmetry.

Because of the very poor thermal conductivity of Bi-2212 crystals, the heating effects are inevitable in measurements, which is also a disadvantage for applications based on mechanism of IJJ. One of the most effective ways to surmount this problem is to intercalate a guest material into pristine Bi-2212 without affecting structural properties of the crystal. If IJJ spectra obtained from $HgBr_2$ intercalated Bi-2212 samples are compared with those from optimally doped ones, it can be easily understood, intercalation can suppress a large amount of Joule heating generated in the crystal. The tunneling conductances of intercalated crystals show pronounced dip and hump structures, which are associated with superconducting phase properties. Although intercalation does not affect the structure of Bi-2212, it causes the decrease of T_c from 77 K to around 74 K. But the locations of the quasiparticle peaks as well as dip and hump structures changed slightly if compared with their expected values. The

superconducting energy gap magnitudes found in IJJ characteristics are between 15-18 meV while this value is exactly 24 meV in SIS and SIN spectrum for $HgBr_2$ intercalated samples. The difference between these consequences is relatively lower if compared with those found in optimally doped crystals, which can be attributed to comparatively less formation of heating in the mesa. The table 5.1 shows the superconducting energy gap values of both nearly-optimally doped and intercalated samples.

Table 5.1. Energy gaps of investigated samples

Sample Type	Junction Type	Sample Code	Energy Gap
Optimally Doped Bi-2212 Single Crystals	SIS	HB2j12	Δ= 32 meV
	IJJ	MC01j06	Δ= 18 meV
		MC03j23	?
$HgBr_2$ Intercalated Bi-2212 Single Crystals	SIN	BH8j05	Δ= 24 meV
	SIS	BH8j11	Δ= 24 meV
	IJJ	BH3ej03	Δ= 16 meV
		BH4d#1j02	Δ= 18 meV
		BH4d#2j01	Δ= 15 meV
		BH4d#3j01	Δ= 16 meV
		BH5b	Δ= 15 meV

Both kinds of samples except MC03 gave IJJ characteristics with reduced energy gap. We can not determine the superconducting energy gap value for MC03 using our tunneling conductances because of high contact resistance. The I-V dependence of this sample neither exhibits any quasiparticle branch up to around 390 mV nor Josephson current at zero bias; which points out the presence of a relatively high resistance between gold film and Bi-2212 single crystal. Because we are not able to count the branches below 390 mV which are indiscernible due to the mentioned effect, we can not obtain the accurate number of IJJ in the mesa. This generates a

controversial value for energy gap of MC03 in calculations, since the quasiparticle peak voltage should be divided by IJJ number in the mesa to obtain the gap value. That is why the gap value of MC03 is emphasized by a question mark in related table. Excessive heat developed in the IJJ stacks is the possible reason of the lower superconducting gap value. The ratio of the gap obtained from IJJ to gap obtained from single junction for BH5b and BH4d#2 is 0.63 which is the closest one to the value of 0.6 found in theory of Owen and Scalapino that considers the nonequilibrium electron distribution caused by excess quasiparticle injection. Therefore such injection effects might be playing a role in the IJJ characteristics. The ratios for other intercalated samples are 0.66 for the sample with Δ=16 meV and 0.75 for the sample with Δ=18 meV. Note that as the value of the IJJ superconducting gap becomes closer to energy gap obtained from SIS junction, the ratio deviates from Owen Scalapino value; which makes weaker the effect of quasiparticle injection resulting in much more reduced amount of heating.

In order to enquire the superconducting origin of the quasiparticle excitation gap in HTSC, we examined the normalized temperature dependence of the normalized gap voltage values. For comparison with the gap behavior of conventional superconductors, BCS temperature dependence was presented in the same plot. According to BCS prediction, the gap magnitude significantly decreases as temperature increases near T_c over all doping ranges. However, the temperature evolution of the gap feature in HTSC shows absolutely different behavior. The existence of pseudogap well above T_c up to a characteristic temperature, T^*, affects the temperature dependence of superconducting energy gap. Pseudogap is believed to come into existence as a depression in the DOS of Bi-2212 above T_c. We can refer the temperature dependence of tunneling conductance to be able to determine the presence of pseudogap in the spectra. We encountered with this feature in tunneling characteristics obtained by optimally doped crystals. Although $HgBr_2$ intercalated samples generally reveal pseudogap, we did not observe this feature in our results.

Because of the inhomogeneous Ar ion etching, the mesa heights can be different even though the same parameters are used while doing ion milling. Therefore, we observed mesas with various heights including different number of IJJ within the same crystal. We presented 3 different mesa characteristics which belong to BH4d single crystal ($HgBr_2$ intercalated sample).

Table 5.2. Investigated IJJ and some related parameters

Sample Code	Sample Type	Mesa Size (μm^2)	Au Height (nm)	Mesa Height (nm)	# of IJJ (calculated)	# of IJJ (counted)
MC01	Optimally Doped	20x20	55	120	43	56
MC03	Optimally Doped	10x10	55	90	23	26(?)
BH3e	$HgBr_2$ Intercalated	20x20	40	80	19	14
BH4d	$HgBr_2$ Intercalated	10x10	35	65	14	12
BH5b	$HgBr_2$ Intercalated	10x10	74	119	21	30

The tunneling conductance of first mesa in concerned sample give the superconducting energy gap relatively at lower bias values (approximately at 427 mV for total number of IJJ) if compared second and third mesas, which means that the number of the IJJ in the first mesa is less than that of others. So we can conclude that the height of the mesa as important as its surface area in terms of overcoming heating problem. Because first mesa displays well-defined dip and hump structures at elevated bias values indicating less heating.

From the tunneling characteristics we found the number of IJJ for all the samples and these results were compared with calculated values for IJJ number obtained by AFM data. The IJJ properties in each investigated sample are presented in Table 5.2.

The general shape of the quasiparticle conductance data for optimally doped and $HgBr_2$ intercalated crystals are similar and especially well-defined dip and hump structures were observed around 3Δ and 4Δ values for IJJ and SIS single junctions.

REFERENCES

Alff, L., Krockenberger, Y., Welter, B., Schonecke, M., Gross, R., Manske, D., Naito, M. 2003. "A Hidden Pseudogap under the Dome of Superconductivity in Electron Doped High Temperature Superconductors", Nature Vol. 422, p. 698.

Ambegaokar, V. and Baratoff, A. 1963. "Tunneling Between Superconductors", Phys. Rev. Lett. Vol. 10, p. 486.

Anagawa, K., Yamada, Y., Shibauchi, T., Suzuki, M., Watanabe, T. 2003. "60 ns Time Scale Short Pulse Interlayer Tunneling Spectroscopy for $Bi_2Sr_2CaCu_2O_{8+\delta}$", Appl. Phys. Lett. Vol. 83, p. 2381.

Bednorz, J. G. and Müller, K. A. 1986. "Possible High Tc Superconductivity in the Ba-La-Cu-O System", Z. Phys. B. Vol. 64, p. 189.

Buchanan, M. 2001. "Mind the Pseudogap", Nature Vol. 409, p. 8.

Chen, J., Zasadzinski, J. F., Gray, K. E., Wagner, J. L., Hinks, D. G. 1994. "Point-Contact Tunneling Study of $HgBa_2CuO_{4+\delta}$: BCS-like Gap Structure", Phys. Rev. B. Vol. 49, p. 3683.

Chu, C. W., Bechtold, J., Gao, L., Hor, P. H., Huang, Z. J., Meng, R. L., Sun, Y. Y., Wang, Y. Q., Xue, Y. Y. 1988. "Superconductivity up to 114 K in the Bi-Al-Ca-Sr-Cu-O Compound System without Rare-Earth Elements ", Phys. Rev. Lett. Vol. 60, p. 941.

DeWilde, Y., Miyakawa, N., Guptasarma, P., Iavarone, M., Ozyuzer, L., Zasadzinski, J. F., Romano, P., Hinks, D. G., Kendziora, C., Crabtree, G. W., Gray, K. E. 1998. "Unusual Strong Coupling Effects in the Tunneling Spectroscopy of Optimally Doped and Overdoped $Bi_2Sr_2CaCu_2O_{8+\delta}$", Phys. Rev. Lett. Vol. 80, p. 153.

Duzer, T. V. and Turner, C. W. 1999. "Principles of Superconductive Devices and Circuits", (Prentice-Hall, New Jersey), pp. 88-91.

Dynes, R. C., Narayanamurti, V., Garno, J. P. 1978. "Direct Measurement of Quasiparticle-Lifetime Broadening in a Strong Coupled Superconductor", Phys. Rev. Lett. Vol. 41, p. 1509.

Esaki, L. 1957. "New Phenomenon in Narrow Germanium p-n Junctions", Phys. Rev. Vol. 109, p. 603.

Fine, B. V. 2005. "Temperature Dependence of the Superconducting Gap in High Tc Cuprates", Phys. Rev. Lett. Vol. 94, p. 157005.

Gao, L., Xue, Y. Y., Chen, F., Xiong, Q., Meng, R. L., Ramirez, D., Chu, C. W., Eggert, J. H., Mao, H. K. 1994. "Superconductivity up to 164 K in $HgBa_2Ca_{m-}$

$_1Cu_mO_{2m+2+\delta}$ (m=1,2 and 3) Under Quasihydrostatic Pressures", Phys. Rev. B. Vol. 50, p. 4260.

Giaver, I. 1960a. "Energy Gap in Superconductors Measured by Electron Tunneling", Phys. Rev. Lett. Vol. 5, p. 147.

Giaver, I. 1960b. "Electron Tunneling Between Two Superconductors", Phys. Rev. Lett. Vol. 5, p. 464.

Giaver, I. and Megerle, K. 1961. "Study of Superconductors by Electron Tunneling", Phys. Rev. Vol. 122, p. 1101.

Hawley, M. E., Gray, K. E., Terris, B. D., Wang, H. H., Carlson, K. D., Williams, J. M. 1986. "Measurement of the Energy Gap in an Organic Superconductor: Evidence for Extremely Strong Coupling", Phys. Rev. Lett. Vol. 57, p. 629.

Hazen, R. M., Finger, L. W., Angel, R. J., Prewitt, C. T., Ross, N. L., Hadidiacos, C. G., Heaney, P. J., Veblen, D. R., Shenh, Z. Z., El Ali, A., Hermann, A. M. 1988. "100 K Superconducting Phases in the Tl-Ca-Ba-Cu-O System", Phys. Rev. Lett. Vol. 60, p. 1657.

Heim, S., Irie, A., Schromm, S., Möβle, M., Rother, S., Kleiner, R., Müller, P. 2000. "Small Size Mesa Structures on $Bi_2Sr_2CaCu_2O_{8+\delta}$ Single Crystals", Physica C Vol. 341, p. 1567.

Huang, Q., Zasadzinski, J. F., Gray, K. E. 1990. "Phonon Spectroscopy of Superconducting Nb Using Point Contact Tunneling", Phys. Rev. B. Vol. 42, p. 7953.

Josephson, B. D. 1962. "Possible New Effects in Superconductivity Tunneling", Phys. Lett. Vol. 1, p. 251.

Kadin, A. M. 1999. "Introduction to Superconducting Circuits", (John Wiley & Sons, New York), pp. 153-157.

Kendziora, C., Kelley, R. J., Skelton, E., Onellion, M. 1996. "Advances in Single Crystal $Bi_2Sr_2CaCu_2O_{8+\delta}$ Supercondcutors", Physica C Vol. 257, p. 74.

Kim, S-J., Latyshev, Yu. I.,Yamashita, T. 1999. "Submicron Stacked Junction Fabrication from $Bi_2Sr_2CaCu_2O_{8+\delta}$ Whiskers by Focused Ion Beam Etching", Appl. Phys. Lett. Vol. 74, p. 1156.

Kleiner, R., Steinmeyer, F., Kunkel, G., Müller, P. 1992. "Intrinsic Josephson Effects in $Bi_2Sr_2CaCu_2O_{8+\delta}$ Single Crystals", Phys. Rev. Lett. Vol. 68, p. 2394.

Kurter, C. and Ozyuzer, L. 2004. "Mesa Structures on High Temperature Superconductors", Proceedings of the 10th Denizli Material Symposium and Exhibition, Denizli, (14-16 April 2004), p.863.

Kurter, C. and Ozyuzer, L. 2005. "Fabrication of Array of Mesas on Superconducting $Bi_2Sr_2CaCu_2O_{8+\delta}$ Single Crystals", J. Optoelectron. Adv. M. Vol. 7, No. 1, p. 415.

Latyshev, Yu. I., Monceau, P.,Pavlenko, V. N. 1997. Intrinsic Josephson Effects on Stacks Fabricated from high Quality BSCCO-2212 Single Crystal Whiskers, Physica C Vol. 293, p.174.

Latyshev, Yu. I., Yamashita, T., Bulaevskii, L. N., Graf, M. J., Balatsky, A. V., Maley, M. P. 1999. "Interlayer Transport of Quasiparticles and Cooper Pairs in $Bi_2Sr_2CaCu_2O_{8+\delta}$ Superconductors", Phys. Rev. Lett. Vol. 82, p. 5345.

Mallet, P., Roditchev, D., Sacks, W., Defourneau, D., Klein, J. 1996. "Vacuum Tunneling Spectroscopy of High Temperature Superconductors: A critical Study", Phys. Rev. B. Vol. 54, p. 13324.

Misra, S. 2004. "Scanning Tunneling Microscopy of The Cuprate Superconductor BSCCO", Ph.D. Thesis, University of Illinois at Urbana-Champaign, Illinois.

Miyakawa, N., Zasadzinski, J. F., Ozyuzer, L., Guptasarma, P., Hinks, D. G. , Kendziora, C., Gray, K. E. 1999. "Predominantly Superconducting Origin of Large Energy Gaps in Underdoped $Bi_2Sr_2CaCu_2O_{8+\delta}$ from Tunneling Spectroscopy", Phys. Rev. Lett. Vol. 83, p.1018.

Miyakawa, N., Zasadzinski, J. F., Ozyuzer, L., Guptasarma, P., Kendziora, C., Hinks, D. G., Kaneko, T., Gray, K. E. 2000. "Superconducting Gap and Pseudogap from Tunneling Conductance on $Bi_2Sr_2CaCu_2O_{8+\delta}$ with Various Oxygen Concentration", Physica C Vol. 341, p. 835.

Miyakawa, N., Zasadzinski, J. F., Asano, M., Henmi, D., Oonuki, S., Sasaki, K., Kaneko, T., Ozyuzer L., Gray, K. E. 2001a. "Universal Features of Tunneling Conductance on High-Tc Cuprates", Physica C Vol. 357, p. 126.

Miyakawa, N., Zasadzinski, J. F., Oonuki, S., Asano, M., Henmi, D., Kaneko, T., Ozyuzer, L. Gray, K. E. 2001b. "Implications of Tunneling Studies on High Tc Cuprates: Superconducting Gap and Pseudogap", Physica C Vol. 364, p. 475.

Miyakawa, N., Tokiwa, K., Mikusu, S., Zasadzinski, J. F., Ozyuzer, L., Ishihara, T., Kaneko, T., Watanabe, T., Gray, K. E. 2003. "Tunneling Studies of Multilayered Superconducting Cuprate (Cu, C)$Ba_2Ca_3Cu_4O_{12+\delta}$" , Int. J. Mod. Phys. B. Vol. 17, p. 3612.

Murakami, H., Ogami, T., Qi, Y., Sakai, K., Ito, T., Shigaki, I., Jansen, A. G. M., Wyder, P. 2000. "Problems in Point-Contact Tunneling Study on BSCCO", Physica B. Vol. 284, p. 573.

Ozyuzer, L., Zasadzinski, J. F., Gray, K. E., 1998, "Point Contact Tunneling Apparatus with Temperature and Magnetic Field Control", Cryogenics Vol. 38, No: 9, p. 911.

Ozyuzer, L. 1999a. “Doping Dependence of Quasiparticle and Josephson Tunneling in High Tc Superconductors”, Ph.D. Thesis, Illinois Institute of Technology, Illinois.

Ozyuzer, L., Miyakawa, N., Zasadzinski, J. F., Yusof, Z., Romano, P., Kendiora, C., Guptasarma, P., Hinks, D. G., Gray, K. E. 1999b. “Simultaneous Quasiparticle and Josephson Tunneling in $Bi_2Sr_2CaCu_2O_{8+\delta}$ Break Junctions”, IEEE T. Appl. Supercond. Vol. 9, No: 2, p. 2898.

Ozyuzer, L., Zasadzinski, J. F., Kendziora, C., Gray, K. E. 2000. “Quasiparticle and Josephson Tunneling of Overdoped $Bi_2Sr_2CaCu_2O_{8+\delta}$ Single Crystals”, Phys. Rev. B. Vol. 61, p. 3629.

Ozyuzer, L., Kurter, C., Zasadzinski, J. F., Gray, K. E., Hinks, D. G., Miyakawa , N. 2005. “Comparison of Intrinsic Josephson Junction and SIS Tunneling Spectroscopy of $Bi_2Sr_2CaCu_2O_{8+\delta}$ ”, IEEE T. Appl. Supercon. Vol. 15, p.181

Pan, S.H., O’Neal, J.P., Badzey, R.L., Chamon, C., Ding, H. , Engelbrecht, J.R. , Wang, Z. , Eisaki, H. , Uchida, S., Gupta, A.K., Ng, K.-W., Hudson, E.W., Lang, K.M., Davis, J.C. 2001. “Microscopic Electronic Inhomogeneity in the High-Tc Superconductor $Bi_2Sr_2CaCu_2O_{8+x}$”, Nature Vol. 413, p. 282.

Petley, B. W. 1971. “An Introduction to the Josephson Effects”, edited by J. Gordon Cook (Milles & Boon Limited, London), pp. 13, 75-78.

Poole, C. P., Horacio, A. F., Richard, J. C. 1995. “Superconductivity”, (Academic Press, California)

Romano, P., Chen, J., Zasadzinski, J. F. 1998. “Josephson and Quasiparticle Tunneling in SIS Junctions $Bi_2Sr_2CaCu_2O_8$ and $Bi_2Sr_2CuO_6$”, Physica C Vol. 295, p.15.

Rowell, J. M. 1963. “Magnetic Field Dependence of the Josephson Tunnel Current”, Phys. Rev. Lett. Vol. 11, p. 200.

Schilling, A., Cantoni, M., Guo, J. D., Ott, H. R. 1993. “Supercondcutivity above 130 K in the Hg-Ba-Ca-Cu-O System”, Nature Vol. 363, p.56.

Schmidt, V. V. 1997. “The Physics of Superconductors”, edited by P. Müller and A. V. Ustinov (Springer- Verlag, Berlin), pp. 155-160.

Shapiro, S. 1963. “Josephson Currents in Superconducting Tunneling: The Effect of Microwaves and Other Observations”, Phys. Rev. Lett. Vol. 11, p. 80.

Soibel, A. 2001. “Visualization of Vortex Lattice Melting Transition and Transport Current Flow in $Bi_2Sr_2CaCu_2O_{8+\delta}$ with Differential Magnetoptical Technique” , Ph.D. Thesis, Weizmann Institute of Technology, Rehovot

Takano, Y., Hatano, T., Ishii, A., Fukuyo, A.,Sato, Y., Arisawa, S., Togano, K. 2001. “Fabrication of Bi2212 Cross Whiskers junction”, Physica C Vol. 362, p. 261.

Tallon, J. L. 2000. “Industry Warms to Superconductors”, Physics World, p. 27.

Tanabe, K., Hidaka, Y., Karimoto, S., Suzuki, M. 1996. "Observation of Both Pair and Quasiparticle Tunneling in Intrinsic Junction Stacks Fabricated on $Bi_2Sr_2CaCu_2O_{8+\delta}$ Single Crystals", Phys. Rev. B Vol. 53, p. 9348.

Ting-Wei Li. 1995. "Studies of Crystal Growth, Oxygen Diffusion, Flux Pinning and Flux Lattice Melting on $Bi_2Sr_2CaCu_2O_x$ Single Crystals ", Ph.D. Thesis, Kammerlingh Onnes Laboratory, Leiden University and Van der Walls-Zeeman Laboratory, University of Amsterdam, Netherlands.

Tinkham, M. 1996. "Introduction to Superconductivity", (Mc Graw-Hill, Singapore).

Tsai, J. S., Fujita, J., Kupriyanov, M. Yu. 1995. "Thin Film Anisotropic Transport Measurement on Tilted $Bi_2Sr_2CaCu_2O_x$", Phys. Rev. B. Vol. 51, p. 16267.

Wolf, E. L. 1985. "Principles of Electron Tunneling Spectroscopy", (Oxford University Press, New York).

Won, H. and Maki, K. 1994. "d-wave Superconductor as a Model of High Tc Superconductors", Phys. Rev. B. Vol. 49, p. 1397.

Wu, M. K., Ashburn, J. R., Torng, C. J., Hor, P. H., Meng, R. L., Gao, L., Huang, Z. J., Wang, Y. Q., Chu, C. W. 1987. "Superconductivity at 93 K in a New Mixed-Phase Y-Ba-Cu-O Compound System at Ambient Pressure", Phys. Rev. Lett. Vol. 58, p. 908.

Yurgens , A., Winkler, D., Zavaritski, N. V., Claeson, T. 1996a. "Gap and Subgap Structures of Intrinsic Josephson Tunnel Junctions in $Bi_2Sr_2CaCu_2O_{8+\delta}$ Single Crystals", SPIE Proceedings Vol. 2699.

Yurgens, A., Winkler, D., Zavaritski, N. V., Claeson, T., 1996b, Strong Temperature Dependence of the c-axis Gap Parameter of $Bi_2Sr_2CaCu_2O_{8+\delta}$ Intrinsic Josephson Junctions, Phys. Rev. B., Vol. 53, p. R8887.

Yurgens, A., Winkler, D., Claeson, T., Hwang, Seong-Ju, Choy , Jin-Ho 1999. "Pseudogap Features of Intrinsic Tunneling in (HgBr2)-Bi2212 Single Crystals", Int. J. Mod. Phys. B Vol. 13, p. 3758.

Yurgens, A. A. 2000. "Intrinsic Josephson Junctions: Recent Developments", Supercond. Sci. Tech. Vol. 13, R85,

Yurgens, A. and Claeson, T. 2001. "Intrinsic Josephson Junctions for Studies of High Tc Superconductors", Physica C Vol. 341, p.2277.

Yurgens, A., Winkler, D., Claeson, T., Ono, S., Ando, Y. 2004. "Reply to the Comment on Intrinsic Tunneling Spectra of $Bi_2(Sr_{2-x}La_x)CuO_6$ ": Auxiliary Information", cond-mat/0309131

Yusof, Z., Zasadzinski, J. F., Coffey, L., Miyakawa, N. 1998. "Modeling of Tunneling Spectroscopy in High Tc Supercondcutors Incorporating Band Structure, Gap

Symmetry, Group Velocity and Tunneling Directionality", Phys. Rev. B. Vol. 59, p. 514.

Zasadzinski, J. F., Ozyuzer, L., Miyakawa, N., Hinks D. G., Gray, K. E. 2000. "High Energy Secondary Peak Structure in Tunneling Spectra (hump) as Possible Magnetic Pseudogap", Physica C Vol. 341, p. 867.

Zasadzinski, J. F., Ozyuzer, L., Miyakawa, N., Gray, K. E., Hinks, D. G., Kendziora, C. 2001. "Correlation of Tunneling Spectra in $Bi_2Sr_2CaCu_2O_{8+\delta}$ with the Resonance Spin Excitation", Phys. Rev. Lett. Vol. 87, p. 067005.